Modelling of Fire and Toxicants Formation - Measures to Reduce Risks

Dissertation

submittet to and approved by the

Faculty of Mechanical Engineering
University of Braunschweig-Institute of Technology

and the

Faculty of Engineering
University of Florence

in candidacy for the degree of a
Doktor-Ingenieur(Dr.-Ing.)/
dottore di Ricerca in Risk Management on the Built Environment *

by
A.F.M. Kamrul Islam

Born 5.11.1977

from Mymensingh, Bangladesh

Submittet on 10 October 2008

Oral examination on 5 December 2008

Professorial advisors Prof. Dr.techn. Reinhard Leithner
Prof.Dr.Ing. G. Manfrida

Prof. Dr.-Ing. D. Hosser

2009

* Either the German or the Italian form of the title may be used.

.

Dedicated to my parents Rokeya Islam and Nurul Islam.

Abstract

This thesis describes a methodology of fire risk simulation and mitigation by developing and implementing a model for toxic chemical species formation from gas and plastic burning at enclosure fire conditions into a conventional Computational Fluid Dynamics (CFD) model and taking appropriate measures.
Roughly two-thirds of all deaths resulting from enclosure fires can be attributed to the presence of Carbon Monoxide (CO) which is a dominant toxicant in fire deaths. Some studies revealed the role of other toxicants in fire deaths. Therefore, a complete fire hazard assessment requires knowledge of toxic chemical species production of $CO, NO_x, SO_x, H_2S, HCN, HCl$ etc. Most existing studies of toxicants assessment have solely relied on data obtained from small scale physical fire models or empirical data concerning CO and soot yield. There is no straight forward method to interpret such data in terms of toxic concentration in real scale fire. In reality, toxic species production varies with combustion conditions (i.e. equivalence ratio, temperature). Therefore, using constant toxic yield value from small scale experiments can lead to a significant error in toxic hazard assessment. Currently available CFD codes have either no implemented toxic species formation model or toxic species formation models (i.e. CO) with inaccurate predictability. There is no model available for other toxicants which may also be produced during enclosure fires.
In this dissertation, detailed investigations of the effect of equivalence ratio and temperature on toxicants formation for different burning substances are conducted through constrained (temperature and equivalence ratio) equilibrium calculations.
Three different CFD fire simulation programs are compared to experimental data and one is chosen based on its local transient temperature predictability while spending same computational time and using same computational resource. CO concentration is calculated as a result of temperature and equivalence ratio at each point as postprocessing. But simulated CO-values are very high in the flame and very low apart from the flame. Therefore, a submodel has been developed to predict local toxicant concentration by solving species transport equation with artificial source terms as postprocessing. Constrained equilibrium concentrations are utilized for the calculation of the artificial source terms. All spatial derivatives are approximated by second order finite differences and flow variables are updated in time using an explicit second order predictor corrector scheme. Explicit 2nd order Adam-Bashforth scheme is utilized for numerical integration of source term with species balance equation. The developed toxic model is coupled with the chosen CFD model-FDS.

Simulations are performed with the developed toxic species formation and transport model. Simulation results are compared with experimental data of full and reduced scale enclosure natural gas fires as well as reduced scale polystyrene fires. Predictions of CO are in reasonable agreement with experimental data although discrepancies occur due to concentrations and temperature discrepancies resulting from the fire simulation. A discussion is presented pointing out scope of further development of the model.

In final part of the thesis, it is shown how the probability of fires and resulting damages i.e. fire risk could be assessed by using fault tree and event tree analysis if satisfying statistical data would be available. By implementing the presented toxic species formation and transport model into usual fire simulation program, the prediction of the probability of fire deaths can be improved. By reducing toxic exposure through choosing appropriate enclosure geometry and ventilation, the probability of fire deaths can be reduced and by improving early fire warning system, the probability of fire can be mitigated. Consequently, both result in mitigation of fire risk e.g. using two detectors for 60 m^2 area instead of one as prescribed e.g. in DIN, can reduce sensors failure probability by 78% and thereby also fire risk.

Zusammenfassung

Diese Arbeit beschreibt eine Methode, das Brandrisiko durch die Entwicklung und Einbettung eines Modells für die Bildung von toxischen Schadstoffen, insbesondere CO, in ein konventionelles Computational Fluid Dynamics Modell (CFD) besser zu beschreiben und durch geeignete Maßnahmen zu verringern.
Ungefähr zwei Drittel aller durch Brände in geschlossenen Räumen entstehenden Todesfälle können auf die Anwesenheit von Kohlenmonoxid im Rauch zurückgeführt werden, welches damit den dominanten letalen Schadstoff darstellt. Allerdings wurden im einigen Studien auch andere toxische Stoffe als Todesursache gefunden. Aus diesem Grund macht eine umfassende Brandbewertung Fachwissen über die Bildung von Schadstoffen wie $CO, NOx, SOx, H_2S, HCN, HCl$ etc. unabdingbar. Ein Großteil der bislang durchgeführten Studien zur Schadstoffbewertungen beziehen sich lediglich auf empirische Daten von (z.B. CO und Ruß) oder auf solche Daten, die aus wenig umfangreichen empirischen Brandmodellen gewonnen wurden. Bisher wurden diese Daten nicht systematisch mit den Konzentrationen der zahlreichen toxischen Schadstoffe in tatsächlichen Bränden verglichen. In der Realität variiert die toxische Schadstoffbildung mit den Stoffen, die verbrennen und den Verbrennungsbedingungen -insbesondere mit dem GER (Global equivalence ratio) (Kehrwert des Luftüberschusses) und der Temperatur. Die Verwendung einer konstanten Schadstoffentstehung aus den wenig umfangreichen Experimenten kann zu einer signifikanten Fehleinschätzung in der toxischen Gefahrenanalyse führen. Aktuell verfügbare CFD Codes haben entweder kein Modell für die toxischen Schadstoffbildung implementiert oder eines mit stark limitierter Vorhersagegenauigkeit nur für CO. Es gibt auch kein Modell für die Bildung anderer toxischer Schadstoffe, die ebenfalls während des Brandes entstehen können.
In dieser Arbeit werden detaillierte Untersuchungen des Einflusses von Luftüberschuss und Temperatur auf die Schadstoffbildung bei der Verbrennung verschiedener Materialien mit Hilfe von chemischen Gleichgewichtsberechnungen durchgeführt.
Dabei werden zuerst die Ergibnisse dreier verschiedener CFD Brandsimulationsprogramme mit experimentellen Daten verglichen und schließlich eines davon wegen der Qualitat seiner lokal instationären Temperatursimulationen ausgewählt. Die drei Simulationsprogramme brauchen die gleiche Rechenzeit auf dem gleichen Rechner. Der CO -Gehalt wird als Funktion der Temperatur und des Luftüberschusses bzw.

Brennstoff-Luft-Verhaltnisses in einem Postprocessing berechnet. Dies ergab teils zu kleine und teils zu hohe Werte. Daher wurde ein Sub-Modell entwickelt, um lokale toxische Schadstoffkonzentration vorherzusagen, indem eine Spezies-Transportgleichung mit künstlichen Quelltermen im Postprocessing gelöst wird. Für die Berechnung dieser Quellterme werden die Gleichgewichtskonzentrationen und Reaktionstemperaturgrenzen verwendet. Alle räumlichen Ableitungen werden durch finite Differenzen 2. Ordnung approximiert und die Strömungsvariablen zeitabhängig aktualisiert, indem ein explizites Predictor Corrector Verfahren 2. Ordnung benutzt wird. Ein explizites Adam- Bashforth wird für die numerische Integration der Spezienbilanzen verwendet. Schließlich wird das entwickelte Modell mit dem ausgewählten CFD Programm-FDS gekoppelt.
Die Ergebnisse der Simulationen mit diesem Programm werden mit experimentellen Daten von Erdgasbränden und Polystyrolbränden teilweise auch in verkleinertem Maßstab verglichen. Die Vorhersage des CO zeigt gute Übereinstimmung mit den experimentellen Daten. Abweichungen in den Schadstoffkonzentration werden teilweise sicher auch durch Temperatur, und Mischungsabweichungen der Brandsimulation hervorgerufen. Ergänzend werden mögliche Weiterentwicklungen des Modells aufgezeigt.
Es wird gezeigt, wie die Wahrscheinlichkeit eines Brandes und Schäden d.h. des Risiko mit Hilfe der Fehlerbaumanalyse und der Ereignisablaufanalyse abgeschätzt werden könnte, wenn ausreichendes statistisches Datenmaterial vorhanden wäre.
Durch die Implementierung des entwickelten Modells für die Bildung toxicher Schadstoffe kann die Wahrscheinlichkeit von Todesfällen besser abgeschätzt werden. Durch die angemessenen Wahl der Raumgeometrie und Belüftung kann die Wahrscheinlichkeit von Todesfällen vermindert werden. Wird zudem durch verbesserte Brandfrühwarnsysteme die Wahrscheinlichkeit von Bränden reduziert, wird des Risiko durch beide Maßnahmen stark vermindert. Die Verwendung z.B. von zwei Rauchsensoren für 60 m^2 Raumfläche anstatt nur eines Rauchsensors, wie in der DIN vorgeschrieben, reduziert die Wahrscheinlichkeit des Versagens der Rauchsensoren und damit auch die Wahrscheinlichkeit der Entstehung eines größeren Brandes um 78% und damit auch das Brandrisiko entsprechend.

Acknowledgments

First and foremost, I am profoundly grateful to my mentor Prof.Dr.techn. Reinhard Leithner for his wise counsel and patient support throughout this dissertation. I thank him for the continuous guidance and advice with which my dissertation has been brought to success. I especially thank Prof.Dr.Ing. G. Manfrida, University of Florence to become my mentor and for providing me the oppurtunity to work with him at his department during my Florence visit. I am thankful to Prof.Dr.-Ing. Hosser for his cooperation and becoming a member of my PhD defense committee. I thank Prof.Dr.-Ing. M. Mönnigmann to preside over the committee.

I would like to thank M.Sc. Md. Khalaquzzaman, Dr.-Ing. Noman Kabir, M.Sc. Faroque Hossain, Dipl.-Math. Timm Pliefke for their help to my dissertation in various ways. I would like to express my gratitude to Dr. Stephen Welch of Edinburgh university for his cooperation. Dr.-Ing. Müller of IWBT for his valuable discussion on CFD. I thank Dr. Per Blomqvist, Dr. Dan Gottuk for sending experimental data. I extend my thanks to Dr. Kevin McGrattan and Dr. Jason Floyd for their prompt answer whenever I have asked about FDS source code. Special thanks go to Dr. Suresh Kumar of BRE, U.K. for providing Jasmine code.

I want to thank my family for their support and encouragement.

Finally I acknowledge financial support of German Research Foundation (DFG) as a framework of International Graduate Program namely IGK 802 of TU Braunschweig and Engineering Faculty, University of Florence for organizing such international PhD programm.

A.F.M.Kamrul Islam

Contents

Tables and Figures

Tables

Figures

List of Symbols

ROMAN

A	pre exponential factor
A_c	area of cell face
A_d	area of door
A_0, A_j, a_i	probability of events
$B(x, \lambda)$	emission source term
C	coefficient for natural convection
C_R	Eddy Break Up model reaction rate factor
C_s	empirical constant for LES turbulence model
$C_{\mu,\rho}$	coefficient
$c_{p,s}$	specific heat capacity (Indices: p..at constant pressure, s..of solids)
D_i	diffusivity (Index: i..species i)
E	surface roughness
E_A	activation energy
$E_{critical}$	critical accumulated flux
$E_i(t)$	probability of basic event i in failed state at time t
e_x, e_y, e_z	unit vectors in x, y, z direction
$f(t)$	function of time (e.g. ramp)
$\vec{\mathbf{f}}$	external forces
F	net heat flux
$\vec{\mathbf{F}}$	specific force related to pressure
F_s	wall shear force at cell face
G_B	buoyancy force
$\vec{g}$	gravitational acceleration
h	enthalpy
h_d	height of door
h_c	convection heat transfer coefficient
$I_\lambda(x, \vec{s})$	radiation intensity at wavelength
$I_b(x)$	Plank function
I_n	radiation intensity integrated over band
k	turbulent kinetic energy
$k_{g,s,LES}$	thermal conductivity (Indices: g..gas,s..solid, LES..Large Eddy Simulation)
L	characteristic length

$M_{\alpha,mix}$	molar mass, Indices: α..of species, mix..of mixture
$m_{f,fu,i,o_2,p}$	mass fraction (Indices: f,fu..fuel, i..species, o_2..oxygen, p..product)
$\dot{m}''$	mass loss rate of fuel
$\dot{m}''_f$	fuel mass loss
$\dot{m}''_a$	air flow rate
$\dot{m}'''_i$	production rate of species i
N	maximum number
n	counting number
p	pressure
Pr	Prandtl number
Prw	Probability
$\dot{Q}$	heat release rate
$\mathbf{q}$	heat flux vector
$\dot{q}'', q_w$	heat flux at solid surface, wall
$\dot{q}''_{c,r,user}$	heat flux to surface (Indices: c..convective, r..radiative, user..user defined)
$\dot{q}'''_{c,r}$	heat release rate per unit volume (Indices: c..chemical reactions, r..radiation)
$\Re$	universal gas constant
Re	Reynolds number
R_{fu}	mean reaction rate of fuel
r	stoichiometric fuel to air ratio
S_{ij}	strain tensor
s	stoichiometric oxygen to fuel ratio
$\overrightarrow{s}$	direction vector
Sc	turbulent Schmidt number
$T_{s,p,w}$	temperature (Indices: s..solid, p..near wall point, w..wall)
t	time
U	tangential velocity
$\mathbf{u}$	velocity vector (u,v,w)
u^+	non-dimensional velocity
u_τ	friction velocity
X_α	volume fraction of α
x	cartesian coordinate
$x^{'}$	CO yield
$Y_{\alpha,i,F}$	mass fraction (Indices: α..of species α, i..of species i, F..Fuel)
Y^*_α	mass fraction of species α from lookup table
y	cartesian coordinate
y^+	non-dimensional distance to surface
Z	mixture fraction
z	cartesian coordinate

GREEK

α	component
β_g	thermal expansion coefficient
$\triangle$	length in the order of the grid cell size
$\triangle H$	reaction enthalpy
$\triangle H_{pyro}$	heat of pyrolysis
$\triangle H_v$	heat of vaporization
δ	thickness
$\delta x \delta y \delta z$	volume of finite element
ε	turbulent dissipation rate
ε_w	emissivity of boundary surface
$\varepsilon_{u,v,w}$	local Courant numbers
κ	von Karman constant
κ_n	mean absorption coefficient inside the band
$\kappa(x, \lambda)$	local absorption coefficient
μ	dynamic viscosity
μ_t	turbulent dynamic viscosity
$\rho_{g,s,char,moisture}$	density (Indices: g..gas, s..solid, char, moisture)
σ	Stefan-Boltzmann coefficient
$\sigma_{h,l}$	laminar Prandtl number
$\sigma_{h,t}$	turbulent Prandtl number
$\sigma_s(x, \lambda)$	local scattering coefficient
σ_t	coefficient in buoyancy term
τ_{ij}	stress tensor
τ_q	characteristic ramp up time
τ_w	wall shear stress
ϕ	global equivalence ratio
Φ	dissipation rate

MATHEMATICAL SYMBOL

∇	Nabla $(\frac{\delta}{\delta x}e_x, \frac{\delta}{\delta y}e_y, \frac{\delta}{\delta z}e_z)$
$\frac{D}{Dt}$	substantial derivative
$\frac{dx}{dt}$	ordinary derivative
$\frac{\delta x}{\delta t}$	partial derivative

ABBREVIATIONS

CFD	computational fluid dynamics
CFL	Courant-Friedrichs-Lewy condition for time steps
DNS	direct numerical simulation
DTR	Discrete Transfer Radiation model
EBU	Eddy Break Up combustion model
EDC	Eddy Dissipation Combustion model
ETA	event tree analysis
FDM	finite difference method
FDS	fire dynamics simulator (FDM -CFD program for fire simulation)
FVM	finite volume method
FTA	fault tree analysis
FSE	full scale enclosure
FPS	fire protection system
GER	global equivalence ratio
HRR	heat release rate
JASMINE	FVM-CFD program for fire simulation
LES	large eddy simulation
ODE	Ordinary Differential Equation
PP	polypropelyne
PDE	partial differential equation
PUF	polyurethane foam
PVC	polyvinyl chloride
QUICK	Quadratic Upstream Interpolation of Convective Kinematics
QUICKER	Quadratic Upstream Interpolation of Convective Kinematics Revised
RANS	Reynolds averaged Navier-Stokes
RSE	reduced scale enclosure
SIMPLE	Semi Implicit Pressure Linked Equation
SIMPLER	Semi Implicit Pressure Linked Equation Revised
SOFIE	FVM-CFD program for fire simulation

CHEMICAL SPECIES

CO	carbon monoxide
HCl	hydrogen chloride
HCN	hydrogen cyanide
NH_3	ammonia
NO_2	nitrogen dioxide
SO_x	sulphur oxide
H_2S	hydrogen sulphide
F	fuel consisting of carbon, hydrogen etc.

Chapter 1

Introduction

1.1 Motivation

The damage done by natural disasters reveals a clearly rising trend [16]. In order to manage risk it is utmost important to analyse, assess and control the effects of hazards to which the built environment may be exposed as a result of natural or anthropogenic disasters. Wind, water with all its different ways of action, earthquakes, landslides, groundwater contamination, waste, air pollution and large scale fires are typical examples. This thesis deals with the reduction of fire risk especially in the field of development of fire modelling and toxic chemical species (toxicants) formation and fire risk management through fire protection design.

Accidental fires result in enormous amount of property damage and endanger people and environment. Fire statistics show that smoke and toxic gas inhalation cause the majority of fire fatalities. Roughly two-thirds of all deaths resulting from enclosure fires can be attributed to the presence of Carbon Monoxide (CO) which is known to be the dominant toxicant in fire deaths [50]. The inhalation of a large concentration of toxic gas and soot may lead to lung edema and inflammation, causing death a short time after the fire [16]. In addition, toxic effluents can either be set free or be produced during a fire and can affect people directly through air, ground water or surface water [54]. Therefore, a complete fire hazard assessment requires knowledge of toxic chemical species production ($CO, NO_x, SO_x, H_2S, HCN, HCl$ etc.). Species production is mainly affected by the chemical properties of burning material and also by the confinement, ventilation, fluid dynamics, thermal environment and mode of burning i.e. by the combustion conditions. In the majority of accidental fires, thermochemical characteristics of the burning material and combustion conditions depend on a lot of accidental influences which lead to more or less different results. Therefore, experimental studies of large fires which are very expensive would have to be repeated several times while condition changes. Numerical simulations provide a promising tool to complement experimental studies and improve our understanding and to allow a stochastic approach for fire safety risk assessment. For calculating very detailed fire effects, e.g. gas concentration in a special area of a confinement , CFD (Computational Fluid Dynamics) models can be used with enormous calculation effort. Most

existing studies of toxicants assessment have solely relied on data from small scale physical fire models or empirical data (i.e. CO and soot yield). There is no straightforward method to interpret such data in terms of toxic concentration in real scale fire. In reality, toxic species production varies with fires conditions. Therefore, using constant toxic yield values from small scale experiments can lead to significant errors in toxic hazard assessment. Currently available CFD codes have either no implemented toxic model or toxic models (i.e. CO) with inaccurate predictability. There are no models available for other toxicants which may also be produced in fire. Fire toxicants assessment in terms of a CFD modelling approach including chemical equilibrium calculation of the burning matter at variable combustion conditions and equivalence ratios is conducted in this thesis. Such model can be utilized to mitigate fire risk through fire hazard assessment and fire protection design. The following parts of the risk management process are involved in the thesis:

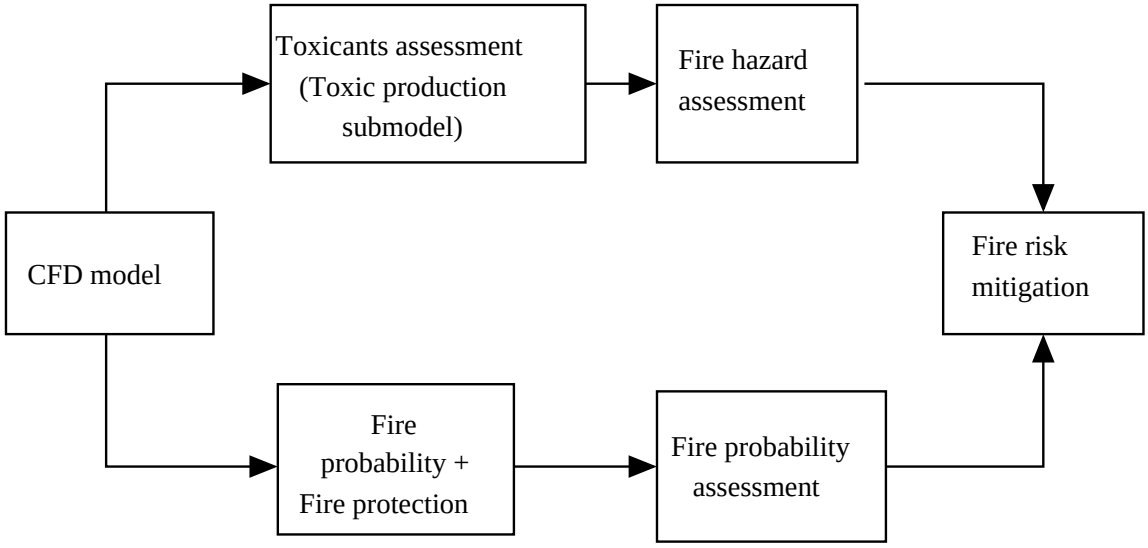

FIGURE 1.1 Risk management process involved in the thesis

1.2 Objective

The objective of this thesis is to develop fire risk mitigation strategies through toxic hazard assessment and fire protection design. To achieve this goal, the thesis is subdivided into different parts:

- Detailed investigations of the effect of equivalence ratio and temperature on fire products for different burning substances. In order to do so calculations of the constrained chemical equilibrium concentrations during the combustion of natural gas, polystyrene, polyurethane, poly vinyl chloride (PVC), polypropylene are conducted.
- Find out a CFD model from conventional models which can compute enclosure fire growth reasonably.
- Develop a model to calculate local toxicants concentration of a specific fire resulting

from the residence time of smoke at different equivalence ratios and temperatures and couple this model with the conventional CFD model which can reasonably calculate local fire conditions (i.e. temperature, equivalence ratio or mixture fraction).

- Assess fire prevention measures like the design of rooms, ventilations and the early fire identification, utilizing the developed model.

1.3 Basics of fire

Fire, which is conventionally defined as uncontrolled diffusion flame spread, is arguably one of the most complex phenomena considered in combustion science. A typical compartment fire (in the absence of attempts to control it) undergoes the following major stages [45]:

- Ignition: Ignition process can be either piloted (caused by flame, spark etc.) or spontaneous (due to accumulation of heat in the fuel). Once ignition occurs, part of the solid fuel in the compartment pyrolyze, releasing gaseous volatiles which burn as they mix with air.

- Growth: Following ignition, fire grows at the rate dependent upon the type of fuel, access to oxygen, compartment configuration and other factors. By heat transfer, contiguous and nearby combustible surfaces can reach temperatures at which they will begin to burn. The gaseous phase may be viewed as a primary energy transmitter between the burning and virgin burning material. During this stage, hot gases produced by the fire rise due to buoyancy entraining the surrounding air, and the fire plume is formed. Impingement of a fire plume on the ceiling of the compartment gives rise to formation of a hot smoke layer in the upper part of the room.

- Flashover: Flashover is a rapid transition from the growth period to a fully developed fire, resulting in the total surface of the combustible material being involved in fire. Flashover represents a thermal instability caused primarily by strong radiation from the smoke layer to the combustible materials within the enclosure.

- Fully developed fire: At this stage the rate of heat release reaches its maximum, and the development of the fire is often limited by the availability of oxygen. The average temperatures in the compartment are very high, in the range of 700-1200°C.

- Decay: During this stage the energy release rate diminishes as the fuel (or oxygen) becomes consumed.

Basic Definitions

Species Yields: The generation of fire products in compartment fires can be quantified in terms of species yields, Y_i, defined as the mass species i produced per mass of fuel burned (g/g):

$$Y_i = \frac{m_i}{m_f} \tag{1.1}$$

Global Equivalence Ratio (GER): The concept of GER can be used to express the overall ventilation of a control volume, such as a fire compartment. However, due to complex interaction between the plume and the upper layer, a compartment equivalence ratio is more appropriate. As a practical note, for fires within a single compartment, the equivalence ratio is calculated (and experimentally measured) based on the the instantaneous fuel mass loss rate, $\dot{m}''_f$, and air flow rate, $\dot{m}''_a$, into the compartment

$$\phi = GER = \frac{\frac{\dot{m}''_f}{\dot{m}''_a}}{r} \tag{1.2}$$

where r is the stoichiometric fuel to air ratio.

Chapter 2

State of the art

2.1 Fire modelling

Fire models are means in the evaluation of the performance of buildings built with new materials and contents. Fire modelling of a compartment can be achieved either using empirical equations based on observations from experiments or mathematical methods that are commonly divided into stochastic (probabilistic) and deterministic models. The emphasis in this document is on the deterministic models , which predict fire development based on solutions of mathematical equations that describe the physiochemical phenomena of fire. There are two types of deterministic fire models called zone models and field models. Field models are also known as CFD models of fire. The zone modelling approach emerged in mid 1970s when efforts to study the developing fire in a compartment were intensified. Massive increases in computer speed accompanied by ever-reducing hardware costs made CFD modelling a common practice in the design and analysis of many practical engineering problems including those associated with fire. A focus of this research is to exploit CFD modelling to fire field, zone modelling approach will not be explained here. Details of zone modelling technology can be found in [31, 30]. This chapter also does not include theoretical underpinning to CFD. Such detail will be found in any text book and review on the topic. A general survey of existing CFD fire models can be obtained in [53, 3]. In this review, we will focus on the different integrated submodels in commonly used CFD fire models. Following sections summarize built in physical models, exploited in this thesis in order to model fire. Detailed descriptions of these models are given in the respective CFD models documentations [1, 4, 5]. The goal of this section is to get a short overview of these CFD models.

2.1.1 Fire Dynamics Simulator (FDS)

FDS is a CFD model of fire driven fluid flow developed at the National Institute of Standards and Technology (NIST), USA. Major features of the model and the underlying physical assumptions will be outlined here. More detailed information about the model can be obtained in [1]. The model solves numerically a form of the Navier-Stokes equations appropriate for low speed, thermally driven flow with an emphasis on smoke and heat

transport from fires.

The Fundamental Conservation Equations

The conservation equations for mass, momentum and energy for a newtonian fluid are presented here.
Conservation of Mass

$$\frac{\partial \rho}{\partial t} + \nabla . \rho \mathbf{u} = 0 \tag{2.1}$$

Conservation of Momentum

$$\frac{\partial}{\partial t}(\rho \mathbf{u}) + \nabla . \rho \mathbf{u}\mathbf{u} + \nabla p = \rho \mathbf{f} + \nabla . \tau_{ij} \tag{2.2}$$

Conservation of Energy

$$\frac{\partial}{\partial t}(\rho h) + \nabla . \rho h \mathbf{u} = \frac{Dp}{Dt} + \dot{q}''' - \nabla . \mathbf{q} + \mathbf{\Phi} \tag{2.3}$$

Equation of State for a Perfect Gas

$$p = \frac{\rho R T}{M} \tag{2.4}$$

This is a set of partial differential equations consisting of six equations for six unknowns, all are functions of three spatial dimensions and time: the density ρ, the three components of velocity $\mathbf{u} = (u, v, w)$, the temperature T, and the pressure p. The sensible enthalpy, h, is a function of temperature. Note that bold faced quantities represent vectors and bold faced quantity with the subscripts ij represent tensors.
The mass conservation equation is often written in terms of the mass fractions of the individual gaseous species

$$\frac{\partial}{\partial t}(\rho Y_i) + \nabla . \rho Y_i \mathbf{u} = \nabla . \rho D_i \nabla Y_i + \dot{m}_i''' \tag{2.5}$$

Summing these equations over all species results in the original mass conservation equation. This implies that the sum of the mass fractions $\Sigma Y_i = 1$, the sum of the production/loss rates $\Sigma \dot{m}_i''' = 0$, and the sum of the diffusion terms $\Sigma \rho D_i \nabla Y_i = 0$.

Numerical Scheme

The PDEs of conservation of mass, momentum and energy are approximated as finite differences and the the solution is updated in time on a three dimensional rectilinear grid. All spatial derivatives are approximated by second order finite differences and the flow variables are updated in time using an explicit second order predictor-corrector scheme.

Physical Models

Turbulence

FDS contains Large Eddy Simulation (LES) and Direct Numerical simulation (DNS). There is no Reynolds-Averaged Navier-Stokes (RANS) capability in FDS. LES is a technique

used to model the dissipative processes (viscosity μ, thermal conductivity k_{LES}, material diffusivity D) that occur at length scales smaller than those that are explicitly resolved on the numerical grid. The parameter μ, k_{LES}, D should be modelled. The dissipation function Φ in the energy equation is the rate at which kinetic energy is converted to thermal energy by viscosity. Following the analysis of Smagorinsky viscosity μ is modelled

$$\mu_{LES} = \rho(C_s\triangle)^2(2\bar{S_{ij}}.\bar{S_{ij}} - \frac{2}{3}(\nabla.\bar{u}))^{\frac{1}{2}}$$

where C_s is an empirical constant and $\triangle$ is a length on the order of the size of a grid cell. The bar above the various quantities denotes that these are the resolved or filtered values, meaning that they are computed on a numerical grid. The other diffusive parameters, the thermal conductivity and material diffusivity, are related to the turbulent viscosity by

$$\begin{aligned} k_{LES} &= \frac{\mu_{LES}c_p}{Pr} \\ (\rho D)_{l,LES} &= \frac{\mu_{LES}}{Sc} \end{aligned}$$

The Prandtl number Pr and the Schmidt number Sc are assumed to be constant for given scenario.

Combustion Model

Combustion is assumed to be mixing controlled. The chemical reaction rate is assumed to be infinitely fast that means when fuel and oxidizer are mixed, they are burnt immediately. All species of interest can be derived in terms of mixture fraction. The mixture fraction is a conserved quantity representing the fraction of material at a given point that is originated in the fuel stream. The relations between the mass fraction of each species and the mixture fraction are known as state relations. The state relations for the oxygen mass fraction provides the information needed to calculate the local oxygen mass consumption rate. The form of the state relation that emerges from classical laminar diffusion flame theory is a piecewise linear function. This leads to a flame sheet model, where the flame is a two dimensional surface embedded in a three dimensional space. The local heat release rate is computed from the local oxygen consumption rate at the flame surface, assuming that the heat release rate is directly proportional to the oxygen consumption rate, independent of the fuel involved.

FDS 5 implemented a methodology to describe incomplete combustion and flame extinction at large scale fire within the basic framework of mixture fraction. In order to account for local flame extinction as well as the production/destruction of CO, mixture fraction is decomposed into three components. Simplest possible two-step CO formation mechanism is assumed [25]:

$$\begin{aligned} Step1 : F + O_2 &\rightarrow CO + Other\ \ Products\ \ (i.e. H_2O\ \ and\ \ soot) \\ Step2 : CO + \frac{1}{2}O_2 &\rightarrow CO_2 \end{aligned} \tag{2.6}$$

There is a possibility that step 1 does not occur at all because fuel and oxygen can mix without burning. This could be considered step 0, along with steps listed above. These three steps demand the inclusion of three variables; one to account for the total unburned fuel present (step 0), one to account for the CO produced (step 1), and one to account for the CO that has oxidized to form CO_2 (step 2). Three variables are defined as

$$Z_1 = Y_F, Z_2 = \frac{M_F}{x^{'} M_{CO}} Y_{CO}, Z_3 = \frac{M_F}{x^{'} M_{CO_2}} Y_{CO_2} \tag{2.7}$$

where $x^{'}$ is the moles of CO formed per mole of fuel burned. M is molar mass and Y is mass fraction and subscript F represents fuel. Transport equations of these three variables are as follows:

$$\frac{DZ_1}{Dt} = \nabla .\ D\rho\nabla Z_1 - \frac{M_F \dot{m}''_{CO,1}}{x^{'} M_{CO}} \tag{2.8}$$

$$\frac{DZ_2}{Dt} = \nabla . D\rho\nabla Z_2 + \frac{M_F \dot{m}''_{CO,1}}{x^{'} M_{CO}} + \frac{M_F \dot{m}''_{CO,2}}{x^{'} M_{CO}} \tag{2.9}$$

$$\frac{DZ_3}{Dt} = \nabla . D\rho\nabla Z_3 - \frac{M_F \dot{m}''_{CO,2}}{x^{'} M_{CO}} \tag{2.10}$$

The source terms for the three equations cancel by design. Thus, the sum of the three components is the mixture fraction:

$$Z_1 + Z_2 + Z_3 = Y_F + \frac{M_F}{x^{'} M_{CO}} Y_{CO} + \frac{M_F}{x^{'} M_{CO_2}} Y_{CO_2} = Z \tag{2.11}$$

Assuming that water vapor and soot have yields that are fixed functions of CO and CO_2, the three quantities Z_1, Z_2, Z_3 can determine the individual mass fractions of N_2, O_2, CO, CO_2, H_2O and unburned fuel. The process via which species are extracted from mixture fraction (state relations) parameters is discussed in [25].

Transport equations are solved for the three components of mixture fraction. At each time step of calculation, individual mass fractions are extracted from the mixture fraction according to built in state relations. Then, an empirical criterion is used to decide whether or not step 1 can occur. If the temperature and the oxygen mass fractions of a given cell and that of its neighbours are too low to support combustion, then step 1 can not occur. The neighbor cells represent either the fuel or oxidizer stream of classical diffusion flame theory. The local flamibility criterion is based on the critical adiabatic flame temperature, as described by Beyler [20]. The criterion determines if the energy released by consuming maximum possible amount of oxygen can raise the local temperature above the critical flame temperature. If so then step 1 is not allowed. If the local condition is assumed to support combustion, step 1 depletes either fuel or oxygen, releasing the corresponding amount of energy and species into the grid cell, upto an empirically-based maximum value. This maximum value is based on two assumptions. First, a flame sheet cannot generate more than $200 kW/m^2$ of energy; second, numerical grid is resolved enough so that any grid cell is cut by only one flame sheet. The limitation of this simple extinction model is that it

is based on the conditions of oxidizer stream not the fuel stream. For any particular grid cell, an adequate oxygen supply in any of its neighboring cells automatically allows step 1 to occur. In reality, low temperatures and/or low concentrations of fuel may still lead to flame extinction. The step 2, the oxidation of CO occurs according to Z_2 to Z_3 conversion, using the source terms in Eq. 2.9 and Eq. 2.10. Conversion of CO is fast if any heat is produced in a grid cell from step 1. If no heat is produced in step 1, existing temperature is the final temperature of the grid cell. The rate of CO oxidation is computed through finite rate computation [23].

Radiation Model

Radiative heat transfer is included in the model via the solution of the radiation transport equation for non-scattering gray gas, and in some limited cases using a wide band model. The radiative transport equation for an absorbing or emitting and scattering medium is

$$\vec{s}.\nabla I_\lambda(x,\vec{s}) = -[\kappa(x,\lambda)+\sigma_s(x,\lambda)]I(x,\vec{s})+B(x,\lambda)+\frac{\sigma_s(x,\lambda)}{4\pi}\int_{4\pi}\Phi(\vec{s},\vec{s}')I_\lambda(x,\vec{s}')d\Phi \quad (2.12)$$

where $I_\lambda(x,\vec{s})$ is the radiation intensity at wavelength λ and $\vec{s}$ is the direction vector of the intensity, $\kappa(x,\lambda)$ and $\sigma_s(x,\lambda)$ are the local absorption and scattering coefficients, respectively, and $B(x,\lambda)$ is the emission source term. The integral on the right hand side describes the in-scattering from other directions. In the case of a non-scattering gas Eq. 2.12 becomes

$$\vec{s}.\nabla I_\lambda(x,\vec{s}) = \kappa(x,\lambda)[I_b(x) - I_\lambda(x,\vec{s})]$$

where $I_b(x)$ is the source term given by the Plank function. This section describes the radiation transport in the gas phase.
In practical simulation the spectral dependence can not be solved accurately. Instead, the radiation spectrum is divided into a relatively small number of bands and a separate radiation transport is derived for each band. The limits of the bands are selected to give an accurate representation of the most important radiation bands of CO_2 and water. The band specific radiation transport equations are now

$$\vec{s}.\nabla I_n(x,\vec{s}) = \kappa_n(x)[I_{b,n}(x) - I_n(x,\vec{s}], n = 1...N \quad (2.13)$$

where I_n is the intensity integrated over the band n, and κ_n is the appropriate mean absorption coefficient inside the band. The source term can be written as a function of blackbody radiation

$$I_{b,n} = F_n(\lambda_{min},\lambda_{max})\sigma T^4/\pi$$

where σ is the Stefan-Boltzmann constant. When the intensities corresponding to the bands are known, the total intensity is calculated by summing over all the bands

$$I(x,\vec{s}) = \sum_{n=1}^{N} I_n(x,\vec{s})$$

From a series of numerical experiments it has been found that six bands are usually enough.

The radiative transport Eqn. 2.13 is solved using techniques similar to those for convective transport in finite volume methods for fluid flow. The unit sphere is divided into a finite number of fixed angles in order to obtain discretized form of the equation. There are several limitations of the model. The absorption coefficient of the smoke laden gas is a complex function of its composition and temperature. Because of the simplified combustion model, the chemical composition of smoky gases, especially the soot content, can effect both the absorption and emission of thermal radiation. Additionally, the radiation transport is discretized via approximately 100 fixed angles. For targets far away from a localized source of radiation like a growing fire, the discretization can lead to a non-uniform distribution of the radiant energy. The problem can be lessened by the inclusion of more fixed angles but compromising computational time.

Solid Phase Model

Solid obstructions consist of multiple layers composed of multiple material components that can undergo multiple thermal degradation reactions are included in FDS. Each reaction forms a combination of solid residue, water vapor and fuel vapor.

The Heat Conduction Equation for a Solid

A one dimensional heat conduction equation for the material temperature, $T_s(x,t)$, is applied in the direction x pointing into the solid where $x = 0$ represents the surface.

$$\rho_s c_s \frac{\partial T_s}{\partial t} = \frac{\partial}{\partial x}(k_s \frac{\partial T_s}{\partial x}) + \dot{q}_s''' \tag{2.14}$$

The following section explains component average material properties, k_s and $\rho_s c_s$. The source term, $\dot{q}_s'''$ represents chemical reactions and radiative absorption:

$$\dot{q}_s''' = \dot{q}_{s,c}''' + \dot{q}_{s,r}''' \tag{2.15}$$

$\dot{q}_{s,c}'''$ is the heat production rate given by the pyrolysis models for different types of solids and fuels, $\dot{q}_{s,r}'''$ is the radiation absorption and emission in depth.

Component-Averaged Thermal Properties

The conductivity and volumetric heat capacity of the solid are expressed as

$$k_s = \sum_{\alpha=1}^{N} X_\alpha k_{s,\alpha}; \rho_s c_s = \sum_{\alpha=1}^{N} \rho_{s,\alpha} c_{s,\alpha} \tag{2.16}$$

N is the number of material components forming the solid. $\rho_{s,\alpha}$ is the component density

$$\rho_{s,\alpha} = \rho_s Y_\alpha \tag{2.17}$$

where ρ_s is the density of the composite material and Y_α is the mass fraction of material component α. The solid density is the sum of the component densities

$$\rho_s = \sum_{\alpha=1}^{N} \rho_{s,\alpha} \tag{2.18}$$

X_α is the volume fraction of component α

$$X_\alpha = \frac{\frac{\rho_{s,\alpha}}{\rho_\alpha}}{\sum_{\alpha'=1}^{N} \frac{\rho_{s,\alpha'}}{\rho_{\alpha'}}} \tag{2.19}$$

where ρ_α is the density of material α in its pure form. Multi-component solids are defined by specifying the mass fractions Y_α and densities $\rho_{\alpha'}$ of the individual components of the composite.

Pyrolysis Model

A pyrolysis model is implemented in FDS version 5 which describes how solid phase reactions and chemical source terms in the solid phase heat conduction equation, $\dot{q}'''_{s,c}$, are modelled [1]. This model has not been employed in this thesis, experimental heat release rate (HRR) has been used as model input in order to get mass loss rate from solid or other fuel. In this instances, the desired HRR is translated into a fuel mass flux $\dot{m}''_f$ at the given solid surface like at the cross-section of a burner:

$$\dot{m}''_f = \frac{f(t)\dot{q}''_{user}}{\Delta H} \tag{2.20}$$

A given heat release rate per unit area of fuel surface is $\dot{q}''_{user}$ and a time function t, usually a ramp $f(t)$, and a reaction enthalpy ΔH is generally used.

Convective Heat Transfer to Wall

The heat fluxes to a solid surface consists of gains and losses from convection and radiation. The radiative flux at the surface is obtained from the boundary condition for the radiation equation. In an LES calculation, the convective heat flux to the surface is obtained from combination of natural and forced convection correlations

$$\dot{q}''_c = h_c \triangle T; \quad h_c = max[C(\triangle T)^{\frac{1}{3}}, \frac{k_g}{L}.037Re^{\frac{4}{5}}Pr^{\frac{1}{3}}]$$

where $\triangle T$ is the temperature difference between the structure and the gas temperature, C is the coefficient for natural convection, L is the characteristic length related to the size of the physical obstruction, k_g is the thermal conductivity of the gas, and Reynolds Re and Prandtl Pr numbers are based on the gas flowing past the obstruction. Since the Reynolds number is proportional to the characteristic length L, heat transfer coefficient is weakly related to L. Therefore, L is taken to be 1 m for most calculations.

Thermal Boundary Conditions

Boundary condition on the front surface is

$$-k_s \frac{\partial T_s}{\partial x}(0,t) = \dot{q}_c'' + \dot{q}_r'' \tag{2.21}$$

If internal radiation is solved for a solid, the radiation boundary condition $\dot{q}_r''$ is not used. On the back surface, adiabatic boundary condition is used if back side is perfectly insulated. The back side boundary condition is similar to that of the front side, if the back surface is assumed to be open to ambient condition or to another part of the computational domain.

Boundary Conditions at Opening

Momentum equation has been simplified so that it can be solved numerically. Pressure term is decomposed as

$$\frac{\nabla \tilde{p}}{\rho} = \frac{\nabla \tilde{p}}{\rho_\infty} + \left(\frac{1}{\rho} - \frac{1}{\rho_\infty}\right) \nabla \tilde{p}$$

$\frac{(\vec{u})^2}{2} + \frac{\tilde{p}}{\rho_\infty}$ is defined as variable H. The pressure term in the momentum equation is to simplify the elliptical partial differential equation obtained by taking the divergence of the momentum equation

$$\nabla^2 H = -\frac{\partial(\nabla.\vec{u})}{\partial t} - \nabla.\vec{F}; \tag{2.22}$$

$$\vec{F} = -\vec{u} \times \omega + \left(\frac{1}{\rho} - \frac{1}{\rho_\infty}\right) \nabla \tilde{p} - \frac{1}{\rho}(\rho - \rho_\infty \vec{g} + \vec{f} + \nabla.\tau_{ij}) \tag{2.23}$$

The pressure on the left hand side (incorporated in variable H) is solved directly. The reason for decomposition of the pressure term is that the linear algebraic system arising from the discretization of Eq. 2.22 has constant coefficients and can be solved by a fast direct method that utilizes Fast Fourier Transforms. No flux or forced flow boundary conditions are specified by asserting that

$$\frac{\partial H}{\partial n} = F_n - \frac{\partial u_n}{\partial t} \tag{2.24}$$

where $\vec{F}_n$ is the normal component of $\vec{F}$ at the vent or solid wall and $\frac{\partial u_n}{\partial t}$ is the prescribed rate of change in the normal component of velocity at a forced vent. Initially the velocity is zero everywhere. At open external boundaries the pressure like term H is prescribed, depending on whether the flow is outgoing or incoming

$$H = (\vec{u})^2/2, \quad \text{outgoing} \tag{2.25}$$

$$H = 0, \quad \text{incoming}$$

The outgoing boundary condition assumes that the pressure perturbation $\tilde{p}$ is zero at an outgoing boundary and that H is constant along streamlines. The incoming boundary condition assumes that H is zero infinitely far away.

Fire Specification

HRR should be specified as input. This can be designated in two ways. First is to prescribe a heat release rate per unit area of burning material. The other is to prescribe the amount of energy required to vaporize a solid or liquid fuel once it has reached its ignition temperature. τ_q is defined as characteristic ramp up time of heat release rate per unit area. τ_q indicates that the thermal quantities are to ramp up to their prescribed values in τ seconds and remain there. FDS uses following functions to ramp up the heat release rate

- if $\tau_q > 0$ heat release rate ramp up like $\tanh(\frac{t}{\tau})$
- if $\tau_q < 0$ heat release rate ramp up like $(\frac{t}{\tau})^2$
- otherwise user can define burning history as input and a linear interpolation is used to fill in intermediate time points.

2.1.2 JASMINE

Jasmine is a fire specific CFD code developed by Fire Research Station in the United Kingdom in the past 20 years. It employs a finite volume method to solve the governing conservation equations of mass, momentum, heat and chemical species.

Numerical Scheme

Jasmine uses a structured, staggered, cartesian grid and SIMPLEST pressure correction algorithm, which is a modified form of the classic SIMPLE algorithm. For a typical smoke movement problem, the program solves transport equations for three velocity components, turbulent kinetic energy and its rate of dissipation, enthalpy, fuel mixture fraction and fuel mass fraction. The above mentioned equations are solved sequentially. A pressure correction scheme is then solved, satisfying the continuity equation and yielding pressure and updated velocity fields. The six-flux radiation equations are solved separately, with a coupling between enthalpy and the radiation field. The upwind interpolation scheme is employed in the discretization of the convection terms of transport equation. Diffusion terms are discretized by a central differencing scheme. Temporal advancement is by the first-order, fully implicit, backward Euler scheme. The pressure correction equation is solved in a fully three dimensional manner, while the set of transport equations are solved as a sequence of two-dimensional planes (slabs). Thus each transport equation is solved at the first slab, then the program proceeds to the second slab etc. At each slab, the linear system is solved for each transport equation by a plane relaxation algorithm, which is similar to Stone's strongly implicit procedure.

Physical Models

The physical models employed in Jasmine are described briefly in the following chapter.

Turbulence

$k-\varepsilon$ model with buoyancy modification is used for turbulence modelling. Turbulent mixing in a rising plume is enhanced by buoyancy while in a stable stratified layer, it will be inhibited. The production term in the k equation associated with the buoyancy forces can be expressed as

$$G_B = -\beta_g \frac{\mu_t}{\sigma_t} \frac{\partial T}{\partial x_j} \tag{2.26}$$

It takes opposite signs in regions of stable and unstable stratification. This term, which describes the exchange of turbulent kinetic energy with potential energy, represents a source in the unstable situation of the fire plumes, where heated gases emerge beneath cool gases, but it becomes a sink in the hot gas ceiling layer, where the opposite occurs.

Combustion

Two options are provided for combustion modelling. In both cases, the process of turbulent combustion is described by a one-step simple chemical reaction where complete oxidation of the fuel is assumed, producing carbon dioxide and water vapor. The one step reaction may be written as

$$fuel + s\ (oxygen) = (1+s)\ combustion\ products \tag{2.27}$$

where s is the stoichiometric oxygen to fuel ratio.

The options are as follows:

- Flame sheet or mixture fraction combustion model: The assumptions of flamesheet model are as mentioned in section 2.1.1.
- Eddy break-up model: The mean reaction rate (R_{fu}), a sink term in the transport equation for m_{fu}, is here controlled by the turbulent mixing of fuel and air, and is given by

  $$R_{fu} = C_R \rho \frac{\varepsilon}{k} min(m_{fu}, \frac{m_{O2}}{s}) \tag{2.28}$$

  The specific heats of individual components (fuel, oxidant, products) are allowed to vary and the heat release is represented either by a balance between heat of formation or by a heat of reaction. Additional transport equations are solved for mixture fraction, fuel mass fraction and enthalpy. These equations are based on the scalar transport equation with modified source terms: mixture fraction-source equal to zero, fuel mass fraction-source equal to rate of fuel consumption given by Eddy break up model, enthalpy equation-source includes the net energy absorbed or emitted by radiation and the rate of heat released is prescribed by the eddy breakup combustion model.

Thermal Radiation

The process of thermal radiation in the gas phase is modelled by a six flux method. The differential transport equation for radiative flux, in the three co-ordinate cartesian directions,

is discretised on the CFD numerical grid. This assumes that radiant transfer is normal to the co-ordinate directions, ignoring the angular dependence of radiant intensity. The six-flux method is suited to the task of calculating radiant heat transfer from stratified hot layers, but it is not appropriate for tasks such as surface flame spread calculations. Here the angular dependency of radiataion intensity is very important for the accurate prediction of the radiative heat transfer to combustible fuels ahead of a spreading flame front. The discrete transfer radiation model would be more appropriate for this purpose.

Boundary Layer Heat and Momentum Transfer

This section describes the model used in JASMINE to calculate the transfer of heat (convected and radiated) to solid surfaces, the temperature of solid surfaces, the momentum losses in the boundary layer next to solid surface. Standard wall functions for enthalpy and momentum are used to describe the turbulent boundary layer adjacent to solid objects.

- The turbulent boundary layer

  The one dimensional description of the turbulent boundary layer uses a non dimensional (tangential) velocity, u^+ and a non-dimensional (normal) distance to surface, y^+

  $$u^+ = \frac{U}{u_\tau} \tag{2.29}$$

  $$y^+ = \frac{\rho y u_\tau}{\mu} \tag{2.30}$$

  Where U is the tangential velocity at a distance y and u_τ is the friction velocity, defined as

  $$u_\tau = \sqrt{\frac{\tau_w}{\rho}} \tag{2.31}$$

  where τ_w is the wall shear stress.

  Jasmine computes y^+ at each node adjacent to a solid boundary, and from this value categorises the local flow regime. Generally, the turbulent boundary layer can be split into laminar, viscous sublayer closest to the wall ($y^+ < 5$), an integral log-law sublayer ($30 < y^+ < 400$) where the flow is fully turbulent but where the shear stress can be considered uniform and between them ($5 < y^+ < 30$) a region of transition between laminar and turbulent flow. A laminar or turbulent flow calculation is performed at each near-node, depending on the value of y^+, and the appropriate momentum, turbulence and enthalpy source terms are prescribed for the cell. No wall source terms are prescribed if the node is in the outer layer. These source terms are described briefly below (momentum, turbulence and convection).

- Momentum loss

  Momentum loss is related to the wall shear force at a cell face, F_s, where

  $$F_s = -\tau_w A_c \tag{2.32}$$

where A_c is the area of the cell face. The momentum loss is translated to a sink in the Navier-Stokes equations. The wall shear stress is given by

$$\tau_w = \frac{\rho U^2}{(u^+)^2} \tag{2.33}$$

In the linear region this reduces to

$$\tau_w = \frac{\mu U}{y} \tag{2.34}$$

while the log-law region τ_w is calculated after using the following expression for u^+

$$u^+ = \frac{1}{\kappa} ln(1.01 + Ey^+) \tag{2.35}$$

where κ is the von Karman constant (0.4187) and E is a surface roughness related parameter (9.793 for smooth surface).

- Turbulence values

  Near node values for k and ε are prescribed on Jasmine, subjected to being in the log-law region, as follows,

$$k = \frac{(u_\tau)^2}{\sqrt{c_\mu}} \tag{2.36}$$

$$\varepsilon = \frac{(u_\tau)^3}{\kappa y_p} \tag{2.37}$$

- Convective heat transfer

  The convective heat flux per unit area to a solid boundary is defined as

$$\dot{q}_c'' = h_c(T_P - T_w) \tag{2.38}$$

  where h_c is the convective heat transfer coefficient. Jasmine allows three options for computing h_c, a) a fixed value, b) a prescribed function of surface temperature and c) boundary layer analysis. Having selected a boundary layer analysis, the form that h_c takes, depends whether the near node is in the linear or log-law region (no heat transfer occurs within the outer region)

$$linear : h_c = \frac{\mu c_p}{\sigma_{h,l} y_P} \tag{2.39}$$

$$log - law : h_c = \frac{\sqrt{\rho}\sqrt{\tau_w} c_p}{T^+} \tag{2.40}$$

  where $\sigma_{h,l}$ is the laminar Prandtl number (0.707) and T^+ is defined as

$$T^+ = \sigma_{h,t}(u^+ + P_j) \tag{2.41}$$

  where $\sigma_{h,t}$ is the turbulent Prandtl number (generally set in the range 0.7 to 0.9) and

P_j is the so called pee-function value for the particular solid material.

- Radiated heat transfer

  In the six-flux model, the radiated heat flux per unit area is defined as

$$\dot{q}_r'' = \frac{2\varepsilon_w}{2-\varepsilon_w}(F - \sigma T_w^4) \tag{2.42}$$

  where ε_w is emissivity of the boundary surface, σ is the Stefan-Boltzmann constant and F is the net flux in the direction normal to surface. In the absence of the six flux model the radiated heat flux may be approximated as

$$\dot{q}_r'' = \sigma(T_p^4 - T_w^4) \tag{2.43}$$

Fire Specification

One of the main inputs to fire growth and smoke movement models is the heat release rate which defines the fire size and its growth. Experimental heat release rate versus time data can be used in Jasmine as input for a specific fire. In addition, four different options of specification of heat release rate are included in Jasmine

- Constant heat release rate: A single rate is used over the specified time interval
- linear variation of heat release rate: Heat varies linearly between the first and last time step.
- An exponential variation: The rate varies exponentially over the given time step.
- The fire doubling time: This option allows the user to provide a time interval over which heat release rate doubles.

Options	Expression	Jasmine input
Constant heat release	$\dot{Q} = constant$	$\dot{Q}_{const}$
Linear variation	$\dot{Q} = tC_1 + C_2$	C_1, C_2
Exponential variation	$\dot{Q} = \dot{Q}_0 \exp \alpha t$	$\dot{Q}_0, \alpha$
Fire doubling time	$\dot{Q} = \dot{Q}_0 \exp t/t_{double}$	$\dot{Q}_0, t_{double}$

Boundary Conditions

Although boundary conditions depend on the problem of concern, some common conditions are explained here. Those for momentum equations at solid boundaries have been outlined above. Naturally ventilated fires, though entrained air from the surrounding environment driven by pressure differences caused by the fires buoyant acceleration. It is thus necessary to represent an infinite physical region in the finite computational domain. This is generally achieved by taking the computational boundary far away from the region of the primary flow. The pressure is fixed at this plane while velocity derivatives normal to the boundary are set to zero. At this free boundary, at points of outflow, the derivatives of scalar fields are set to zero while at points of inflow, ambient conditions are specified. Heat will be

lost from the fire into the structure at a rate determined by both thermal properties of the bounding walls and time. Assuming a solid boundary is a semi-infinite, implying a thickness greater than the thermal penetration depth, the expression for the penetration depth takes the form

$$\delta = 2\sqrt{\frac{k_s t}{c_s \rho_s}} \tag{2.44}$$

where k_s, c_s, ρ_s are the thermal conductivity, specific heat and density of solid respectively. The item t is either the true transient time or a user prescribed 'time to steady state' value. The surface temperature is then calculated by balancing the convected and radiated fluxes with the conducted flux into the solid. This balance equation is, in general, nonlinear with respect to the surface temperature T_w and therefore solved iteratively.

2.1.3 SOFIE

Sofie is a finite volume based CFD model developed under the umbrella of a consortium including a number of European fire research laboratories: BRE, Technical Research Center of Finland, Swedish National Testing and Research Institute, CSTB, Lund University, Health and Safety Laboratory, Home Office Fire Safety Engineering Group. This consortium was initiated at Cranfield University.

Numerical Scheme

Sofie has been written in a general non-orthogonal coordinate system, where the velocity vector is represented in the terms of its cartesian components and the Navier-Stokes equations are solved in a general coordinate system. The governing transport equations are expanded in terms of the orthogonal and and non-orthogonal contributions. When a Cartesian grid is employed, the non-orthogonal and curvature related terms equate to zero. The transport equations are discretized by integrating the respective equations over a control volume and using an interpolation scheme to evaluate the values of variables on the faces of each control volume. Sofie incorporates a number of interpolation scheme called upwind, hybrid, second order upwind (SOUP), QUICK and TVD in order to determine the value of the dependent variable at a cell face. Sofie employs a SIMPLEC pressure correction scheme. It uses TDMA/Bilinear/ILU/IC PCCG/SIP solvers. Transient solution is performed through first order fully implicit approach. Details can be obtained in [5].

Turbulence Model

$\kappa - \varepsilon$ turbulence model with buoyancy modifications is used. Boundary conditions for turbulent flow are imposed using a conventional high Reynolds number wall function approach in which wall shear stress is approximated by fitting an empirical log-law expression across the near wall boundary layer.

Combustion Model

Sofie provides two options of combustion model namely Eddy Break Up model and Flamelet model. Sofie employs standard form of the Eddy Break Up model, with no Arrhenius terms included. The rate of combustion is assumed to be controlled by the minimum of the rate at which oxidant or fuel arrives through turbulent mixing at the combustion site.

$$R_{fu} = -\rho\frac{\varepsilon}{k}min(c_f m_{fu}, \frac{c_o m_{o2}}{s}, \frac{c_p m_p}{1+s}) \tag{2.45}$$

In the above expression, s is the stoichiometric oxygen to fuel ratio and m_{fu}, m_{o2}, m_p are the mass fractions of fuel, oxidant and products, respectively. Standard values of the constants (c_p, c_0, c_f) are employed.

The specific heats of individual components (fuel, oxidant, products) are allowed to vary and the heat release is represented either by a balance between heats of formation or by a heat of reaction. Additional transport equations are solved for mixture fraction, fuel mass fraction and enthalpy. These equations are based on the scalar transport equation with modified source terms: mixture fraction-source equals zero, fuel mass fraction-source equal to rate of fuel consumption given by Eddy Break Up model, enthalpy equation -source includes the net energy absorbed or emitted by radiation and the rate of heat released is prescribed by the Eddy Break Up combustion model.

Heat Transfer

Heat transfer to and within solid boundaries utilizes the conjugate heat transfer approach with temperature dependent material properties. Conjugate heat transfer describes a procedure for computing the temperature and heat transfer at the gas solid interface due to Patankar [58]. The method determines the temperature field within both fluid and solid by solving the convection-conduction problem throughout the domain of interest. Since there is no fluid flow inside the solid, solution of energy equation reduces to a pure conduction problem. In the resulting solution, the temperature field in the gas and solid is automatically matched at the interface and the heat transfer rate can be obtained. Heat transfer to solid boundaries is modelled via a predicted heat transfer coefficient for convection and a defined emissivity for radiation. Heat transfer from external walls is modelled by prescribing an ambient temperature and an external heat transfer coefficient. Convective heat transfer coefficients are predicted using a modified wall function approach

$$T^+ = \frac{(T_p - T_w)C_p\rho\mu_t}{q_w} = \sigma_{h,t}[u^+ + P_j] \tag{2.46}$$

with T_p equal to the temperature at near wall point y_p, T_w is the wall temperature and q_w is the wall heat flux. The function P_j is the pee-function.

$$h_c = \frac{q_w}{T_p - T_w} = \frac{C_p\rho\mu_t}{T^+} \tag{2.47}$$

$$C_p = \frac{c_p}{y_P \rho} \tag{2.48}$$

Radiation Model

Discrete transfer radiation (DTR) model is used. This model is particularly well suited to coupled flow and heat transfer calculations in arbitrarily shaped geometries. This is because it is superimposed, without modification, upon the CFD grid, and because boundary conditions are easily incorporated. It utilizes features of the zone, flux, and Monte Carlo methods by tracing rays of electromagnetic radiation through the computational domain between boundaries. Radiation transfer is based on a deterministic ray tracing approach using DTR model with incorporation of soot effects via non-adiabatic laminar flamelets together with appropriate weighted sum of grey gas representations of the absorption-emission characteristics of the participating media. Soot distributions are described either by convection of a conserved scalar or by modelling the formation and oxidation according to simple rate equations or via laminar flamelets.

Flame Spread

The main empirical parameters of the flame spread model are the critical accumulated flux, $E_{critical}$, which determines the time to ignition, and an effective heat of gasification parameter which governs the rate of production of volatiles. In computing the accumulated flux, a minimum critical incident heat flux, below which no ignition will occur ($\dot{q}_{min}$), is also included.

$$E_{critical} = \int_0^{t_{ignition}} \dot{q} dt = \sum_0^{t_{ignitiont}} max(\dot{q}_{net} - \dot{q}_{min}, 0) \triangle t \tag{2.49}$$

where t is time, $\triangle t$ is the simulation time step and $t_{ignition}$ is the time to ignition. Other parameters required by the flame spread model are the densities of virgin material and char, the thickness of combustible, the ignition temperature which sets the temperature of any volatiles released and finally two empirical factors which characterize the shape of the heat release curve during pyrolysis.

Boundary Conditions

Solid wall (with wall functions), zero gradient outflow, fixed value inflow, fixed static pressure can be used as fluid boundary conditions. Isothermal, fixed heat flux, fixed external heat transfer coefficient, conjugate heat transfer and semi-infinite solid can be used as heat transfer boundary conditions.

TABLE 2.1
Fire Models Comparison

Models	FDS	Jasmine	SOFIE
Numerical Algorithm	Explicit predictor corrector scheme, second order accurate in time and space	Upwind discretization, first order fully implicit scheme transient	Upwind Hybrid, Power law, QUICK, SOUP, TVD, first order fully implicit scheme transient; Dynamic memory allocation at run time
Discretization	FDM	FVM	FVM
Turbulence	LES with buoyancy modification	$k-\epsilon$ with buoyancy modification	$k-\epsilon$ with buoyancy modification
Combustion Model	Mixture fraction	Flame sheet, Eddy Break Up	Flamelet, EDC
Radiation	Radiation transport equation for non scattering gray gas	Six flux Model, DTR model coupled with Truelove grey gas model for emissive model	DTR model, gaseous radiative property model
Fire growth	model input	model input	model input
Fire Spread	Pyrolysis /solid combustion model	no model	Cumulative flux model

TABLE 2.2
Fire Models Comparison (continued)

Models	FDS	Jasmine	SOFIE
Soot production	Over Simplified empirical model. Fuel is being burned with constant yields of soot, no growth, oxidation or after burning, valid for well ventilated fire	no model	Heptane chemical kinetics is utilized to include nucleation, coagulation and surface growth of soot. Includes the effect of radiative loss on soot formation rate by means of fully coupled calculations based on flamelet libraries
Toxic Model	CO formation model which input is CO and soot yield from well ventilated post-flame measurements	no implemented model	no implemented model
Visualization	PLOT3D format	PLOT3D format	Structured data output in PLOT3D format
Programming language	Fortran 90/C	Fortran /C	Fortran 77/90

2.1.4 Fire Models Comparison

Main features of the above mentioned CFD fire models are enlisted in Tables 2.1 and 2.2. One type of physical or chemical submodels may better predict the relevant phenomena in fire than another type. For instance LES model allows more direct computation of the turbulence field to be performed than $k-\varepsilon$ model. It is still under investigation whether LES or $k-\varepsilon$ is best suited for fire modelling. Similarly, Discrete Transfer Radiation (DTR) model overcome problems encountered in six-flux model which is unable to handle radiation transfer at angles oblique to the Cartesian grid. The fast chemistry approach (Mixture fraction or Flamesheet model) to combustion is generally used for fire modelling. However, an Eddy Break Up (EBU) model has become a more popular choice recently [62]. Fuel mass fraction serves as a second variable along with mixture fraction in the EBU model. Since none of the models utilizes detailed chemical kinetics of combustion. These models are not capable of modelling underventilated fires reasonably. FDS contains a more detailed pyrolysis model while Sofie uses a very simple empirical model for fire spread (see Sec.2.1.1 , 2.1.3). Considering sophistication of individual physical models, Sofie, Jasmine and FDS may have advantages over one another. These models are compared based on local transient temperature prediction capability and required computational time.

2.1.5 Simulations with Jasmine

The fire literature contains comparisons of simulations with Jasmine with experimental data [36, 37, 24, 39, 60, 43] in different cases. This is always recommended to validate a specific fire scenario of interest in order to further proceed with the model for desired purpose. A test case has been simulated which is explained in the following section.

Test compartment

The experiments were performed in a 500 m^3 compartment, built in VTT, Finland [55]. Test compartment layout and dimensions are shown in Fig.2.1. The walls of the test compartment were made of 2 mm thick steel with fiberglass insulation. Ceiling material was 2 mm thick steel without insulation and floor of the compartment was made of concrete. One ventilation opening of size $2m \times 2m$ was left open during the experiments. A wood crib was used in the experiments as fire source. The construction of the wood crib is shown in Fig.2.2.

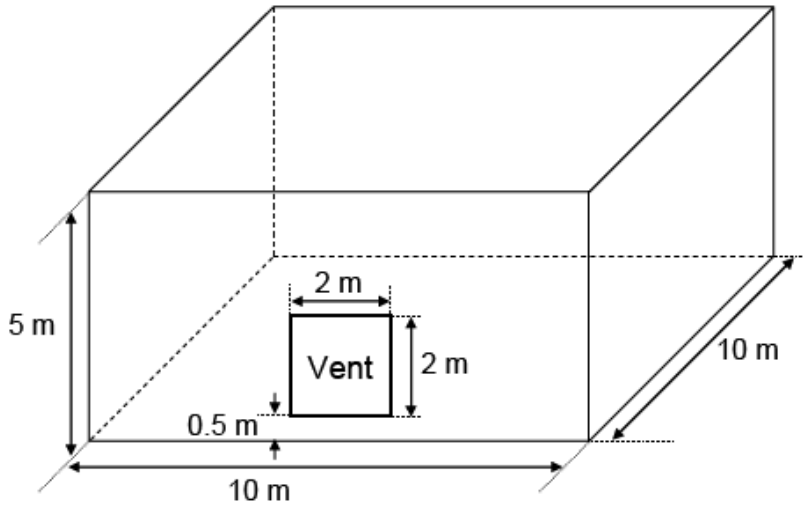

FIGURE 2.1 Test compartment used in experiments [55]

Simulations

Simulations have been performed using Jasmine version 3.23d CFD fire models which includes the internal room and the external surrounding environment outside the opening. The free pressure boundary condition is applied on the extended domain boundary where conditions were assumed to be ambient. For opening, boundary conditions have been applied as described in section.2.1.2. The geometry of the compartment has been modelled using 111020 ($61 \times 65 \times 28$) grid cells or in other words, 0.18 m uniform grid cell size has been used. 1 s time step has been used and 6 days on a 2.21 GHz AMD Athlon 64 processor were needed for 1200 seconds simulation time. Fire source has been modelled as five burning surfaces like a cube without bottom. Submodels used for the simulation are listed

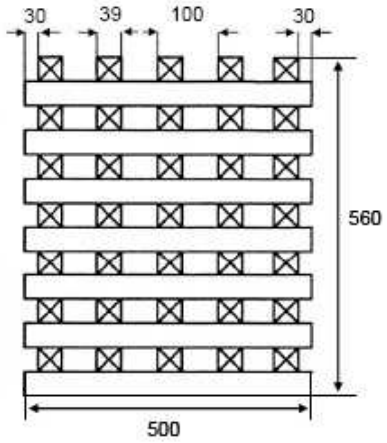

FIGURE 2.2 Wood crib used in experiments, units in mm
[55]

in Table 2.3. Janaf specific heat coefficients for gas properties and database fuel properties of Jasmine have been utilized. Experimental heat release rate (HRR) curve is shown in Fig. 2.3. The curve has been used as input for Jasmine.

TABLE 2.3
Submodels used in simulation by Jasmine

Phenomena	Submodel used
Turbulence	$k-\varepsilon$
Combustion	Eddy Break Up
Radiation	Six-flux
Heat transfer	General wall function

Temperature profile at different heights (x=5 m, y=7.5 m) are shown in Fig. 2.4–2.7. These comparisons of the Jasmin simulations with experimental data show an overprediction of temperatures in all cases. Results are reasonable at the height of 4.5 m and 3.5 m whereas close to the fire plume the prediction is not satisfactory. Simulations fail to predict temperatures reasonably at the steady growth stage of fire. There could be several possible reasons for such discrepancy other than numerical diffusion:

- The simplified combustion model assumes fast chemistry approach which leads to overprediction of temperatures.
- DTR model may lead to better prediction than six-flux model. DTR model requires more computational resources than the six-flux model.
- Experimental uncertainty near to fire flame as well as radiation from the thermocouple during measurement may result in errors of the experimental data.

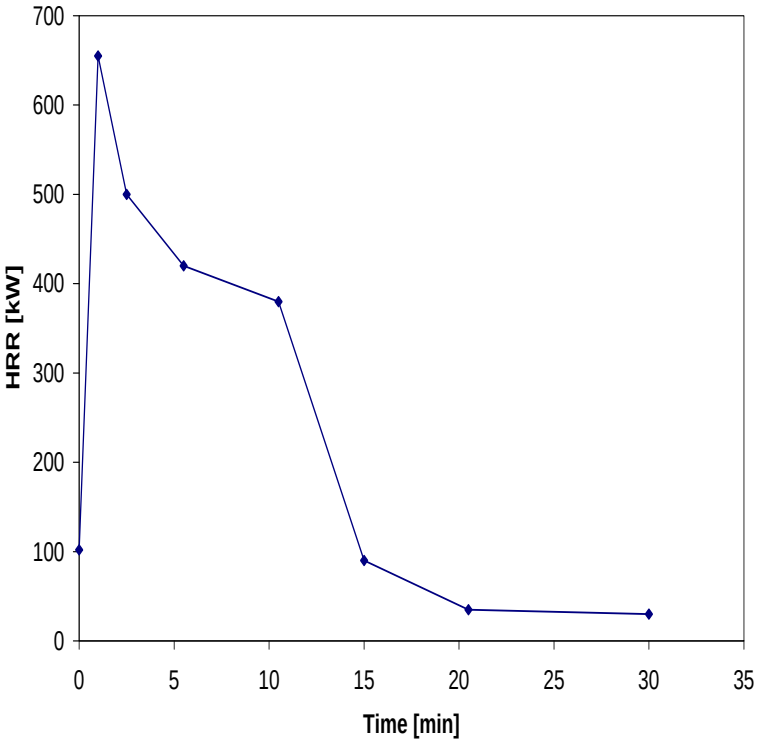

FIGURE 2.3 Heat Release Rate curve for the test

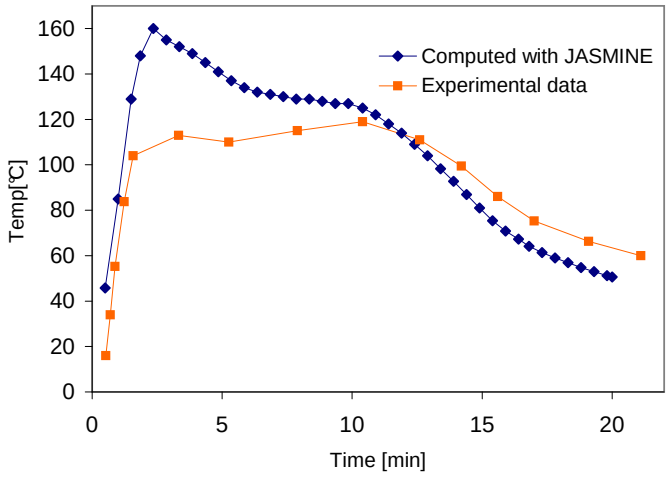

FIGURE 2.4 Transient temperature at location (5 m, 7.5 m, 4.5 m) simulated with Jasmine compared to experimental data

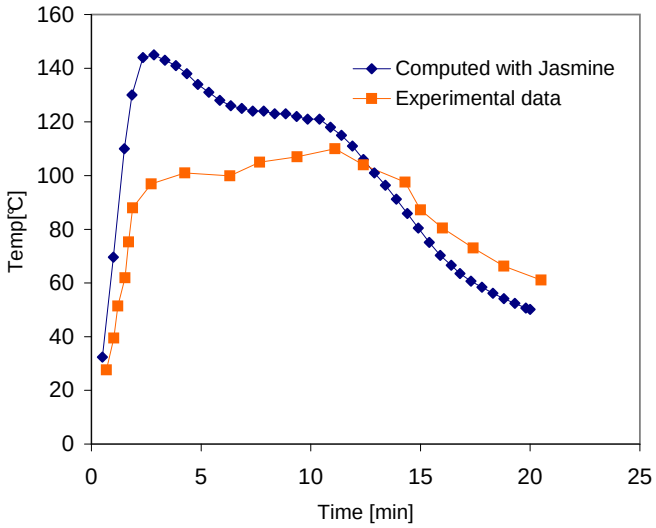

FIGURE 2.5 Transient temperature at location (5 m, 7.5 m, 3.5 m) simulated with Jasmine compared to experimental data

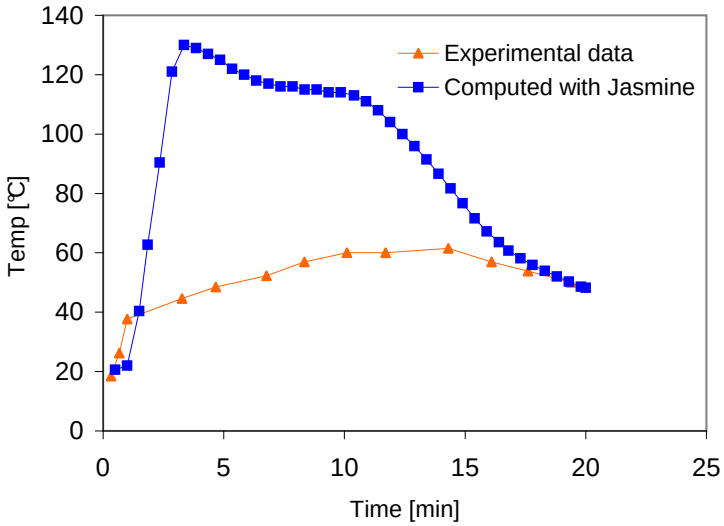

FIGURE 2.6 Transient temperature at location (5 m, 7.5 m, 2 m) simulated with Jasmine compared to experimental data

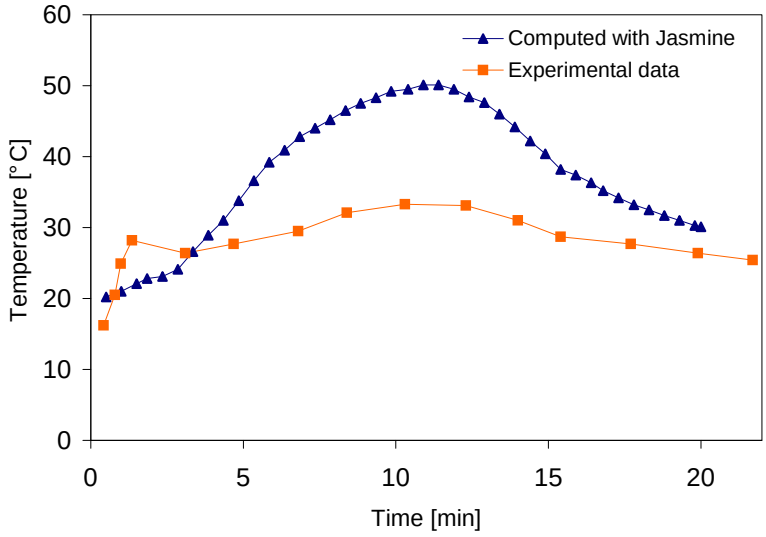

FIGURE 2.7 Transient temperature at location (5 m, 7.5 m, 0.5 m) simulated with Jasmine compared to experimental data

Discussion

Generally, simulation results are sensitive to the grid when cell size is relatively coarse but should independent of grid when cell size is fine enough. To examine the sensitivity related to grid cell size three different numerical test cases have been conducted each using uniform grid cell size of 0.35 m ($37 \times 39 \times 21$), 0.18 m ($61 \times 65 \times 28$) and 0.1 m ($112 \times 123 \times 55$) for 5 minutes. The boundary conditions and submodels used have been kept the same for these simulations like for the simulation as explained in the previous section. Fig. 2.8 shows the comparison of the predicted temperatures at the location of $(5m, 7.5m, 4.5m)$ to experimental data for different cell sizes. Simulation with 0.35 m cell results in an unstable solution. The simulation results are closer to the experimental data with smaller cell size (O.18 m). Simulation with 0.1 m which is expected to provide better prediction, needs large computational time and processor speed. Simulation with 0.1 m cell has been run and estimated finish time was more than a month for only a 5-minute fire simulation. Usually such long computational time is not feasible for fire modelling. It should be noted that Jasmine does not have parallel computation option.

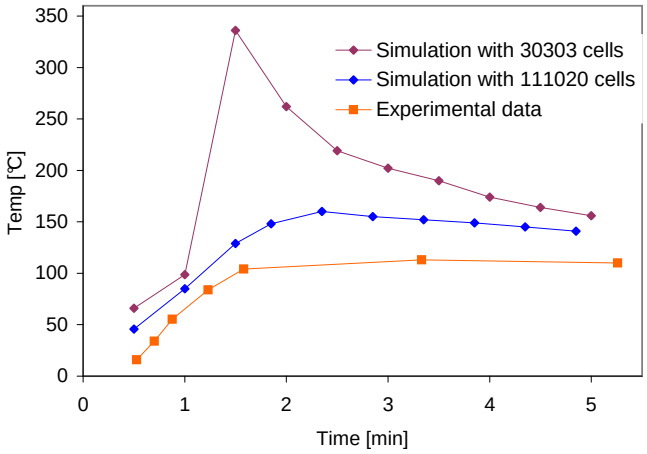

FIGURE 2.8 Grid sensitivity of the simulation

2.1.6 Simulations with SOFIE

The same test cases as described above have been simulated with SOFIE using 0.18 m grid size on the same processor. 7 days computing time were required for 1200 s simulation. Simulation with smaller grid size was not possible with the used processor due to the lack of memory allocation. Built in $k-\varepsilon$ turbulence model, Eddy Dissipation Combustion model and DTR radiation model were used for the simulation. Pyrolysis model was not used. Instead of such pyrolysis models, experimental HRR data as a function of time (see Sec. 2.3) were used as model input like Jasmine and FDS simulations.

2.1.7 Simulations with FDS

The test case simulated with Jasmine and Sofie was also simulated with FDS. 0.18 m, 0.10 m and 0.05 m uniform grid cells have been used for 20 minute-fire simulations with the same processor. The first and second case needed about 20 hours and 6 days computational time respectively. The latter case failed to run due to memory allocation failure.

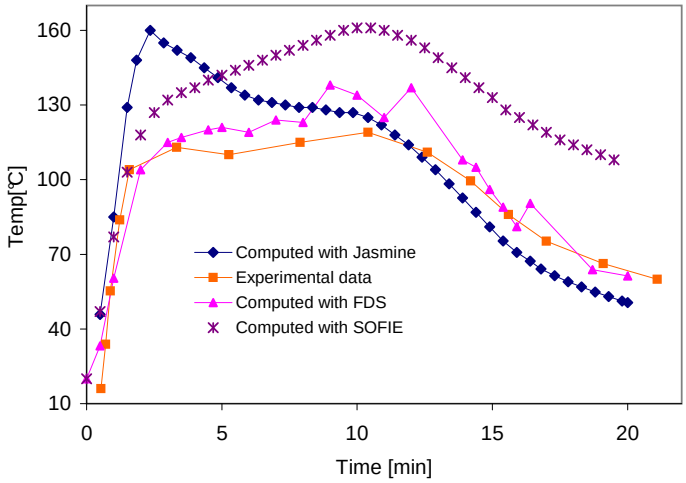

FIGURE 2.9 Transient temperatures at location (5 m, 7.5 m, 4.5 m) simulated with Jasmine, Sofie and FDS compared to experimental data

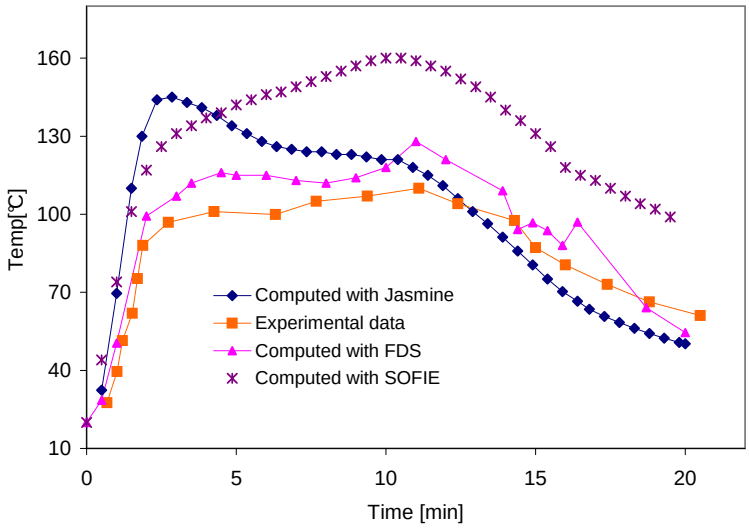

FIGURE 2.10 Transient temperatures at location (5 m, 7.5 m, 3.5 m) simulated with Jasmine, Sofie and FDS compared to experimental data

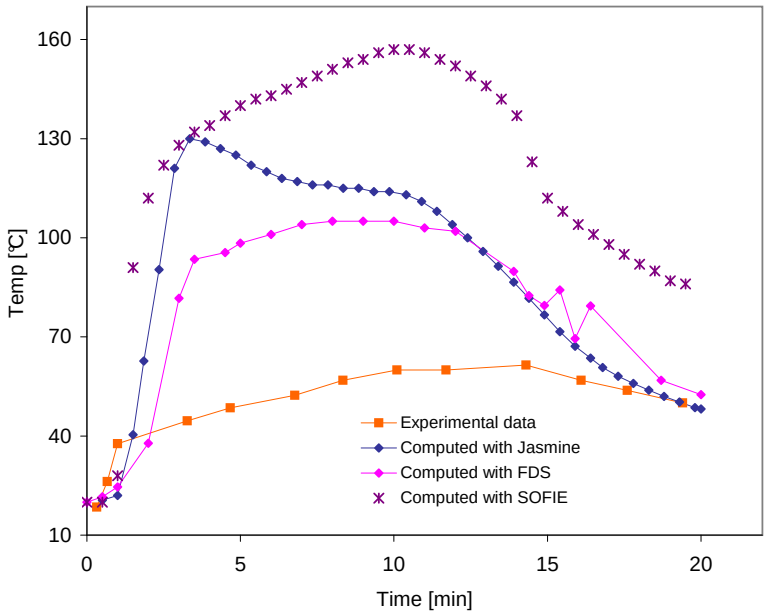

FIGURE 2.11 Transient temperatures at location (5 m, 7.5 m, 2 m) simulated with Jasmine, Sofie and FDS compared to experimental data

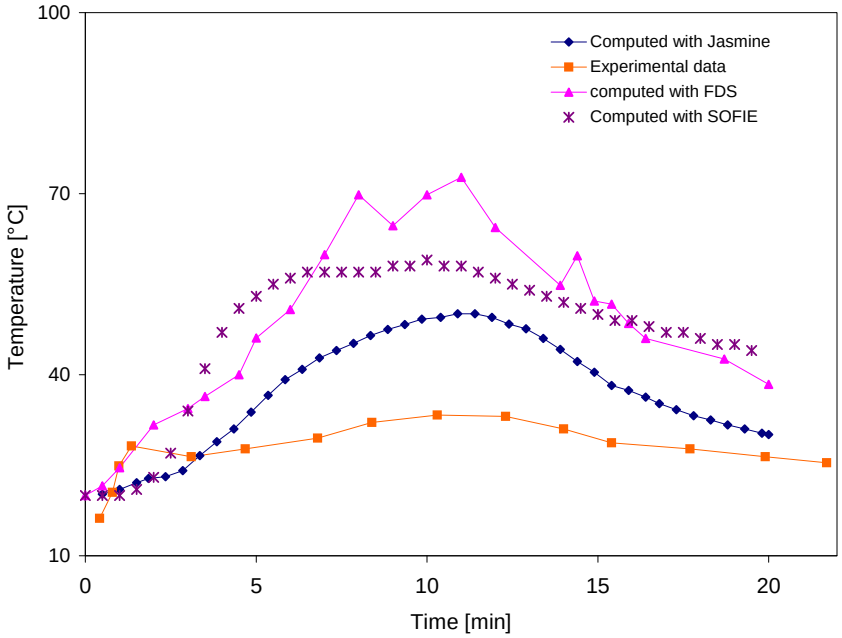

FIGURE 2.12 Transient temperatures at location (5 m, 7.5 m, 0.5 m) simulated with Jasmine, Sofie and FDS compared to experimental data

Discussion

Figure 2.9, 2.10, 2.11 and 2.12 represent the results of the simulations compared to experimental data. 0.18 m uniform grid size is used. Local transient temperature prediction is used to compare between the CFD models predictions and experimental data. Considering the discrepancy of the predictions, FDS predicts the temperature profile relatively better compared to others except at the location (5 m, 7.5 m, 0.5 m) while spending almost same computational time and resources. Temperature prediction is not reasonable close to the fire flame at the height of 2 m and 0.5 m for all these models. The reason for this discrepancy may lie in utilizing fast chemistry assumption of the combustion models. All the combustion models of these CFD softwares account for complete combustion whereas in fires underventilated conditions prevail with incomplete combustion. In order to get precise predictions, detailed chemical kinetics of combustion is required and smaller length and time scales are needed to be resolved for combustion processes with detailed kinetics. This takes enormous computational time. Therefore, the mixture fraction model is utilized with Large Eddy Simulation (LES) and coarse grids, which are not fine enough to resolve the diffusion of fuel and oxygen. However, detailed kinetics implementation is not feasible for large scale problems of the fire safety community [1]. Apart from this, chemical kinetics of most of the burning materials is beyond the state of the art of fire research.

Ignoring significant elementary reaction steps leads to errors in local combustion heat release rate. Additionally, detailed experimentation is required to improve our understanding of underventilated burning conditions. Other physical models (turbulence, radiation etc.) may also contribute to the discrepancies of individual predictions of CFD models. For instance, FDS uses LES simulation for turbulence modelling while Jasmine and SOFIE use $k - \varepsilon$.

2.2 Toxicants formation in enclosure fire

2.2.1 Experimental results

During the past few years, a number of computer programs have been developed which are designed to estimate the life-safety hazards associated with enclosure fires. A major limitation of such models is that the production rates of molecular species as a function of fuel-loss rate are needed as input parameters. The understanding of the mechanism responsible for the formation of CO and other toxic species in fires is far too limited to allow accurate predictions of the generation of these species. This is particularly true with regard to extremely intense fires, where such high generation rates of gaseous fuel occur (either directly as gas, vaporized liquid, or pyrolized solid) that the fire becomes underventilated. Temperatures are usally high, and such fires tend to be "flashed over" [50]. A major step in the understanding of CO formation in enclosures fires has been performed through experiments in the last 30 years. The most important finding of these studies is that major chemical species can be correlated in terms of the Global Equivalence Ratio (GER). This concept indicates the generation rates of combustion species are a function of GER

which generally underpredicts the amount of CO formed in the underventilated enclosure fire. Some findings reveal that CO formation also depends on upper layer temperature in compartment fires.

Hood experiments [15, 19] allow detailed measurements of species concentrations in the upper layer. Beyler was the first to attempt to correlate his measurements of gas concentrations in the upper layer with the GER. He studied a variety of solid, liquid and gaseous fuels. By varying the fuel, Beyler demonstrated that the product concentrations were fuel dependent, but that data for a range of fuels supported the GER concept. The major conclusions of Beyler's work can be summarized as [49]:

- Major flame species including CO can be correlated with GER
- Relatively constant concentrations of CO are observed at low (< 0.5) and high (> 1.3) GER.
- The generation of CO under rich conditions is considerably greater than for fuel-lean conditions.
- The concentrations of CO generated for rich conditions are fuel dependent, but can be correlated with fuel structure. Oxygen containing fuels generate the highest CO levels while thermally stable fuels, such as toluene, generate the lowest. Hydrocarbon fuels fall in the middle.

Several different hood experiments have been performeed by Toner and Morehart [34]. They also observed species concentrations in terms of GER. Unfortunately, Morehart's results revealed a new uncertainty concerning the GER concept. His results showed systematic differences between his measurements of the products of incomplete combustion and those of Toner. Morehart concluded that the variations were real and were the result of differences in layer temperatures between the two experiments.

Morehart tried to address the temperature effect by performing detailed chemical-kinetic calculations of a plug-flow reactor for a rich mixture typical of his upper layer. The calculations showed that such a mixture becomes reactive for temperatures greater than 700 K in agreement with his experimental findings, but that the calculated changes in upper-layer composition were not consistent with the differences between the Toner and Morehart experiments. Pitts [49] has reported similar calculations using the experimental concentrations of combustion gases observed by Morehart as starting concentrations. Calculations were performed over a range of temperatures (700 - 1300 K), GER (0.5-2.83) and residence times (0 - 20 s). Effects of mixing behavior and heat loss variation were investigated by considering possible extremes: infinitely fast (perfectly stirred reactor model) and infinitely slow (plug flow reactor model) mixing models and by considering conditions for which the reactor temperature was held constant by allowing heat transfer to or from the reactor surroundings (isothermal case) and adiabatic case. Briefly, codes provided by the combustion research facility of the Sandia National Laboratory were used, a series of Fortran based subroutines known collectively as CHEMKIN form the basis of the calculations. Sandia also provided "drivers" to allow detailed chemical modelling for a plug flow

reactor (SENKIN) [40] and a perfectly stirred reactor (PSR) [28]. The major findings of the numerical study are:

- Upper-layer gases are unreactive for temperatures less than 700 K
- Upper-layer combustion gases become reactive for temperatures greater than 800 K
- Reaction rates increase with temperature. For the lowest temperatures, residence times of 10 s were required for complete reaction, while periods of less than 1 s were required at 1300 K.
- The products generated varied for lean and rich conditions and with temperatures. For lean conditions products of complete combustion (i.e. water and carbon dioxide) were produced. For rich conditions, CO was produced in preference to CO_2. At lower temperatures (less than 1100 K) water was generated in preference to hydrogen, but for temperatures greater than 1100 K hydrogen was the major product. Since hydrogen does not require an oxygen atom, more oxygen is available for oxidation of fuel and higher concentrations of CO were formed at the higher temperatures.
- The reaction behavior was not strongly affected by the mixing conditions.
- For adiabatic conditions, reactions resulted in an increase of temperatures. In some cases the effects of the temperature increase on the amounts of final products were small for the same initial temperature. In other cases, the changes in the final product distributions for the two heat loss conditions were quite dramatic.

Bryner et al. [47] studied CO formation in Full-Scale (FSE) and Reduced-Scale Enclosure (RSE) with single doorway. FSE is a ISO 9705 room and RSE is its $\frac{2}{5}$ scale model. The fire was fueled by a single natural gas burner centered in the room. Upper layer concentrations of CO, O_2, CO_2 as well as vertical temperatures were measured for locations in the front and rear of the enclosures. The results show that very low concentrations of CO were generated when fire was overventilated, but CO concentrations increase rapidly when the fire became underventilated. Results also demonstrate that FSE and RSE with similar GER did not produce similar concentrations and temperatures. In the FSE higher CO were observed than in RSE. The temperatures of the upper layer of the FSE were significantly higher than in the RSE. This indicates that higher temperatures enhances CO formation. The GER concept fails to predict CO in these cases.

Pitts [51] summarized the experiments where the GER concept fails to predict CO. Conditions where the GER concept is inappropriate for CO formation in enclosure fire are as follows [50]:

- Fires having $GER > 0.5$ and intermediate temperatures (700 - 900 K) in the upper layer: Hood experiments demonstrated that upper layer temperature influences the relative generation rates of combustion products for this condition. Reaction can occur within the upper layer itself and is dependent on the layer residence time. The use of GER concept for these conditions would be inappropriate.

- Fires for temperatures $> 900K$ for which oxygen enters a fuel rich upper layer directly: Both detailed chemical kinetic analysis and experiments indicate that for these cases, any oxygen reaching the upper layer directly reacts with fuel rich gases producing CO as opposed to CO_2. GER concept underestimates CO concentration for the case.

Therefore, there are limited conditions for enclosure fires for which the GER concept will allow accurate predictions of toxic gas formation.

GER concept has its limitations and Beyler [14] presented a methodology to describe external burning from under ventilated fires by calculation of an ignition criterion called ignition index. Forell [26] utilized this concept and derived an extended GER concept to predict CO source terms. Forell reviewed experimental findings in the literature coming up with CO yields as a function of GER for different materials at different scale (i.e. small scale and ISO room). These results show no clear tendency. Although Forell developed a methodology considering occurance of external combustion, upper layer temperature effect and fuel pyrolysis in the upper layer, this approach relies on specific experimental findings (i.e CO yield) of materials burning. Such algorithm may not be valid for different materials burning at various fire conditions.

Gottuk et al. [29] showed that the production of CO in compartment fires as correlated by the GER concept also depends on temperature. The effect of changing temperatures on compartment fire upper layer composition is two-fold: 1) the generation of species in the fire plume is changed 2) the oxidation of post flame gases in the layer is affected. Elevated temperatures correlate with increased fire plume temperatures and more complete oxidation of the fuel to CO_2 and water within the plume. The layer temperature dictates post-flame oxidation in the layer. For most situations, upper layer temperatures below 800 K indicates a chemically unreactive layer. In such cases combustion within the fire plume dictates the final CO production in the compartment. Reactions in the upper layer dictate final CO levels when upper layer temperatures are about 900 K and higher. Richter [54] investigated pollutant formation from Corbel, Basamid, Pyramin DF etc. depending on various GER and temperature of oven. He concluded that GER and temperature determine the concentration of toxic species in the fire product of specific material.

The mechanisms responsible for the generation of high concentrations of CO in fires are not well understood so far. Due to the lack of a substantial database for CO formation in full-scale enclosure fires and lack of understanding of the physiochemical processes responsible for the generation of CO, it has been impossible to provide an engineering correlation or fundamental approach for predicting CO formation for the most fire scenarios. Pitts [49] summarized a large number of investigations designed to characterize the formation of CO in enclosure fires. It includes the reviewed analysis of the studies from the basis of the GER concept. He focused on whether the GER concept can be used to predict the generation rates for these gases. It is found that CO formation not only depends on GER but also on fuel (burning material) type and upper layer temperature of two layered enclosures and therefore no simple universal predictive method can be provided. Other studies analyzed CO production in enclosure using chemical kinetics modelling and experimental data in the literature to provide insights into the effect of temperature on CO production.

Markert et al. [41] investigated toxicants formation from bulk chemicals (polypropylene, nylon etc.) by choosing four different test scales (micro, small, medium and large) under the EU project TOXFIRE. The fire conditions were characterized using GER. Results show no clear tendency in prediction between the different experimental setups. The scaling hypothesis that GER is the only parameter to explain results has been found incorrect and other parameters like temperature and residence time are important to explain all results.

2.2.2 Modelling

Nakaya [42] has proposed a model for the formation of CO in enclosure fires based on the assumption that combustion gas in the upper layer is in chemical equilibrium. Temperatures in access of 1300 K are required for chemical species to reach equilibrium within usual residence times. The highest temperature generally observed in enclosure fires are in the order of 1300 K. Therefore local thermal equilibrium assumption is invalid for fires. Bundy et al. [17] calculated chemical equilibrium for natural gas and showed local chemical equilibrium assumption results in high overprediction compared to measured data at fuel-rich (underventilated) conditions.

Wang et al [63] developed a CFD model of toxic species prediction using empirical models of toxic species yields for plastic fuels available in literature. These empirical models of toxic species yields are found in small scale experiments which may not be valid for different fire conditions or in large scale fires. Cleary [22] developed and implemented a Conditional Moment Closure (CMC) combustion model to predict species concentration in hood fires. Detailed chemical mechanism of methane fuel combustion is used for natural gas fuel. Predictions are reasonable but less satisfactory at fuel rich conditions and results are very sensitive to the choice of chemical mechanisms. One of the major limitations of such modelling techniques is that it requires detailed chemical kinetics mechanisms of fuel burning. Chemical kinetics mechanism of burning materials like plastics, wood etc are beyond the state of the art of fire research.

FDS 5 [1] has the following two options to model CO formation in enclosure fire:

- Well ventilated compartment: The yields of CO and soot are input of the model for CO prediction in fire where yields are based on "well-ventilated" or post-flame measurements. The mixture fraction, Z, is defined in terms of fuel and the carbon carrying products of combustion as

$$Z = Y_F + \frac{M_F}{x' M_{CO_2}} Y_{CO_2} + \frac{M_F}{x' M_{CO}} Y_{CO} + \frac{M_F}{x' M_S} Y_S \tag{2.50}$$

  where, M is molar mass of species and x' is the CO yield.

- Underventilated fires: In underventilated fires soot and CO are produced at higher rates, a single set of fixed yields based on post-flame measurements are not able to predict CO accurately. A Two-step CO production model is implemented in FDS 5 as described in Sec. 2.1.1 in order to account for CO formation at the flame envelop or within a hot upper layer. This model still needs post-flame CO yield like

well-ventilated case but the two-step algorithm contributes to additional CO yield at under-ventilated fires. Floyd [25] validated the model with measured data for steady fire conditions but no transient CO prediction is validated. However, it is claimed that transient CO in fire can be tracked by the model [1]. The transient CO, computed with FDS 5, is compared to measured data which is presented in Sec. 4.2.3 of this dissertation. The input of the model are fuel composition, the soot and CO yields. Other toxic species like $NO_x, SO_x, H_2S, HCN, HCl$ etc. are also produced in some fire cases. If nylon is burning, HCN will be produced and HCN is 35 times more toxic than CO. Model for these other toxic species are not included in FDS.

There is no CO model implemented in Jasmine and Sofie.

Chapter 3

Implementation of toxicants formation model into fire simulation

3.1 Simulation of flow with chemical reactions

In a reacting flow, different chemical and physical processes occur simultaneously on many different time and space scales. For instance, any temperature increase due to chemical reactions causes a local expansion of the gas and at the same time reactions are occurring. The coupling of different processes in a unified computational method is cumbersome. A detailed discussion and numerical methods for reactive flows are explained in [48]. The objective of this section is to summarize parameters needed for reactive flow simulation accurately and to compare this to the state of the art in fire simulation for toxic species prediction. Table 3.1 presents such a comparison.

Table 3.1
Simulation of Reactive Flows

Parameter	Correct approach	FDS 5	Approach of this thesis
Time	Reaction kinetics is needed, time scale of reactions have an important role in determining interaction with fluid dynamics	Time has no influence, very fast reactions are assumed, only CO and soot can be predicted	All reactions are very fast, using this reaction data an artificial source term is derived and used with fluid dynamics
Temperature	At low temperatures no reaction occurs	Temperature influence is included according to empirical model	Temperature influence is included according to constrained equilibrium calculations
Turbulence mixture	Concentrations of substances are included in calculations	Mixture fraction model	Mixture fraction influence according to constrained equilibrium calculations

3.2 Global model and simplification

3.2.1 Combustion of polymers

Solid polymeric materials undergo both physical and chemical changes when heat is applied. In fire, thermal decomposition of solid materials generate gaseous fuel vapors which can burn above the solid materials. In order to continue the production of gases, fuel vapors or volatiles, burning gases need to feedback sufficient heat to the material. Heat transferred to the polymer causes the generation of flammable volatiles which react with the oxygen in the air above the polymer to generate heat, carbon dioxide, water, toxic chemical species, soot and a part of this heat is transferred back to the polymer to continue the process. The chemical processes are responsible for the generation of flammable volatiles while physical changes, such as melting and charring can alter the decomposition and burning characteristics of materials.

Polymeric materials are involatile and quite large molecules must be broken down into smaller molecules that can vaporize. In most cases, a solid polymer breaks down into a variety of smaller molecular fragments made up of a number of different chemical species. The lighter of the molecular fragments will vaporize immediately upon their creation while

other heavier molecules will remain in the condensed phase for some time. These heavier molecules may undergo further decomposition to lighter fragments which are more easily vaporized. However, often, not all the original fuel becomes fuel vapors since solid residue are left behind. These residue can be carbonaceous char, inorganic or a combination of both. Charring materials such as wood leave large fractions of the original carbon content as carbonaceous residue, often as a porous char. When thermal decomposition of deeper layers of such a material continues, the volatiles produced must pass through the char above them to reach the surface. During this transport, the hot char may cause secondary reactions to occur in the volatiles. Carbonaceous char when appropriately formed can have intumescent layers, which slow down further thermal decomposition. On the other hand, inorganic residues can form glassy layers constraining any further thermal breakdown. Unless such inorganic barriers are formed, purely carbonaceous chars can always be burned by surface oxidation at higher temperatures. The mechanisms of these thermal decomposition processes and product composition depend on both the physical properties of the original materials and its chemical decomposition. There are a number of general classes of chemical mechanisms important in the thermal decomposition of polymers:

- random chain scission, in which chain scission occurs at apparently random locations in the polymer chain,
- end-chain scission, in which individual monomer units are successively removed at the chain end,
- chain-stripping, in which atoms or groups are not part of the polymer chain are removed,
- cross-linking, in which bonds are created between polymer chains.

These are discussed in some details in [21]. In short, combustion of polymer materials is characterized by a complex coupling between condensed phase and gas phase phenomena. Furthermore, the phenomena in these phases consist of a complex coupling of chemical reactions with heat and mass transfer processes. The kinetics describing the processes can be quite complex. Because of lack of understanding of basic combustion mechanisms of polymers theoretical models able to predict combustion phenomena and flamibility properties are not available. Available simplified models do not have the capability to predict the evolved rate of decomposition products for these polymers except in a few limited cases that exclude any transport process. Some of the difficulties are lack of kinetic constants for specific decomposition reactions such as intermolecular transfer reactions, which are not only a function of temperature but also of the mobility of polymer chains [35]. Furthermore, if these kinetic constants are available, generally these are measured at much lower heating rates than those encountered in fires.

3.2.2 Simplified models of toxicants formation

Fire is an uncontrolled combustion and mass, momentum, energy, chemical species balance equations are used in combustion simulation. Chemical source term in species balance

equations is highly nonlinear especially concerning temperatures. Turbulence chemistry interaction is crucial to the modelling of mean chemical reaction rate. Damkoehler number is commonly used to define this interaction which is the ratio of mixing time to the chemical reaction time. Therefore, the goal of any combustion simulation is to know detailed chemical kinetics which consist of many reactions simultaneously in order to get detailed results. In case of unavailability of detailed kinetics, a simplified solution is to use global kinetics. Detailed kinetics of polymer burning in fire conditions is unknown as we discussed in Sec. 3.2.1. Because of the multitude of burning materials in fire, simplified solutions can be conducted through

- Global CO formation kinetics and for other toxicants (*i.e.*HCN, NH_3, HX, NOx *etc.*)
- Full chemical equilibrium but dependent on range of temperatures and range of GERS (defined as constrained equilibrium)

3.3 Constrained equilibrium calculations

Thermochemical software FactSage [12] equilibrium module is utilized to calculate complex heterogenous constrained equilibrium of material burning reactions. The methodology of calculation is based on the determination of the combination of moles, gas partial pressure at a specific temperature and pressure that minimizes the total Gibbs energy of the system. One needs to define elementary components of the system and their amounts. After Gibbs energy is minimized for fixed values of temperatures and pressures varying the amount of possible products under the constraint of elemental conservation.

The constrained chemical equilibrium concentrations of toxic species during the combustion of methane, Polystyrene (PS), Polypropylene (PP), Polyurethane (flexible) PU, Polyvinyl chloride (PVC) have been calculated at various temperatures and equivalence ratios (GERs) and 1 bar atmospheric pressure by using FactSage. Calculations were performed over a temperature range of 300 K to 1600 K and GER values from 0.5 to 4 for which products of incomplete combustion were observed. GER values up to 20 are chosen for methane burning in order to analyse CO formation in some details. The temperature and GER effect on the production of toxicants during above mentioned combustion processes can be explained based on the results of the calculations. Other toxic chemical species like hydrogen halides (HX), hydrogen cyanide (HCN), ammonia (NH_3), nitrogen oxide (NO_x) can also be produced depending on the chemical structure of material and burning conditions.

Figures 3.1-3.31 show how calculated toxicant concentrations in the products from the above materials vary with GERs and temperatures. Concentrations of the toxic chemical species have been expressed in vol% (1 $ppm = 10^{-4}$ $vol\%$). Toxicants concentration produced below the allowable concentration limit (i.e. for NO_2 5 ppm) can be ignored as those are not hazardous. Therefore, NO_2 production from PP, PU and PVC at any fire conditions can be ignored. CO production is significant above GER = 1 and above 500 K for all the above materials burning.

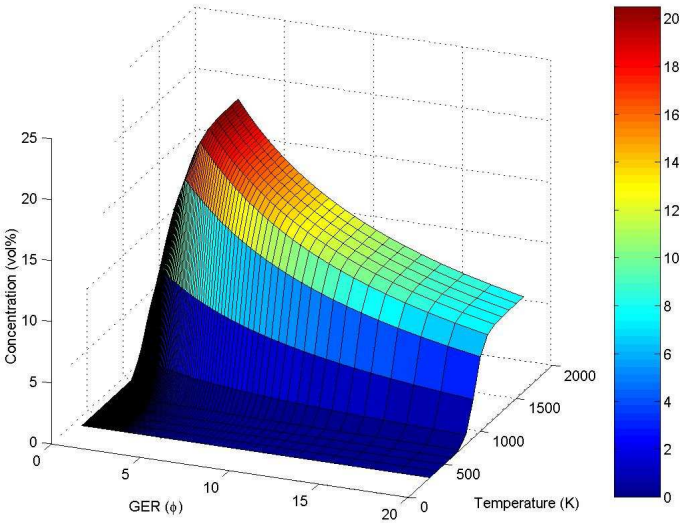

FIGURE 3.1 CO (vol%) formation from methane burning at different GERs and temperatures

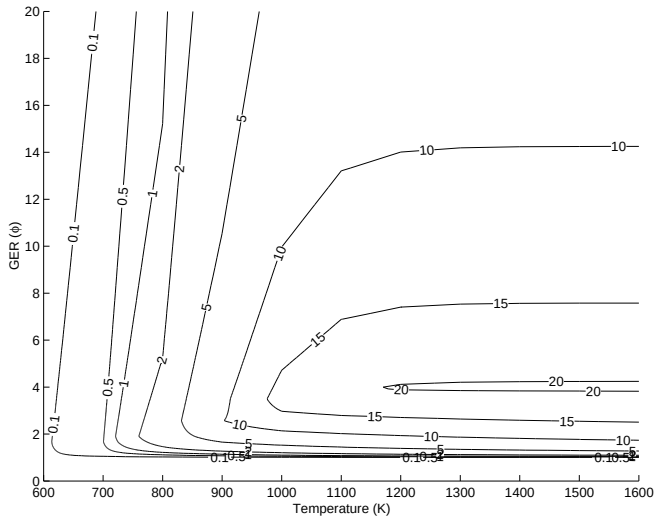

FIGURE 3.2 CO (contour in vol%) formation from methane burning at different GERs and temperatures

The results of calculations need to be compared with experimental data to check their validity. Because of the lack of experimental data of toxic species formation as a function of temperature, fully quantitative comparisons were not possible. Bryner [47] reported CO concentration increases with higher temperature at the same GER from natural gas fires. Results of the calculation (see Fig. 3.1) agree qualitatively with experimental findings as CO concentration increases with increasing temperature at a specific GER.

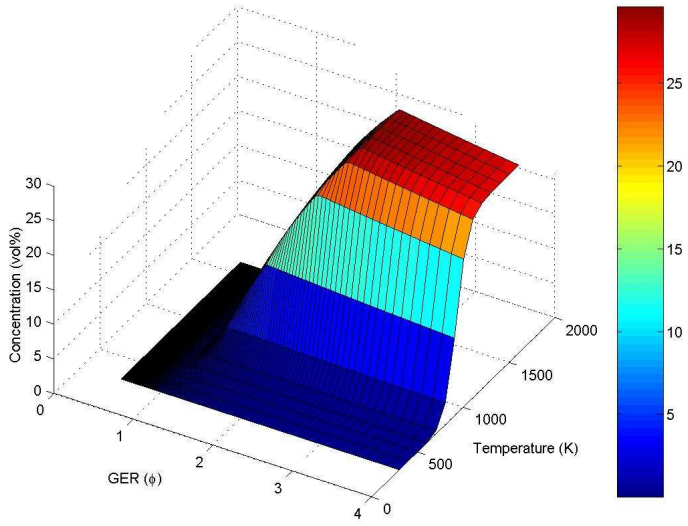

FIGURE 3.3 CO (vol%) formation from polystyrene burning at different GERs and temperatures

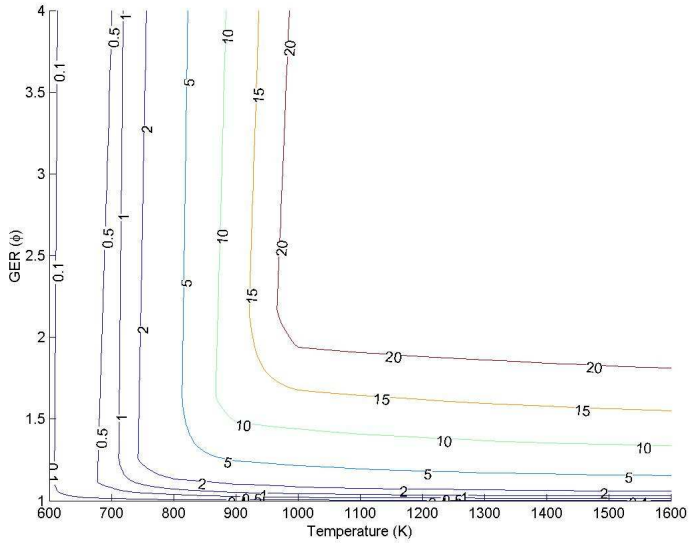

FIGURE 3.4 CO (contour in vol%) formation from polystyrene burning at different GERs and temperatures

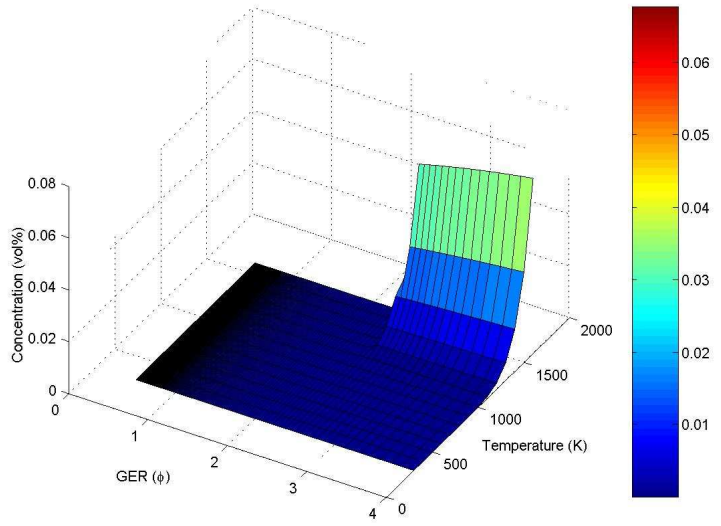

FIGURE 3.5 HCN (vol%) formation from polystyrene burning at different GERs and temperatures

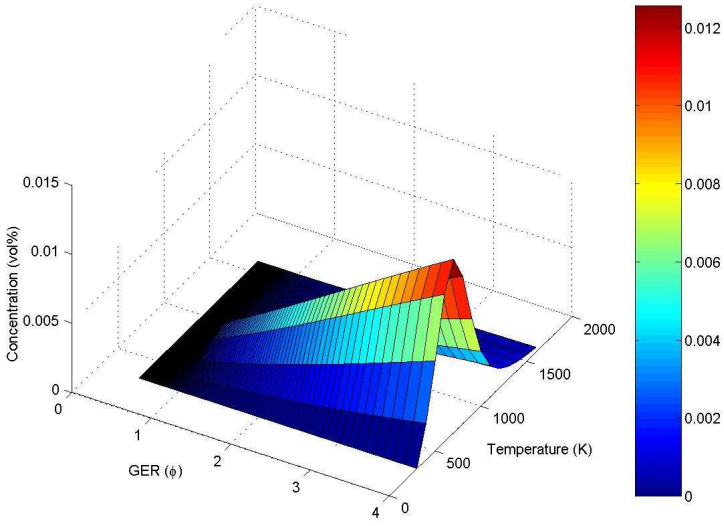

FIGURE 3.6 NH_3 (vol%) formation from polystyrene burning at different GERs and temperatures

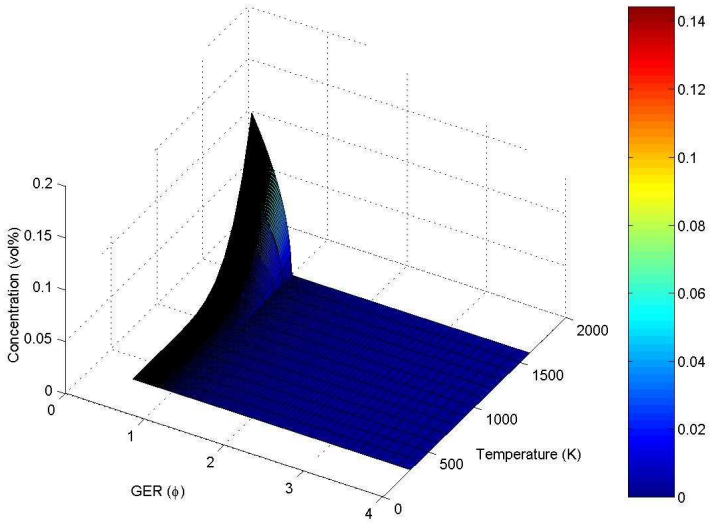

FIGURE 3.7 *NO* (vol%) formation from polystyrene burning at different GERs and temperatures

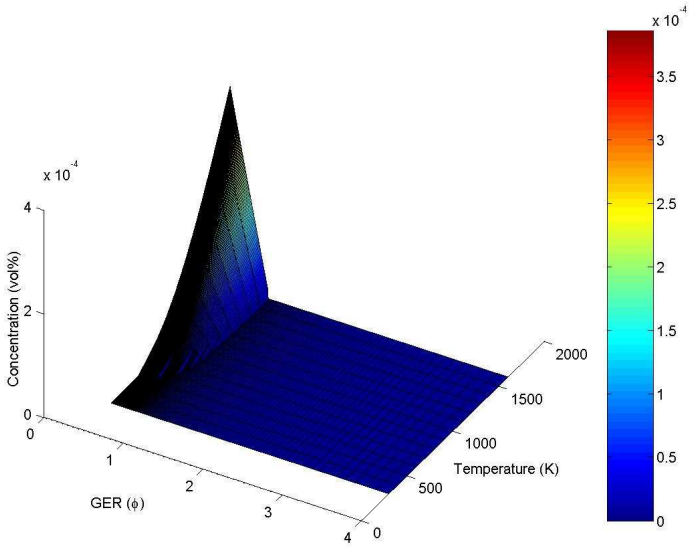

FIGURE 3.8 NO_2 (vol%) formation from polystyrene burning at different GERs and temperatures

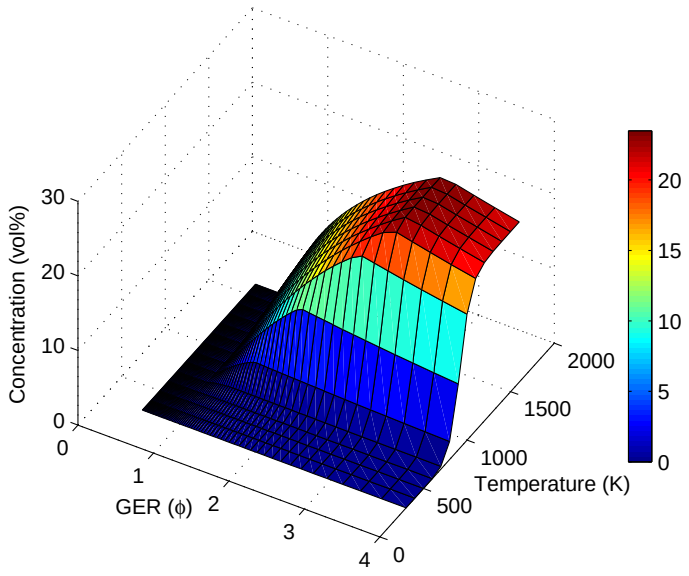

FIGURE 3.9 CO (vol%) formation from PP burning at different GERs and temperatures

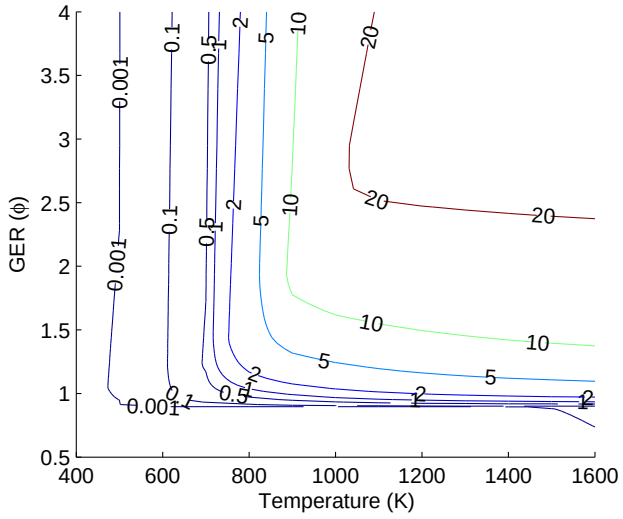

FIGURE 3.10 CO (contour in vol%) formation from PP burning at different GERs and temperatures

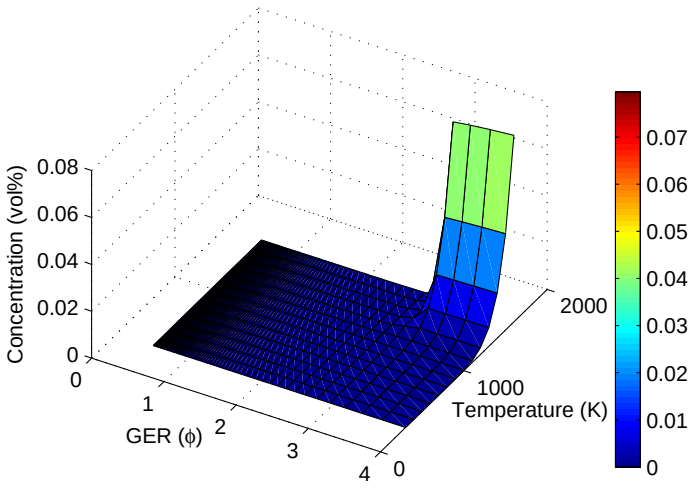

FIGURE 3.11 HCN (vol%) formation from PP burning at different GERs and temperatures

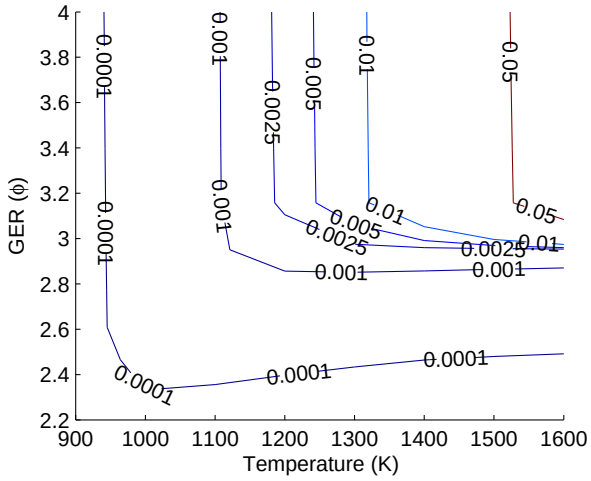

FIGURE 3.12 HCN (contour in vol%) formation from PP burning at different GERs and temperatures

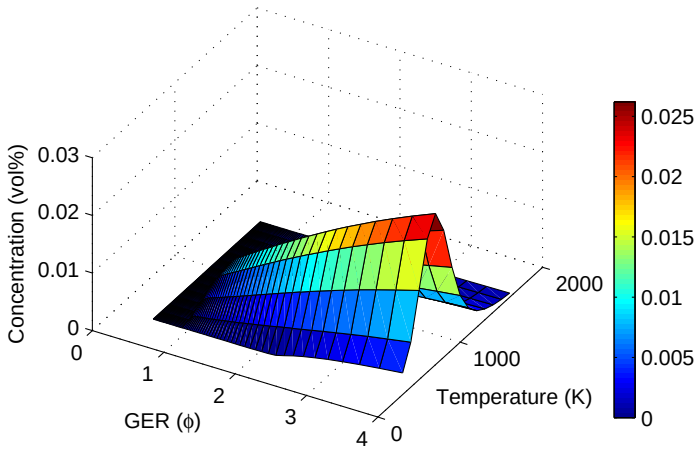

FIGURE 3.13 NH_3 (vol%) formation from PP burning at different GERs and temperatures

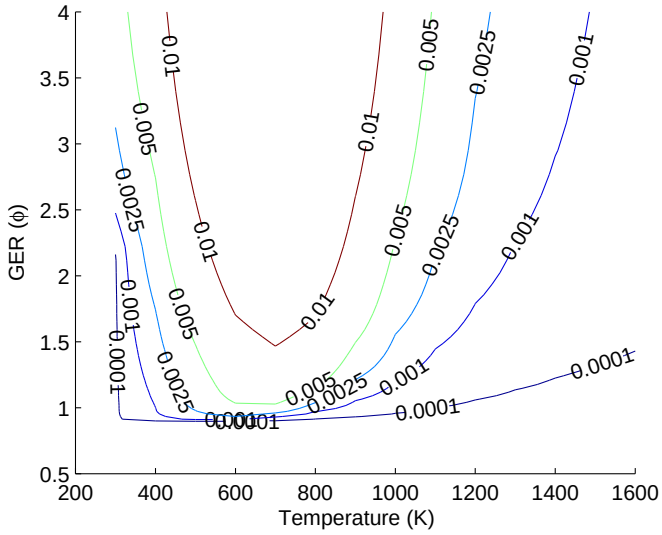

FIGURE 3.14 NH_3 (contour in vol%) formation from PP burning at different GERs and temperatures

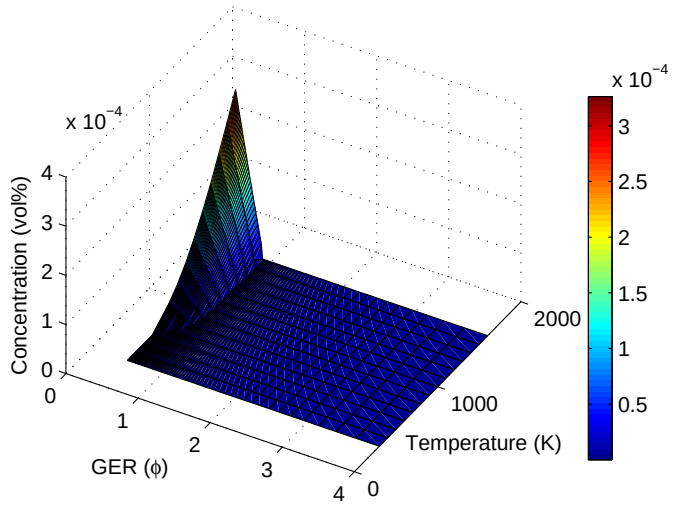

FIGURE 3.15 NO_2 (vol%) formation from PP burning at different GERs and temperatures

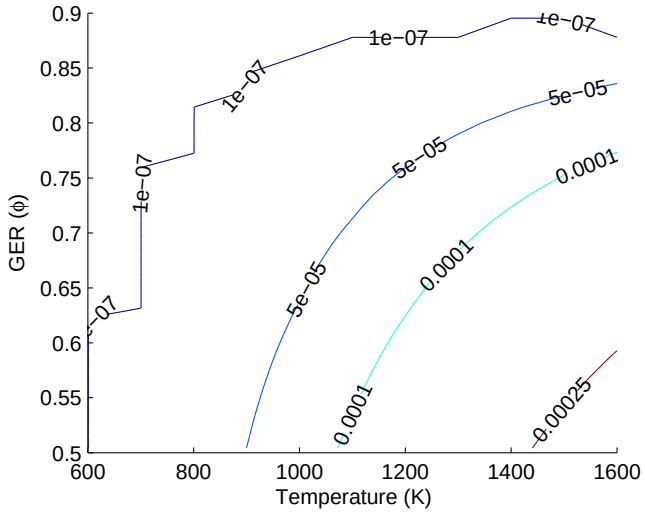

FIGURE 3.16 NO_2 (contour in vol%) formation from PP burning at different GERs and temperatures

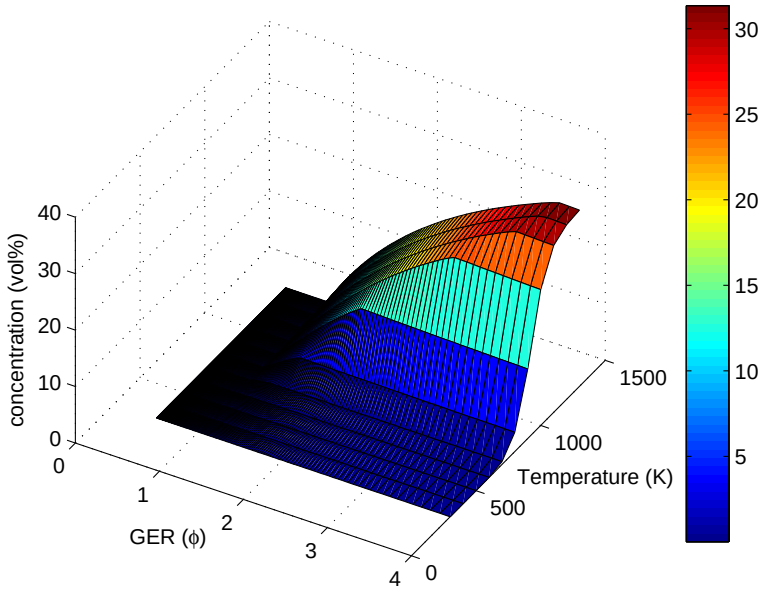

FIGURE 3.17 CO (vol%) formation from PUF burning at different GERs and temperatures

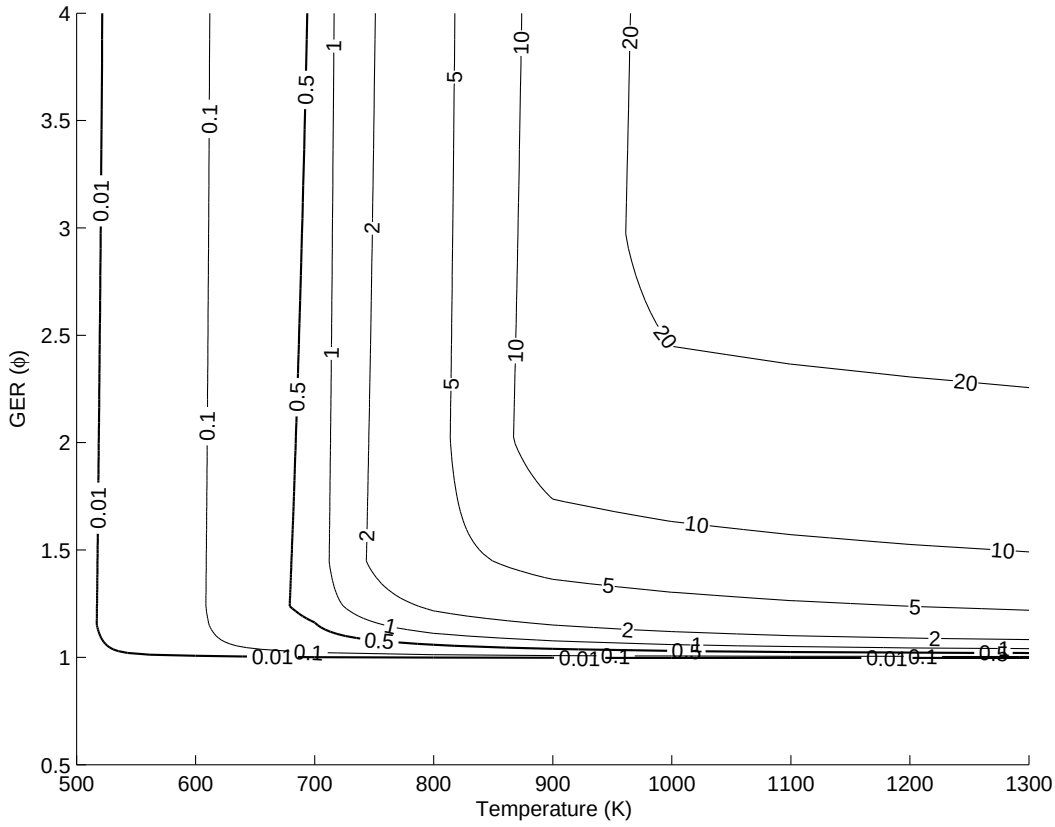

FIGURE 3.18 CO (contour in vol%) formation from PUF burning at different GERs and temperatures

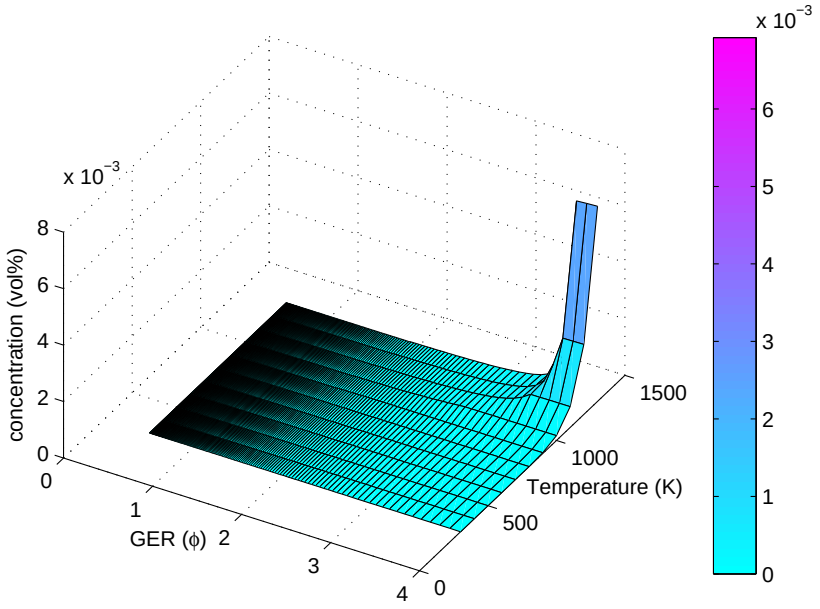

FIGURE 3.19 HCN (vol%) formation from PUF burning at different GERs and temperatures

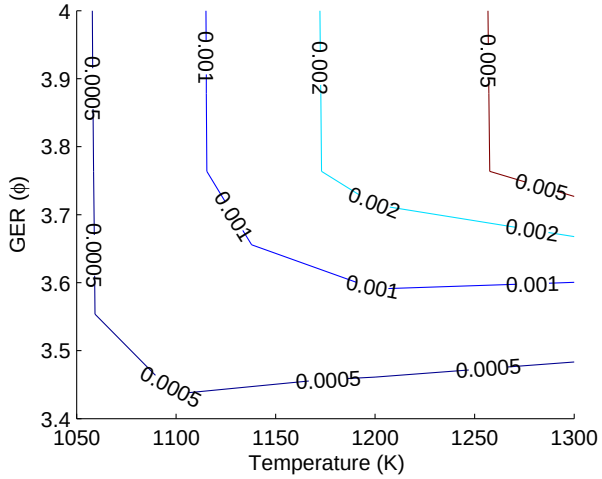

FIGURE 3.20 HCN (contour in vol%) formation from PUF burning at different GERs and temperatures

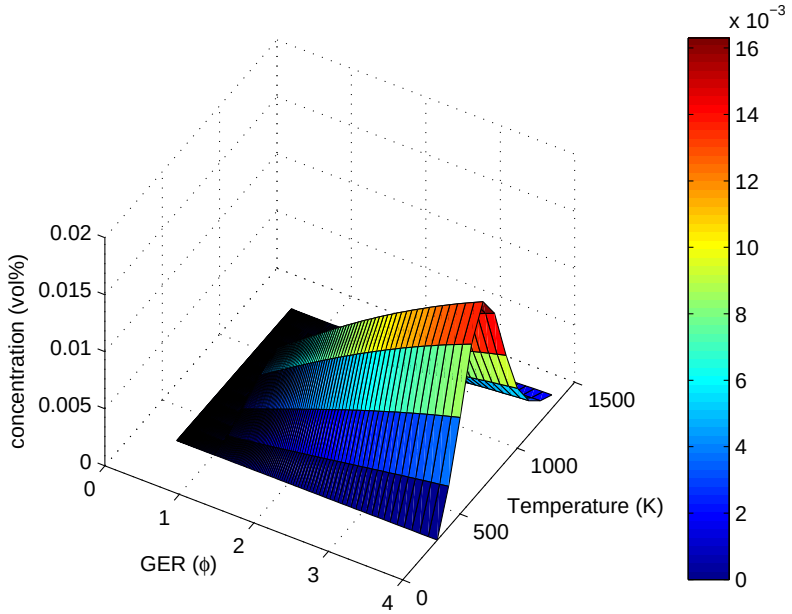

FIGURE 3.21 NH_3 (vol%) formation from PUF burning at different GERs and temperatures

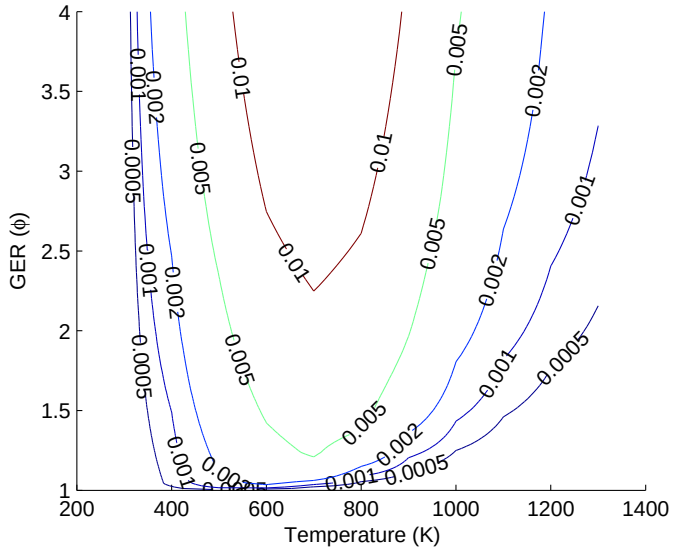

FIGURE 3.22 NH_3 (contour in vol%) formation from PUF burning at different GERs and temperatures

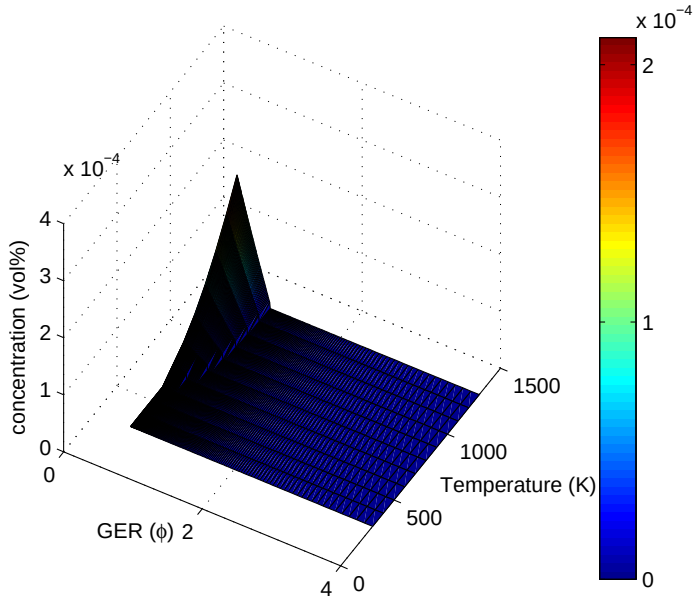

FIGURE 3.23 NO_2 (vol%) formation from PUF burning at different GERs and temperatures

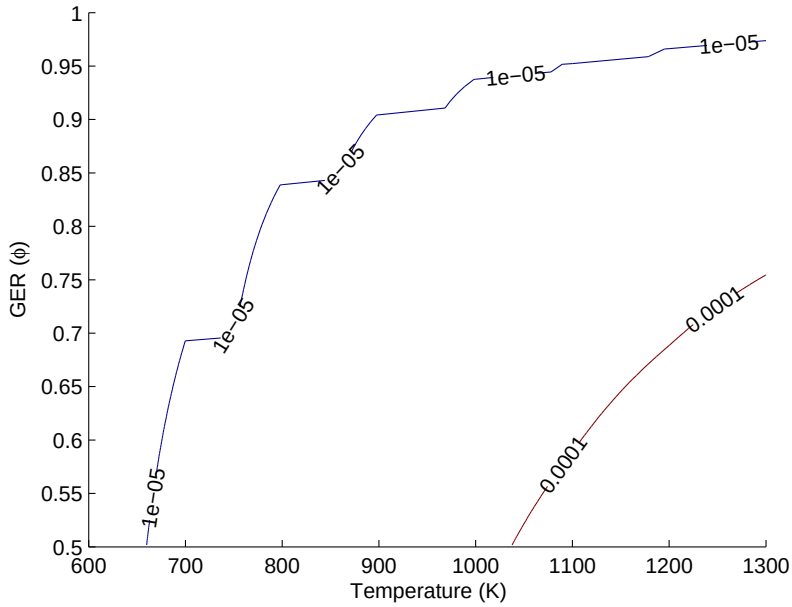

FIGURE 3.24 NO_2 (contour in vol%) formation from PUF burning at different GERs and temperatures

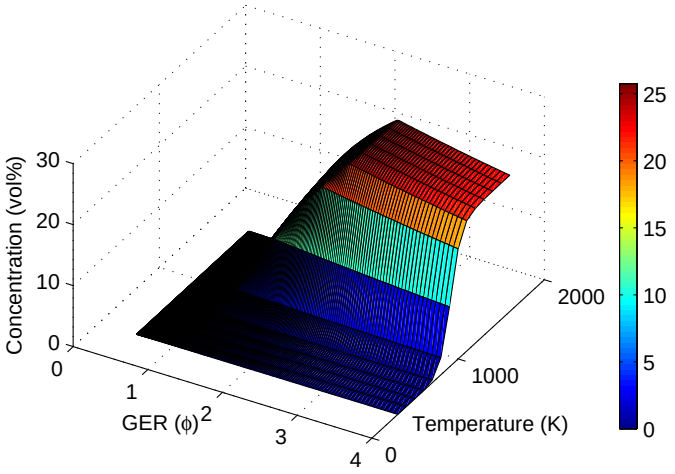

FIGURE 3.25 CO (vol%) formation from PVC burning at different GERs and temperatures

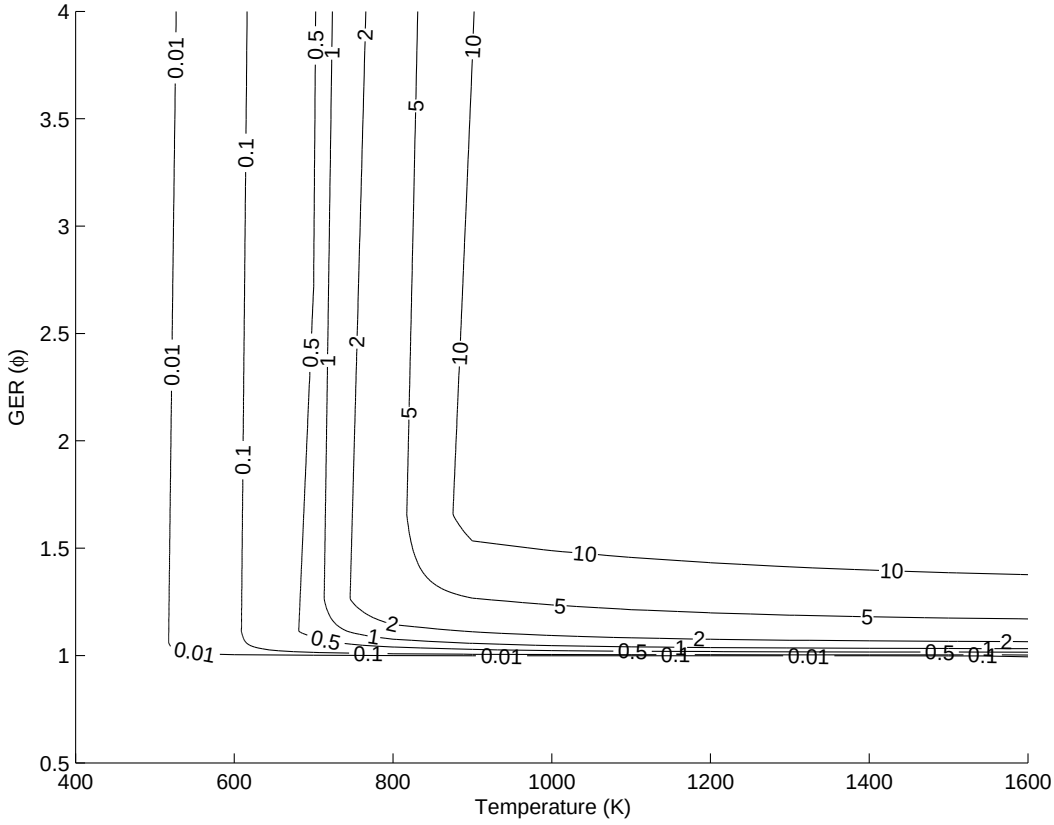

FIGURE 3.26 CO (contour in vol%) formation from PVC burning at different GERs and temperatures

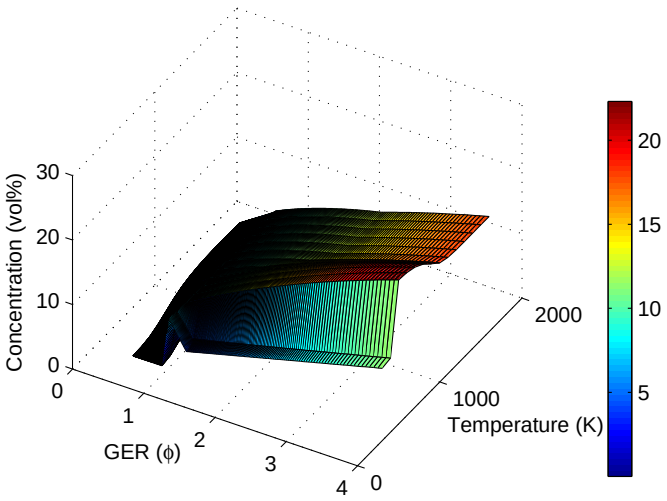

FIGURE 3.27 HCl (vol%) formation from PVC burning at different GERs and temperatures

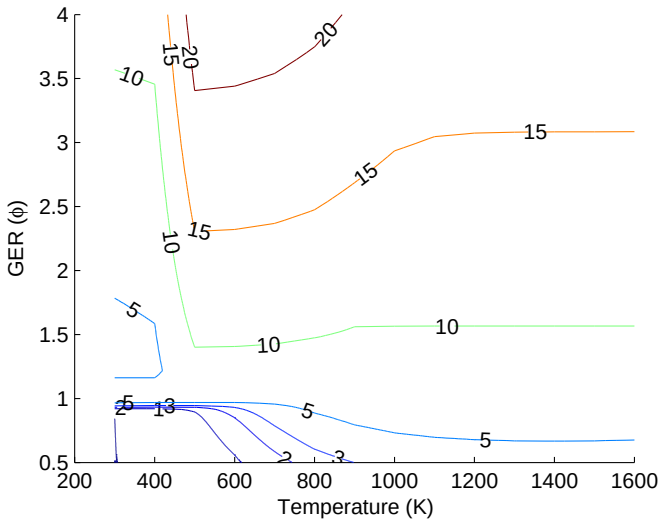

FIGURE 3.28 HCl (contour in vol%) formation from PVC burning at different GERs and temperatures

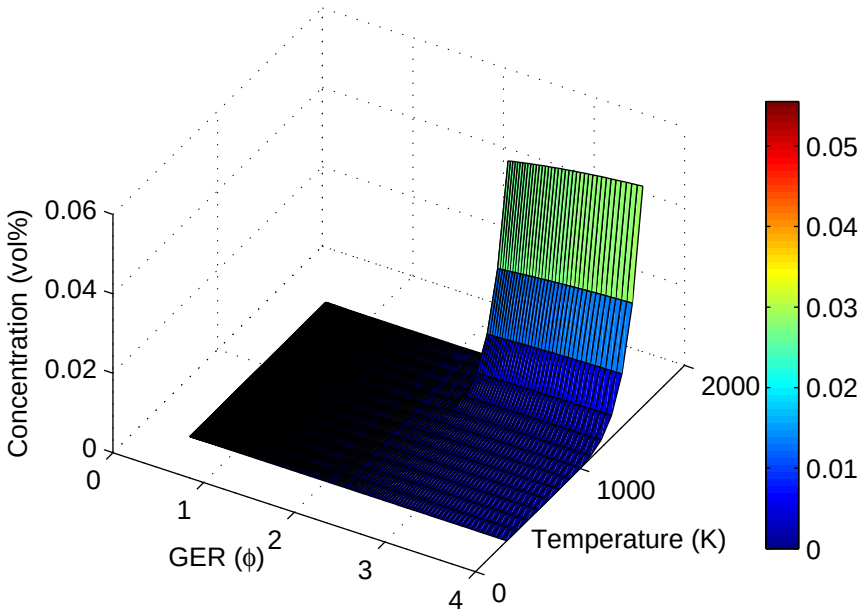

FIGURE 3.29 HCN (vol%) formation from PVC burning at different GERs and temperatures

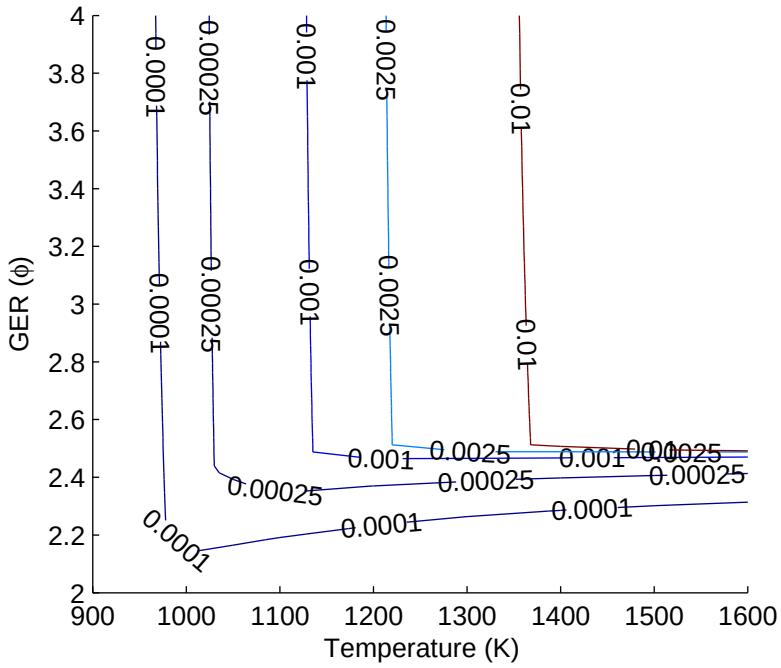

FIGURE 3.30 HCN (contour in vol%) formation from PVC burning at different GERs and temperatures

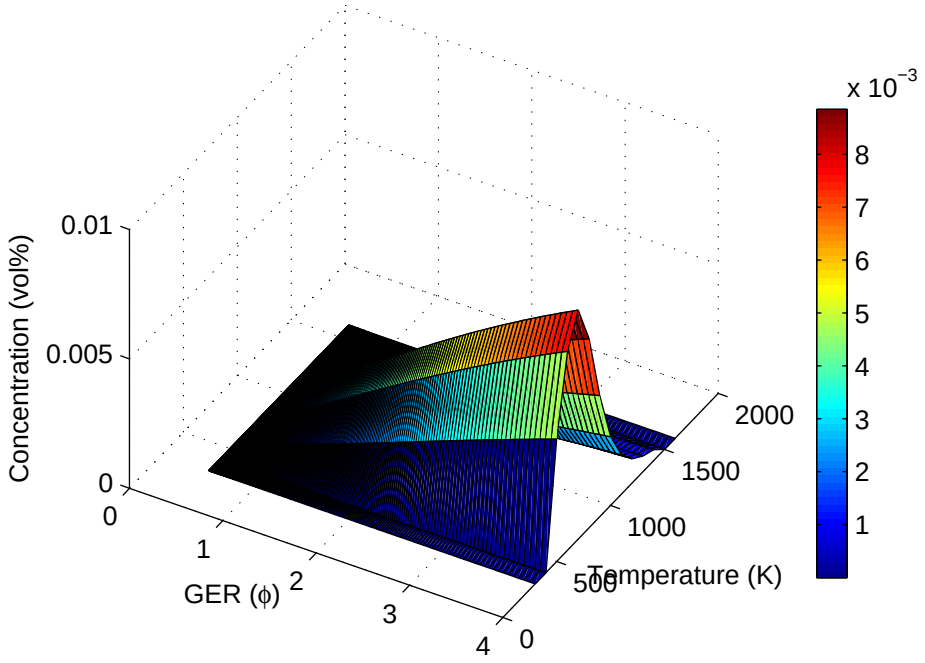

FIGURE 3.31 NH_3 (vol%) formation from PVC burning at different GERs and temperatures

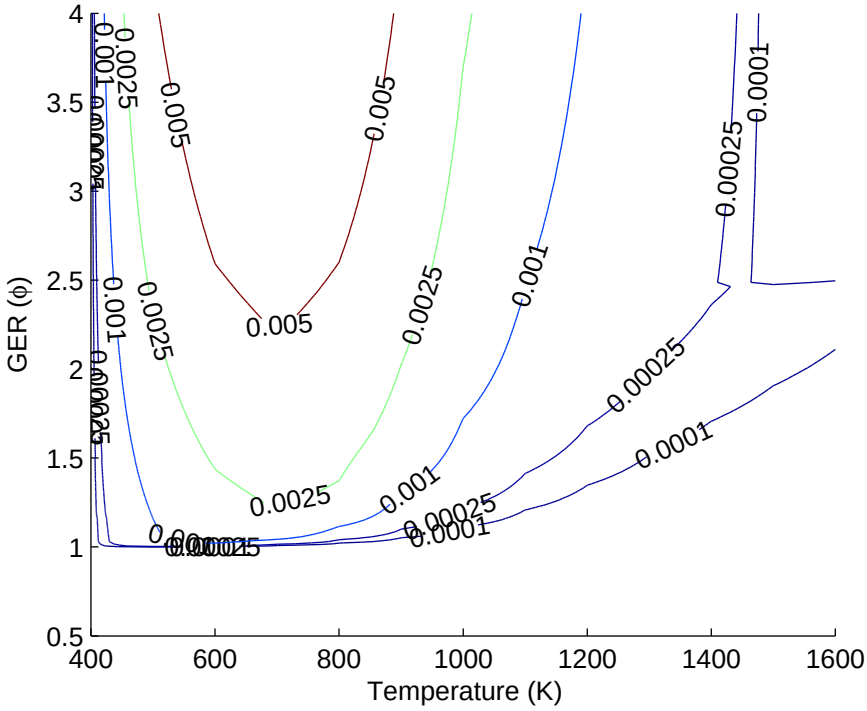

FIGURE 3.32 NH_3 (contour in vol%) formation from PVC burning at different GERs and temperatures

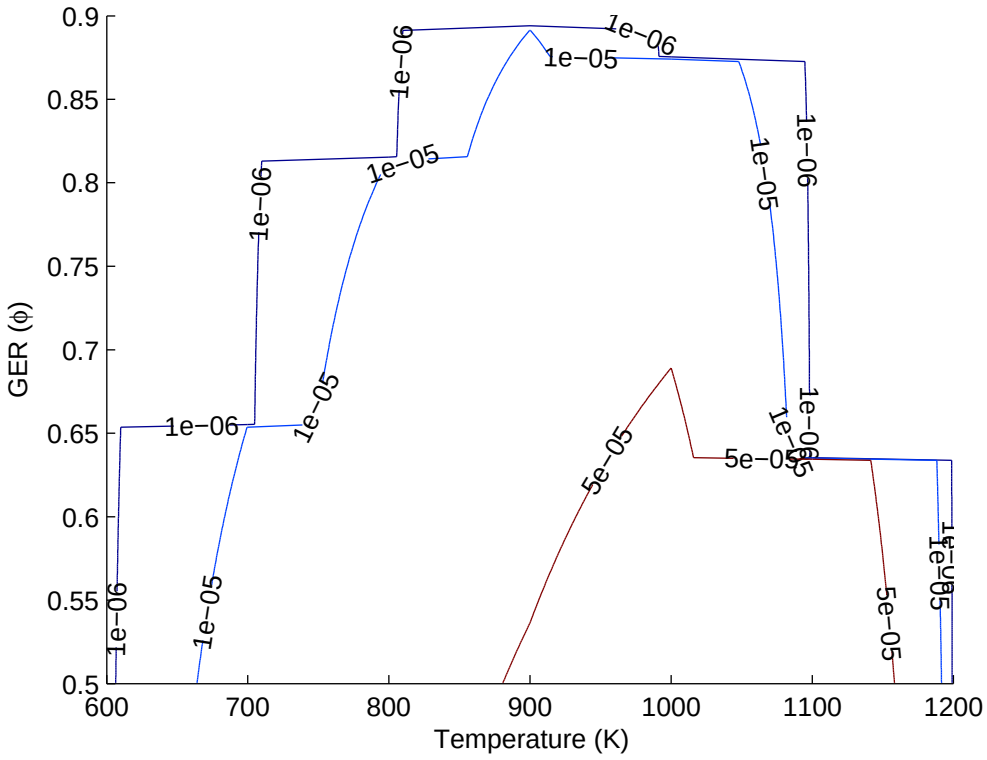

FIGURE 3.33 NO_2 (contour in vol%) formation from PVC burning at different GERs and temperatures

In all the above cases, almost no CO forms at $GER < 1$. CO formation increases drastically above $GER > 1$ and reaches peak values at about GER = 4. Further increase of GER reduces CO formation. Very low amount of CO forms at very high GER ($GER >>$ 20). Increment of GER means depletion of oxygen. Very low amount of oxygen is available for reaction at very high GERs. The maximum temperature during enclosure fire is in the range of 1300 K to 1500 K [27]. CO formation increases dramatically above 800 K and reaches highest value at maximum temperature. NH_3 and HCN have a peak at about 1000 K and higher GERs. NH_3 and HCN are not stable at further increasing temperatures due to chemical bonding breaks down at temperatures greater than 1000 K and at higher GERs. Highest NO_2 and NO forms at lower GERs ($GER < 1$ or excess oxygen) and at about 1000 K. Conditions which favor these species formation or break down depend on chemical affinity of elements forming these species at those combustion conditions.

3.4 Fire simulation including toxic formation

3.4.1 Description of experiments

Experimental data of transient local toxic concentrations in enclosure fire are not easy to find. National Institute of Standard and Technology (NIST) conducted Full Scale Enclosure (FSE) and Reduced Scale Enclosure (RSE) natural gas fire experiments [47, 46]. The FSE

is a ISO/ASTM standard room which is 2.44 m wide, 2.44 m tall, 3.66 m deep with 0.76 m wide and 2.03 m tall doorway centered at the bottom of the front wall (see Fig. 3.34 and 3.35). The room was built with a sheet metal stud framework which was lined with three layers of 0.0127 m thick gypsum board and single layer of 0.0127 m thick calcium silicate board. Two trees of bare chromel-alumel thermocouple were placed 0.5 m from a side wall and 0.5 m from the front and rear wall as shown in Fig. 3.34 and 3.35 as dots and a third tree of ten aspirated thermocouples were utilized to monitor temperatures vertically across the doorway. The 0.35 m burner was centered in the enclosure with upper burner lip 0.38 m above the floor. Fire size was controlled by setting the metered flow of the natural gas fuel.

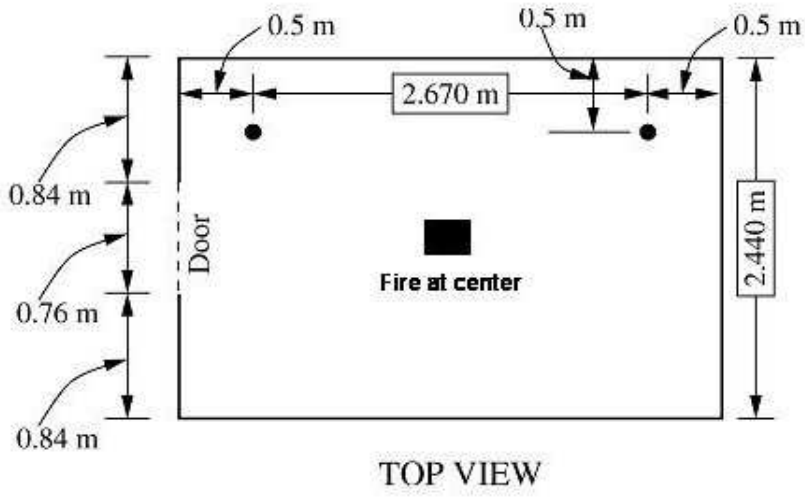

FIGURE 3.34 Top view of FSE

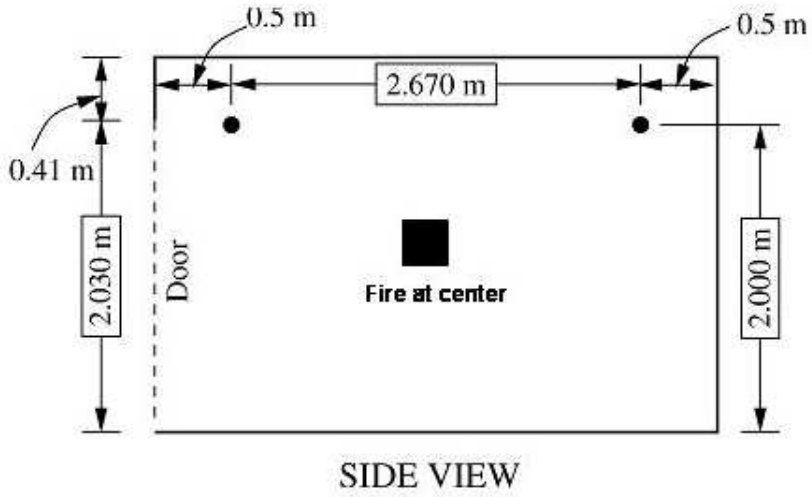

FIGURE 3.35 Side view of FSE

The RSE was designed as 40 percent scale model of the standard room. RSE is scaled geometrically from FSE which is 0.98 m wide, 0.98 m tall and 1.46 m deep. The area of the doorway was scaled following $A_d\sqrt{h_d}$ enclosure ventilation scaling parameter where A_d is the total area of the ventilation opening and h_d is the height of the opening. This results in a 0.48 m wide and 0.8 m tall door for RSE. The RSE steel frame was lined with sheet metal to form an airtight enclosure. Two layers of 0.0127 m thick calcium silicate board were added within the inner walls. Two thermocouple trees were positioned 0.2 m from the side wall and 0.2 m from the front and rear corner. Figure 3.36 and 3.37 show layout of RSE including thermocouple locations.

Natural gas fires with 2700 kW HRR in FSE and fires with 400 kW HRR in RSE have been selected for simulations. Fires of 400 kW HRR in RSE and fires of 2700 kW in FSE are underventilated where estimated GERs are greater than 2 for both cases [47]. Temperatures and CO concentrations were recorded 0.8 m above and 2 m above the floor for RSE and FSE respectively.

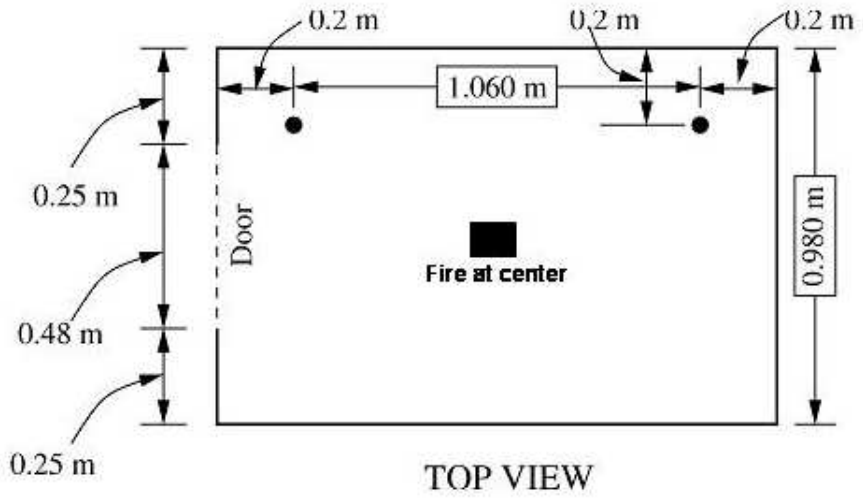

FIGURE 3.36 Top view of RSE

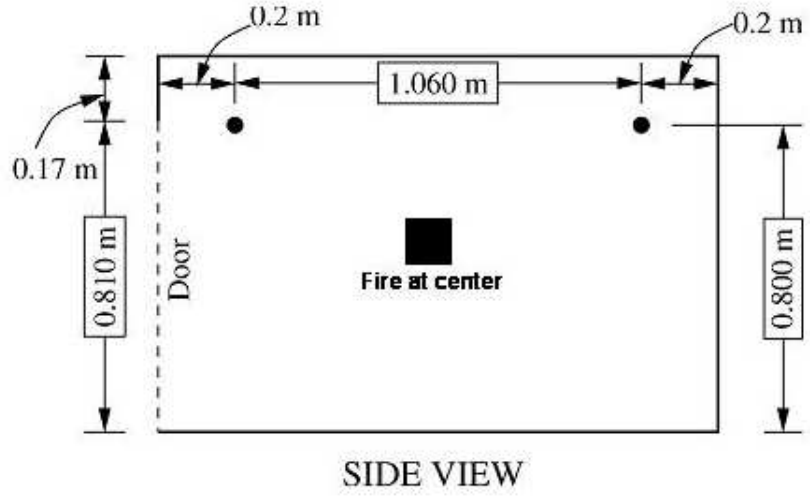

FIGURE 3.37 Side view of RSE

3.4.2 Application of chemical equilibrium calculations

Constrained equilibrium combustions are calculated for natural gas by using FactSage to get toxic species concentration as described in Sec. 3.3. 2-D (temperature and global equivalence ratio, ϕ) "Lookup" tables have been calculated for toxicants product concentration (i.e. CO) from these materials burning. FDS 5 is used to calculate local temperatures and mixture fractions converted to global equivalence ratio ϕ by the formula 3.5. Following local chemical equilibrium assumption, local concentrations are the concentrations taken from "Lookup" table according to local temperatures and mixture fractions. The transient concentrations at front and rear location of enclosures (see Fig. 3.38) are about to zero as mixture fraction and therefore also global equivalence ratio is zero or about to zero at those locations which are away from fire. Equilibrium calculations (see Fig. 3.2) show that concentrations are close to zero at GER less than one, whatever the temperatures are. Experimental data (see Fig. 3.38) shows high concentration profile at front and rear locations with time. Computed CO concentration (see Fig. 3.39) at a location (0.5 m, 1.3 m, 0.2 m) of RSE which is situated inside the fire shows very high concentrations. No experimental data was available to compare this calculation.

These results indicate that equilibrium assumption is unable to predict local concentration of enclosure fire. Equilibrium assumes very fast chemical reactions or mixed is burnt. In reality, CO reactions are slow and convection and diffusion play a significant role in toxicants distribution. Toxic species are produced at certain reaction rates during pyrolysis and in the flame or outside the flame if appropriate reaction conditions prevail and simultaneously transported through flow field. Transport equation with toxic species kinetics source terms need to be solved in order to get realistic local toxic species concentration.

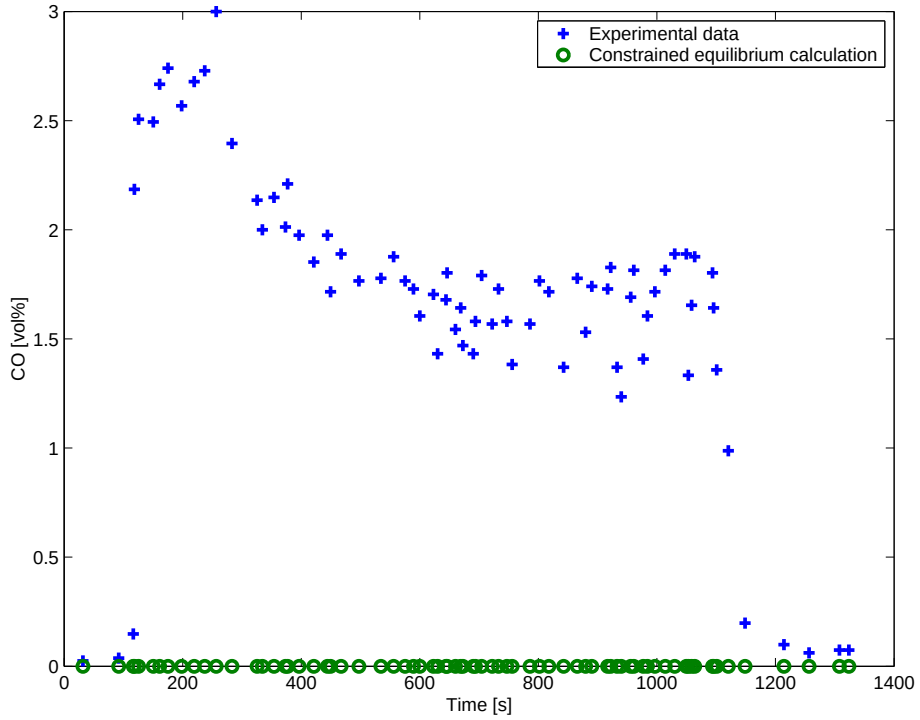

FIGURE 3.38 Comparison of CO concentration at position (0.2 m, 1.26 m, 0.8 m) of RSE natural gas fire

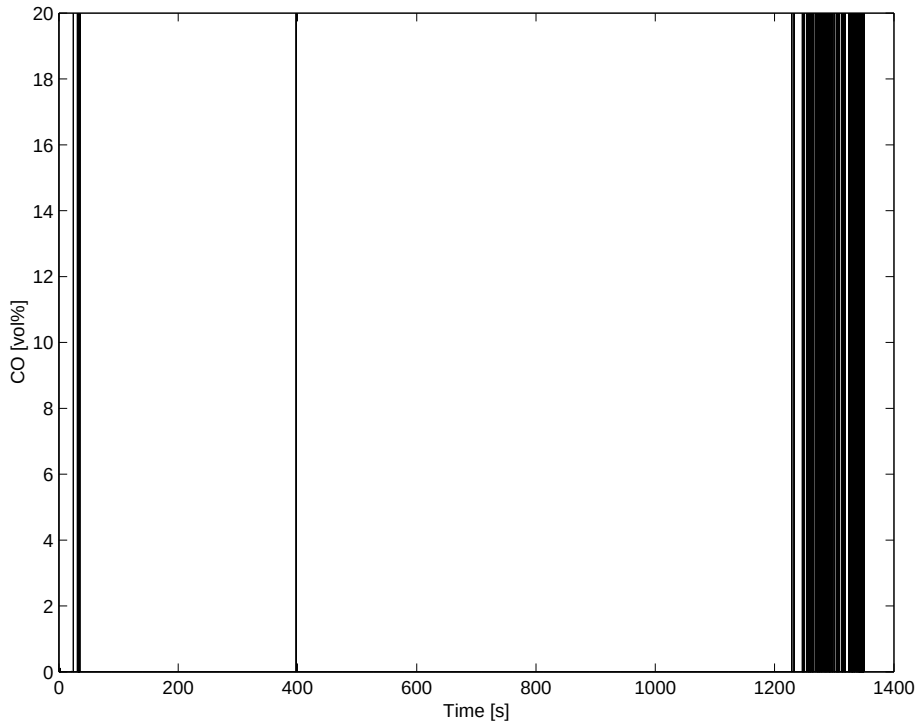

FIGURE 3.39 Computed CO concentration at position (0.5 m, 1.3 m, 0.2 m) of RSE natural gas fire

3.4.3 Transport calculations including kinetic source and sink terms

Chemical kinetics of toxic species production or destruction is essential in order to predict local toxicant concentration. Such kinetics of plastic burning are not known and are not the state of the art of fire research. Global CO formation kinetics are known and used for simulation of combustion chambers of power plants [38] but chemical kinetics of other toxic species are not available and difficult to establish. On the other hand the implementation of chemical equilibrium does not produce realistic results. Results (Fig. 3.38 and 3.39) show that near the fire CO values are too high and apart from fire CO concentrations are too low. This indicates that at least at lower temperatures equilibrium is not reached immediately i.e. the toxicants like CO formed in the region of higher temperatures are transported into regions of lower temperatures where these toxicants are not immediately destroyed as assumed while assuming local equilibrium. Therefore, a submodel has been developed solving species transport equation with calculated source terms from constrained equilibrium calculations.

3.4.4 Calculations of source terms from constrained equilibrium calculations

Source terms can be computed using species balance equation where concentration values can be taken from constrained equilibrium calculations. The species balance equation is as follows:

$$\frac{\partial}{\partial t}(\rho Y_\alpha) + \frac{\partial}{\partial x_i}(\rho u_i Y_\alpha) = \frac{\partial}{\partial x_i}(\rho D_\alpha \frac{\partial Y_\alpha}{\partial x}) + S_\alpha \tag{3.1}$$

Equation 3.1 can be rearranged and source or sink terms can be written as

$$\begin{aligned} S_\alpha &= \frac{\partial}{\partial t}(\rho Y_\alpha^*) + \frac{\partial}{\partial x_i}(\rho u_i Y_\alpha^*) - \frac{\partial}{\partial x_i}(\rho D_\alpha \frac{\partial Y_\alpha^*}{\partial x}) && (3.2)\\ &= accumulation(storage) + convection - diffusion && (3.3)\\ &= S_{\alpha,1} + S_{\alpha,2} - S_{\alpha,3} && (3.4) \end{aligned}$$

Where Y_α^* are the mass fractions of species taken from constrained equilibrium calculations. Discretization of these terms are described in Sec. 4.1 and 4.5. In case of CO, below 600°C CO reactions (production and destruction) are very slow. This means in regions where temperature is below this limit, CO source and sink term should be taken zero.

3.4.5 Transport calculations with source terms derived from equilibrium calculations

A submodel has been built solving PDE's of species balance as postprocessing. All spatial derivatives are approximated by second order finite differences and flow variables are updated in time using an explicit second order predictor corrector scheme. Explicit 2nd order Adam-Bashforth scheme is utilized for numerical integration of storage part of source

Chapter 4

Carbon monoxide prediction in enclosure fire and validations

4.1 Numerical methods

Density, velocity, temperature and mixture fraction prediction by FDS 5 at each time step and at each grid cell are employed for solving toxic species balance equation for CO as postprocessing.

In FDS 5 the density at the center of the *ijk*-th cell is updated in time with the following predictor-corrector scheme. In the predictor step, the density at *(n+1)*th time step is estimated based on information at the nth level.

$$\frac{\rho_{ijk,n+1}-\rho_{ijk,n}}{\delta t}+(\nabla.\rho\mathbf{u})_{ijk,n}=-\rho_{ijk,n}(\nabla.\mathbf{u})_{ijk,n} \tag{4.1}$$

Density is corrected by

$$\frac{\rho_{ijk,n+1}-0.5(\rho_{ijk,n}+\rho_{ijk,n+1})}{0.5\delta t}+(\nabla.\rho\mathbf{u})_{ijk,n+1}=-\rho_{ijk,n+1}(\nabla.\mathbf{u})_{ijk,n+1} \tag{4.2}$$

The convective terms are discretized as upwind biased differences in the predictor step and downwind biased differences in the corrector step [1]. In the equation, the symbol $\pm$ means + in the predictor step and - in the corrector step.

$$\begin{aligned}(\nabla.\rho\mathbf{u})_{ijk} \;=\; & \frac{1\mp\varepsilon_u}{2}u_{ijk}\frac{\rho_{i+1,jk}-\rho_{ijk}}{\delta x}+\frac{1\pm\varepsilon_u}{2}u_{i-1,jk}\frac{\rho_{ijk}-\rho_{i-1,jk}}{\delta x}\\ & +\frac{1\mp\varepsilon_v}{2}v_{ijk}\frac{\rho_{i,j+1,k}-\rho_{ijk}}{\delta y}+\frac{1\pm\varepsilon_v}{2}v_{i,j-1,k}\frac{\rho_{ijk}-\rho_{i,j-1,k}}{\delta y}\\ & +\frac{1\mp\varepsilon_w}{2}w_{ijk}\frac{\rho_{ij,k+1}-\rho_{ijk}}{\delta z}+\frac{1\pm\varepsilon_w}{2}w_{i,j,k-1}\frac{\rho_{ijk}-\rho_{ij,k-1}}{\delta z}\end{aligned} \tag{4.3}$$

These are simple central difference approximations without inclusion of ε. The $\varepsilon's$ are local Courant numbers, where $\varepsilon_u=u\delta t/\delta x, \varepsilon_v=v\delta t/\delta y, \varepsilon_w=w\delta t/\delta z$ where velocity components are those local values. Their role is to bias the differencing upwind at the predictor step.

The species conservation equations are defined as follows at predictor step

$$\frac{(\rho Y_\alpha)_{ijk,n+1} - (\rho Y_\alpha)_{ijk,n}}{\delta t} + (\mathbf{u}.\nabla \rho Y_\alpha)_{ijk,n} = (\nabla.\rho D_\alpha \nabla Y_\alpha)_{ijk,n} + S_{\alpha,ijk,n+1} \tag{4.4}$$

The convective term in the species transport equation $(\mathbf{u}.\nabla \rho Y_\alpha)_{ijk}$ is defined in a similar way like Eqn. 4.3. For corrector step following equation is used:

$$\frac{(\rho Y_\alpha)_{ijk,n+1} - 0.5((\rho Y_\alpha)_{ijk,n} + (\rho Y_\alpha)_{ijk,n+1})}{0.5\delta t} + (\mathbf{u}.\nabla \rho Y_\alpha)_{ijk,n+1} = (\nabla.\rho D_\alpha \nabla Y_\alpha)_{ijk,n+1} + S_{\alpha,ijk,n+1} \tag{4.5}$$

For the material diffusion terms, central differences are used with no upwind or downwind bias, thus they are defined in both predictor and corrector steps in the same way:

$$\begin{aligned}
(\nabla.\rho D_\alpha \nabla Y_\alpha)_{ijk} &= \frac{1}{\delta x}[\rho D_{\alpha,i+\frac{1}{2},jk} \frac{Y_{\alpha,i+1,jk} - Y_{\alpha,ijk}}{\delta x} - \rho D_{\alpha,i-\frac{1}{2},jk} \frac{Y_{\alpha,ijk} - Y_{\alpha,i-1,jk}}{\delta x}] \\
&+ \frac{1}{\delta y}[\rho D_{\alpha,i,j+\frac{1}{2},k} \frac{Y_{\alpha,i,j+1,k} - Y_{\alpha,ijk}}{\delta y} - \rho D_{\alpha,i,j-\frac{1}{2},k} \frac{Y_{\alpha,ijk} - Y_{\alpha,i,j-1,k}}{\delta y}] \\
&+ \frac{1}{\delta z}[\rho D_{\alpha,ij,k+\frac{1}{2}} \frac{Y_{\alpha,ij,k+1} - Y_{\alpha,ijk}}{\delta z} - \rho D_{\alpha,ij,k-\frac{1}{2}} \frac{Y_{\alpha,ijk} - Y_{\alpha,ij,k-1}}{\delta z}]
\end{aligned} \tag{4.6}$$

where $\rho D_{\alpha,ijk} = \frac{\mu_{t,ijk}}{Sc}$, μ_t is the turbulent viscosity and Sc is the turbulent Schmidt number.

The most crucial part of this model is the numerical integration of source term with convection-diffusion term. Generally, chemical reaction source is a stiff Ordinary Differential Equation (ODE). Different numerical schemes [32, 18, 59, 10, 33] are available for the numerical integration of stiff ODEs. Explicit 2nd order Adams-Bashforth scheme are employed for numerical integration of storage part of source term

$$S_{\alpha,1,ijk,n+1} = \frac{1}{2}(3S_{\alpha,1,ijk,n} - S_{\alpha,1,ijk,n-1}) \tag{4.7}$$

Since we do not know the production or destruction rate of chemical species α, S_α, because of the lack of availability of chemical kinetics, an artificial source term can be calculated as described in Sec. 3.4.4. For all the simulations of this chapter, only storage part of source term is used and concentrations are used from "Lookup" table:

$$S_{\alpha,1,ijk,n} = \frac{Y^*_{\alpha,ijk,n} - Y^*_{\alpha,ijk,n-1}}{\delta t}\ \rho_{mixture}\ (\delta x \delta y \delta z) \tag{4.8}$$

$$Y^*_{\alpha,ijk,n} = f(T_{ijk,n}, Z_{ijk,n}) \quad \textit{Lookup table} \tag{4.9}$$

where mass fractions of species are converted from volume fraction by following formula

$$Y^*_\alpha = X_\alpha \frac{M_\alpha}{M_{mix}} \tag{4.10}$$

Where T and Z are the temperature and mixture fraction of grid cell respectively. Species mass fraction, Y^*_α, of the source term of transport equation have been used from

"Lookup" table according to temperatures and mixture fractions which are predicted by FDS 5 at each grid cell at each time step. Consequently, this model is very sensitive to temperature and mixture fraction prediction capability. The better the temperature and mixture fraction prediction, the better toxicant prediction.

The 2nd order finite difference scheme used here is as like FDS. In case of coarse grid, steep gradient of species mass fraction can cause local over-shoots and under-shoots. An over-shoot occurs if mass fraction of species is greater than its permissible maximum, typically 1. An under-shoot occurs if species mass fraction is less than its minimum value, zero. In other words numerical methods transport into or out more mass than physically possible. The overall numerical scheme is mass conserving but non-physical in region of high gradients. The mass flux correction is performed in predictor-corrector scheme like in FDS where for species calculations two loops are performed over computational domain. First loop searches to correct under-shoots and second one to correct over-shoots [1].

Boundary conditions at wall is zero gradient of species mass fraction and derivatives of species mass fraction at outflow is used as zero.

4.2 Gas Fire

4.2.1 Simulations

Numerical simulations have been conducted for FSE and RSE fires both by FDS 5 and by the developed toxic formation model. Natural gas fires with same areas as that in the tests have been set as fire sources. HRR of these fires have been set according to the heat release rate per unit area (HRRPUA) in FDS 5. Experimental HRR versus time profile for these fires were not available. Only maximum HRR are known. The HRR-time profiles are used as user input for simulations as shown in Fig. 4.1 and 4.2. The HRR-time profiles have been set for FDS input file following the experimental data of local temperature profiles of FSE and RSE respectively.

The internal boundary materials of the simulated FSE and RSE have been set to be same as in the experiments. The computational domain has been extended beyond the doorway by one third of the compartment length and 0.02 m uniform grid has been used for all simulations. All the numerical simulations have been conducted on a 2.93 GHz Intel(R) Xeon(TM) CPU and simulation times have been chosen according to the respective fire duration of the test cases.

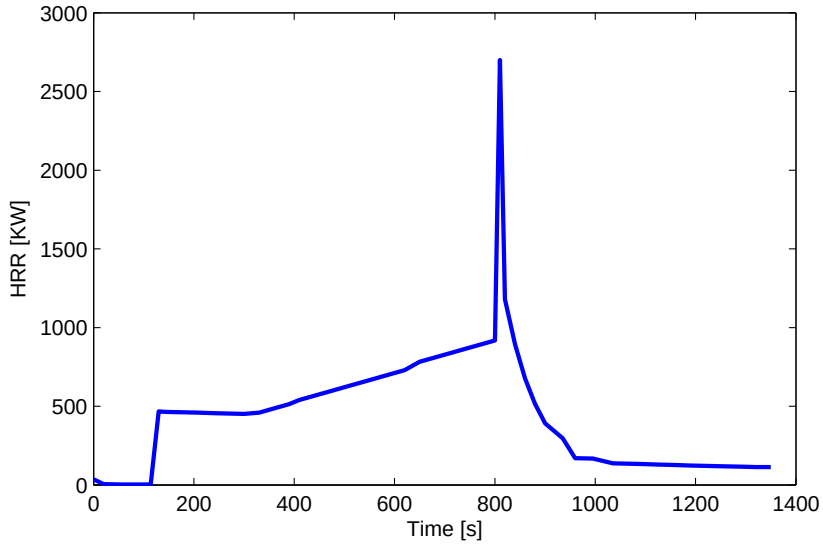

FIGURE 4.1 HRR input of FSE natural gas fire

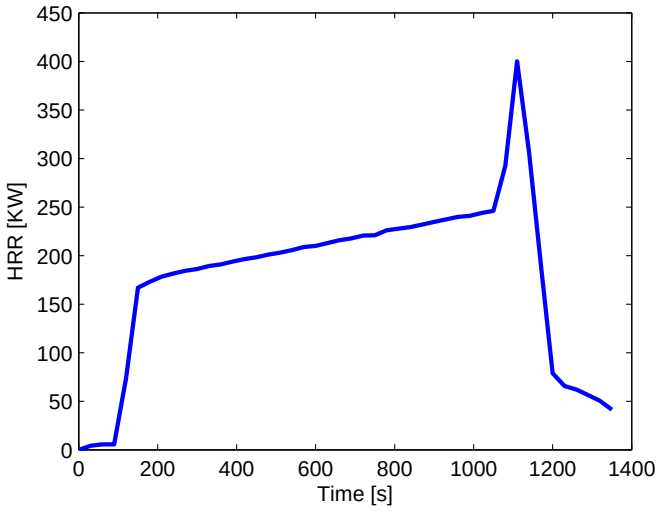

FIGURE 4.2 HRR input of RSE natural gas fire

4.2.2 Temperature predictions and validations

Temperature profiles predicted by FDS 5 simulations have been compared to the data collected from the reported measured values [47] for 2700 kW (FSE) and 400 kW (RSE) fires. The simulation of FSE for 2700 kW fire overpredicts temperatures by about 300 K at the slowly growing phase (130 s to 825 s) at the front and by about 300 K in the rear of enclosure (See Fig. 4.3). In case of 400 kW RSE fire, the computed temperatures at the front are about 300 K higher than the measured data (See Fig. 4.4) and at the rear location computed temperatures are about 400 K higher than the experimental data.

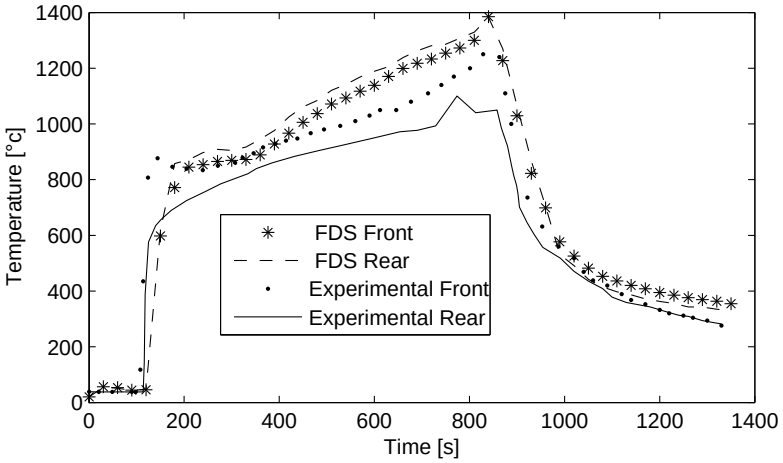

FIGURE 4.3 Transient temperatures at front and rear location of FSE natural gas fire

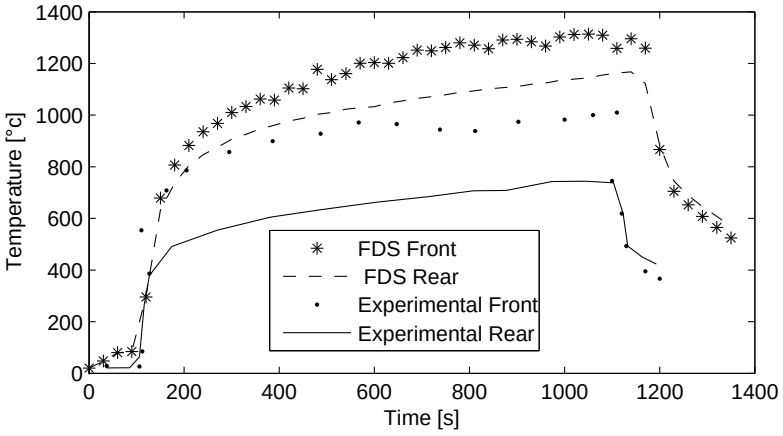

FIGURE 4.4 Transient temperatures at front and rear location of RSE natural gas fire

Such discrepancies result mainly due to the simplified combustion model employed in FDS 5. FDS 5 predicts temperatures reasonably for near stoichiometric or overventilated conditions while prediction quality deteriorates with underventilated burning conditions [1]. In order to predict temperature reasonably for underventilated condition, detailed chemical kinetics of combustion is required. In addition smaller length and time scales are needed for combustion processes with detailed kinetics. This needs enormous computational time. Therefore, mixture fraction model is utilized in FDS with Large Eddy Simulation (LES) where the grid is not fine enough to resolve the diffusion of fuel and oxygen. However, detailed kinetics implementation is not feasible for large scale problems of the fire safety community [1]. Apart from this, chemical kinetics of most of the burning materials are beyond the state of the art of fire research due to its variety and complexity. In spite of all these limitations and in order to get better predictions, multi-step reaction mechanism in form of mixture fraction approach can be applied in combustion modelling. The most

significant reaction stages for such sooting flames combustion are

- complete combustion products when air is in excess,
- carbon monoxide production at GER above 1, i.e. fuel rich conditions,
- production of carbon soot and termination of combustion reaction above still higher GER, i.e. more excess fuel,
- co-existance of unburnt fuel with combustion products.

Ignoring significant elementary reaction steps leads to errors in heat release rate of combustion simulation. However, inclusion of more mixture fraction variables will increase computational time but result in realistic prediction of different burning conditions. Additionally, experiments are also required to improve our understanding of underventilated burning conditions.

4.2.3 Carbon monoxide predictions and validations

CO prediction both by the new developed toxic formation model as well as by FDS 5 are recorded at the location where experimental CO data are available. FDS 5 CO model for underventilated fire is achieved for CO prediction (See Sec. 2.2.2). 0.37 CO yield is used for CO prediction by FDS 5. This is the maximum CO yield measured at underventilated methane burning [57]. In fact, CO yield should be taken from the well-ventilated postflame measurement [1]. In such case, FDS 5 CO prediction further deteriorates. (0.5 m, 0.5 m, 2.0 m) is the front location and (0.5 m, 3.17 m, 2.0 m) is the rear location inside the FSE. (0.2 m, 0.2 m, 0.8 m) is the front and (0.2 m, 1.26 m, 0.8 m) is the rear location inside RSE. Figures 4.5, 4.7, 4.8 and 4.10 show comparison of predictions with experimental data. FDS 5 CO model underpredicts CO concentrations at both locations. The new developed toxic formation model overpredicts CO concentrations and results show fluctuating behavior of CO at a specific location with time. Simulations are conducted for 0.10 m, 0.05 m and 0.02 m in order to check grid dependency of simulations. Consistent results are obtained by using 0.02 m grid. Predicted mixture fraction-time profile by FDS 5 at front locations are monitored which are zero with some sudden increases as shown in Fig. 4.6 and 4.9. There was no mixture fraction experimental data for this location to compare to the prediction. Fluctuations of mixture fraction in a specific location may lead to fluctuations in CO prediction. Now effect of temperatures prediction on CO prediction will be analyzed. Predictions of temperatures are discussed in sec. 4.2.2. Computed temperature profile at FSE front is reasonable and predicted CO profile is reasonable as well. Computed temperature profile at FSE rear is about 300°C higher than experimental data. This overprediction could result in about 3 vol% overprediction of CO concentration (see Fig. 3.2) at a particular GER according to constrained equilibrium calculations of natural gas (95% methane). Figure 4.7 shows CO overprediction varying from 0 to 2 vol%. Furthermore, computed temperature at RSE rear is about 400°C higher than experimental one and Fig. 4.10 shows CO concentration is about 3 vol% higher than experimental data.

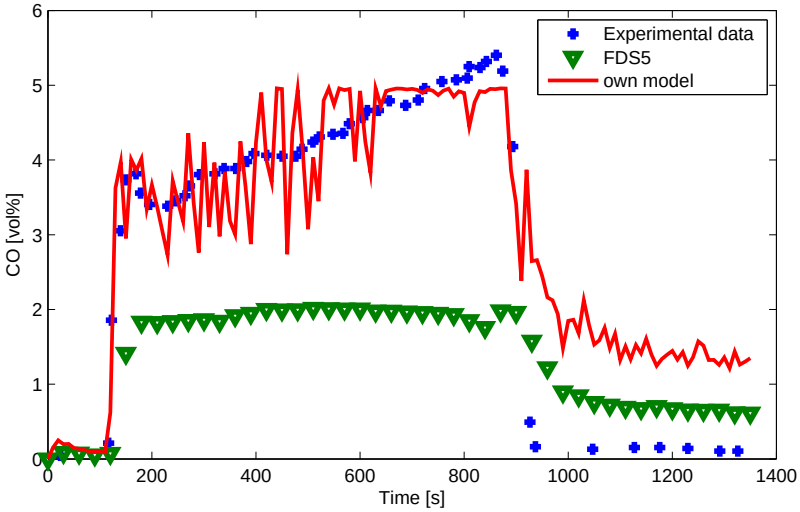

FIGURE 4.5 Validation of computed CO concentrations at front location (0.5 m, 0.5 m, 2.0 m) of FSE natural gas fire

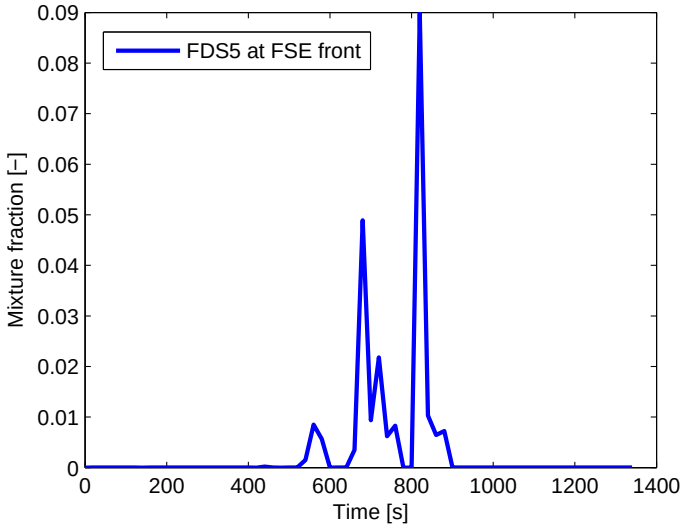

FIGURE 4.6 Mixture fractions computed by FDS 5 at front location (0.5 m, 0.5 m, 2.0 m) of FSE natural gas fire

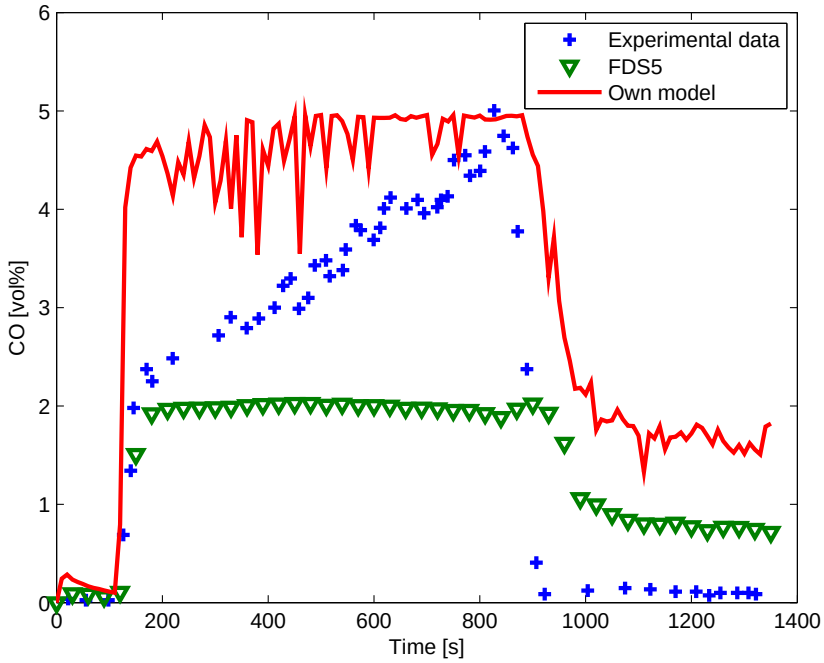

FIGURE 4.7 Validation of computed CO concentrations at rear location (0.5 m, 3.17 m, 2.0 m) of FSE natural gas fire

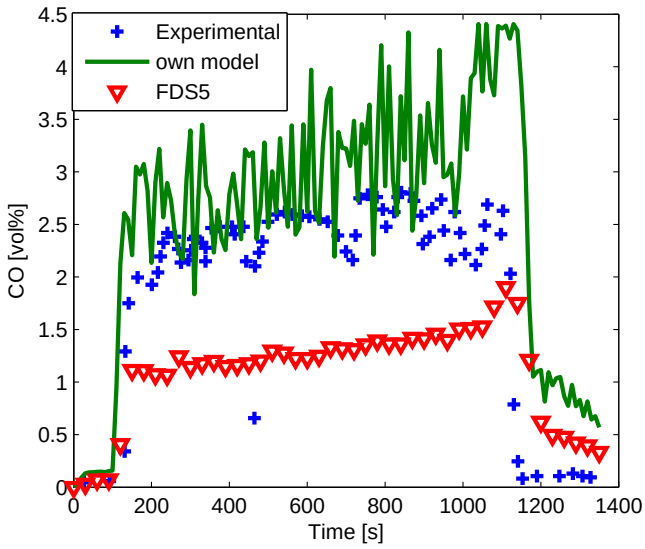

FIGURE 4.8 Validation of computed CO concentrations at front location (0.2 m, 0.2 m, 0.8 m) of RSE natural gas fire

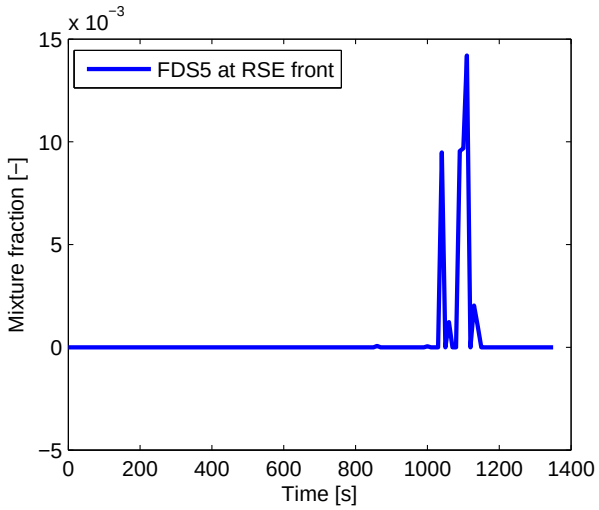

FIGURE 4.9 Mixture fractions computed by FDS 5 at front location (0.2 m, 0.2 m, 0.8 m) of RSE natural gas fire

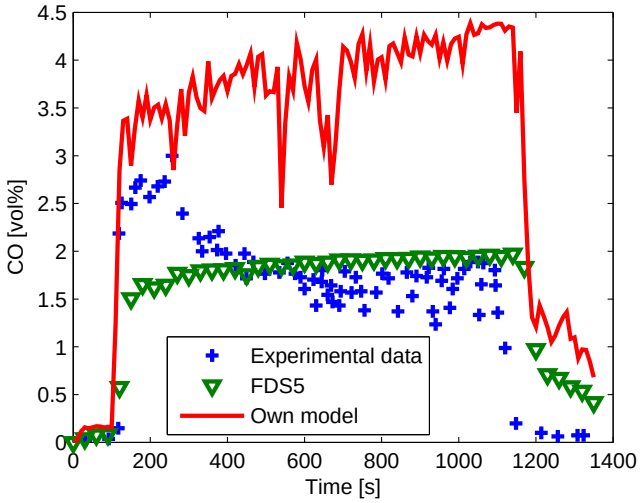

FIGURE 4.10 Validation of computed CO concentrations at rear location (0.2 m, 1.26 m, 0.8 m) of RSE natural gas fire

4.3 Plastic fire

NIST conducted experiments using an enclosure that is roughly a 2/5 scale replicate of the ISO 9705 room (RSE explained in sec. 4.2). The original RSE dimension was 0.98 m wide × 0.98 tall × 0.146 m deep, however for this experiment internal dimensions were measured as 0.95 m wide × 0.98 m tall × 0.142 m deep, with pre burn uncertainty of less than 1 cm on each dimension. The standard doorway geometry was 0.81 m tall × 0.48 m wide and centered horizontally on the 95 cm front wall. The steel frame of the enclosure was lined with 2 layers of 0.127 m thick insulation boards. Different fuels (i.e. Natural gas, Heptane,

Toluene, Polystyrene etc) including gases, liquids and solids at ambient temperatures are used in experiments which included local measurements of temperatures and species compositions. Polystyrene test case is chosen to simulate because this is the only one plastic material available with transient local concentration data. A rigid self supporting ceramic fiber (alumina and silica) board was used during the test case of polystyrene pellets burning in the enclosure. Polystyrene pellets were burned using a round pan of 0.60 m diameter. Burners were centered on the floor. The polystyrene fuel was clear granulated with average molecular mass of 230.8 kg/mol. Details of the experiment is available in NIST technical report [17].

4.3.1 Simulations

Numerical simulations have been conducted for the test case both by FDS 5 and developed toxic formation. CO yield used for FDS 5 simulation is 0.2 whereas well-ventilated CO yield is 0.05 [11]. Polystyrene pan fire with same area as that in the tests have been set as fire source. HRR of these fires have been set according to the heat release rate per unit area (HRRPUA) in FDS 5. Experimental HRR versus time profile for these fire is set as user input for the simulation as shown in Fig. 4.11.

The internal boundary material of the RSE has been set to be same as in the experiment. The computational domain has been extended beyond the doorway by one third of the compartment length and 0.02 m uniform grid has been employed for the simulation. The numerical simulation has been conducted in 2.33 GHz Intel Core Duo CPU and simulation has been run for 1100 s. Simulated CO concentrations at (0.2 m, 0.2 m, 0.8 m) and (0.2 m, 1.26 m, 0.8 m) have been compared with experimental data.

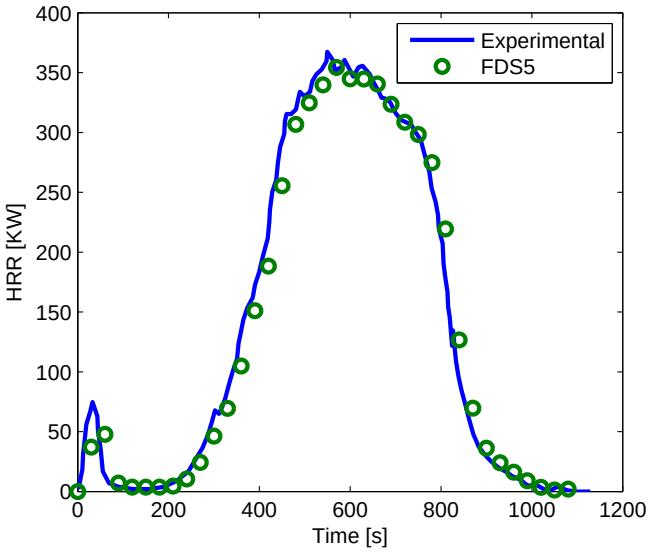

FIGURE 4.11 HRR input of RSE polystyrene fire simulation and experimental data

4.3.2 Carbon monoxide predictions and validations

The model overpredicts CO concentrations at both locations (see Fig. 4.12 and Fig. 4.14). Mixture fraction profile (see Fig. 4.13) predicted by FDS 5 is fluctuating like in the other FSE and RSE simulations. Experimental temperature profiles at front and rear were not available to compare temperature predictions. However, temperature overprediction certainly occurs due to simplified combustion model of FDS 5.

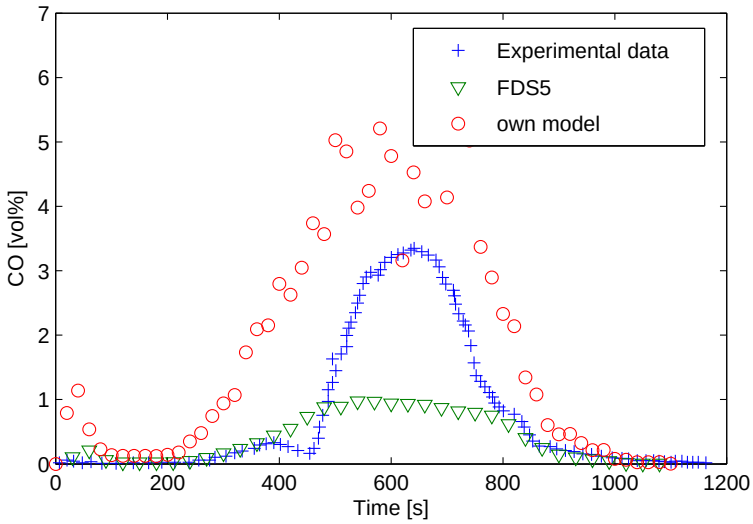

FIGURE 4.12 Validation of computed CO concentrations at position (0.2 m, 0.2 m, 0.8 m) of RSE polystyrene fire

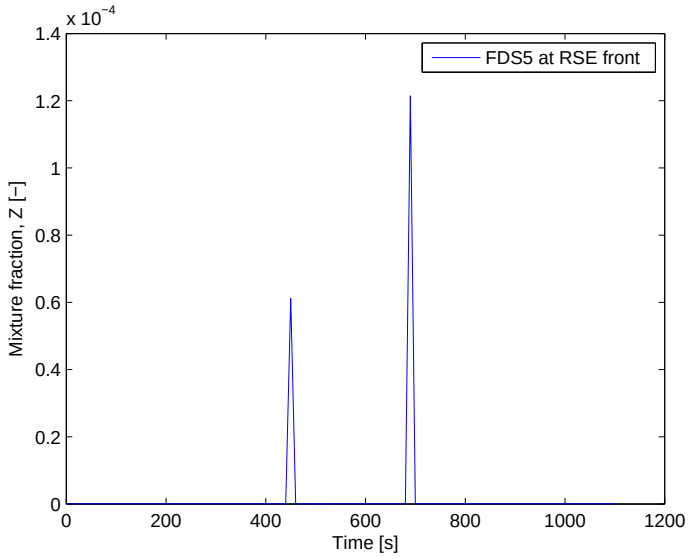

FIGURE 4.13 Mixture fractions computed by FDS 5 at location (0.2 m, 0.2 m, 0.8 m) of RSE polystyrene fire

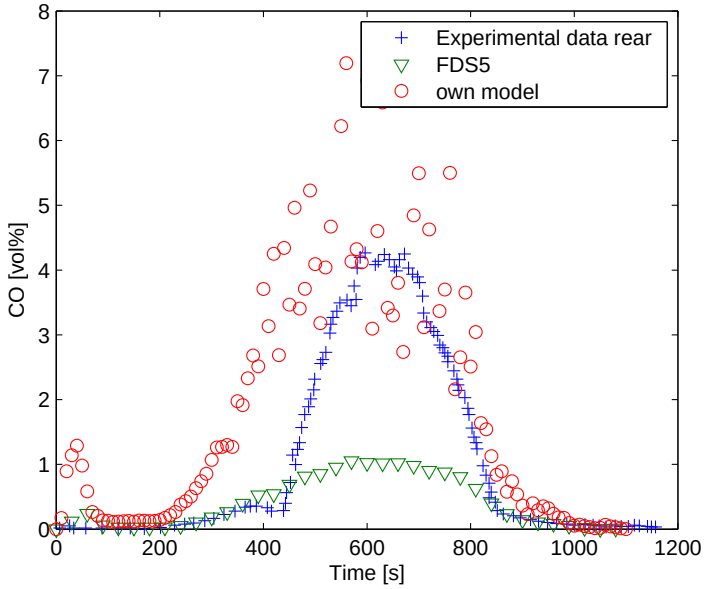

FIGURE 4.14 Validation of computed CO concentration at position (0.2 m, 1.26 m, 0.8 m) of RSE polystyrene fire

Since the CO source term used in the transport equation depends on temperature and mixture fraction prediction of FDS 5, significant discrepancies in concentrations occur due to temperature and mixture fraction overprediction. Further development of the CO prediction is possible through development of the existing combustion model for better temperature and mixture fraction prediction. An approach of further development of the combustion model is proposed in sec. 4.2.2. The FDS 5 combustion model and the developed toxic formation both assume very fast chemical reactions. In reality, combustion reaction rate plays a significant role in the combustion processes. Fuel and oxygen mixing or turbulence mixing and reaction interaction determine total heat production. Additionally, the developed toxic formation ignores heat balance of CO formation during calculation as it is constructed as postprocessing.
The limitation of this model is that it can not be used for steady state condition because the source term becomes zero. Despite of all these limitations, this simplified model can also be utilized to predict other toxicants (HCN, HCl etc.) in enclosure fire. No experimental data was found to compare other toxicants concentrations inside enclosure with the model prediction. Experimental data of other toxicants as well as for other burning substances are required for further testing of the model.

4.4 Sensitivity of simulations

It has been discussed already that the results of simulations are highly sensitive to temperature and mixture fraction prediction. Sensitivity of simulations to time step are to be explained in this section. The time step is constrained by Courant-Friedrichs-Lewy (CFL)

condition where convective transport dominates diffusive transport especially in large scale conditions. CFL condition is

$$\delta t \; max(\frac{|u_{ijk}|}{\delta x}, \frac{|v_{ijk}|}{\delta y}, \frac{|w_{ijk}|}{\delta z}) < 1 \tag{4.11}$$

CFL condition implies that the time step should not be larger than the time that allows a parcel of fluid to cross a grid cell. However, Von Neumann criterion should be used for finely gridded domains (i.e. LES calculation with grid cells of 5 mm) [1]. Minimum 2 cm grid size have been used for all the simulations. Therefore, CFL condition is maintained. Polystyrene fire is simulated with three different time steps in order to check sensitivity of the simulation to time step. Figure 4.15 shows simulated CO concentrations at different time steps. This reveals that CO concentrations are not significantly sensitive to time step when CFL condition is followed.

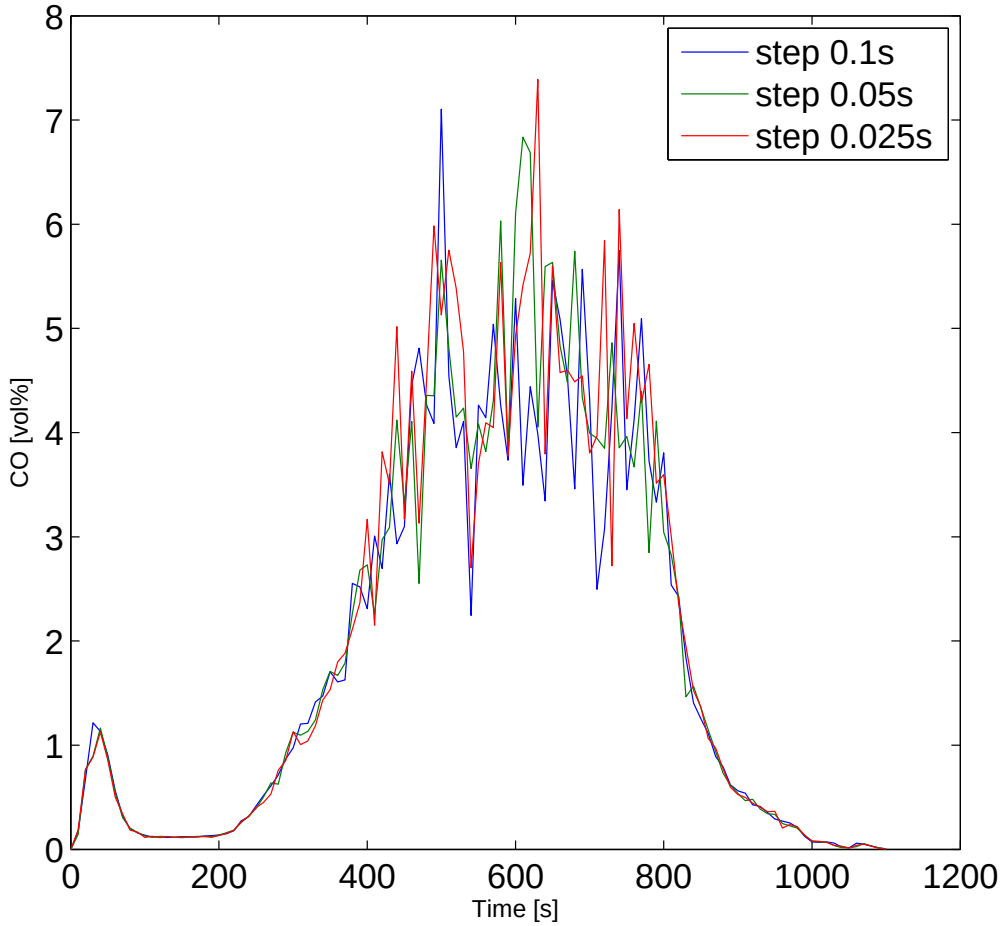

FIGURE 4.15 Sensitivity of simulations to time step

4.5 Simulation with three parts of source terms

Convective parts of source term is discretized as follows

$$\begin{aligned} S_{\alpha,2} &= u_{ijk,n}\rho_{i+1,jk,n}\frac{Y^*_{ijk,n}-Y^*_{i+1,jk,n}}{\delta x} + u_{i-1,jk,n}\rho_{i-1,jk,n}\frac{Y^*_{ijk,n}-Y^*_{i-1,jk,n}}{\delta x} \\ &+v_{ijk,n}\rho_{i,j+1,k,n}\frac{Y^*_{ijk,n}-Y^*_{i,j+1,k,n}}{\delta y} + v_{i,j-1,k,n}\rho_{i,j-1,k,n}\frac{Y^*_{ijk,n}-Y^*_{i,j-1,k,n}}{\delta y} \\ &+w_{ijk,n}\rho_{ij,k+1,n}\frac{Y^*_{ijk,n}-Y^*_{ij,k+1,n}}{\delta z} \\ &+w_{ij,k-1,n}\rho_{ij,k-1,n}\frac{Y^*_{ijk,n}-Y^*_{ij,k-1,n}}{\delta z} \end{aligned} \tag{4.12}$$

Diffusive part of source term is discretized as

$$\begin{aligned} S_{\alpha,3} &= \frac{1}{\delta x}(\rho D)_{\alpha,i+\frac{1}{2}}\frac{Y^*_{ijk,n}-Y^*_{i+1,jk,n}}{\delta x} + \frac{1}{\delta x}(\rho D)_{\alpha,i+\frac{1}{2}}\frac{Y^*_{ijk,n}-Y^*_{i-1,jk,n}}{\delta x} \\ &+\frac{1}{\delta y}(\rho D)_{\alpha,i+\frac{1}{2}}\frac{Y^*_{ijk,n}-Y^*_{i,j+1,k,n}}{\delta y} + \frac{1}{\delta y}(\rho D)_{\alpha,i+\frac{1}{2}}\frac{Y^*_{ijk,n}-Y^*_{i,j-1,k,n}}{\delta y} \\ &+\frac{1}{\delta z}(\rho D)_{\alpha,i+\frac{1}{2}}\frac{Y^*_{ijk,n}-Y^*_{ij,k+1,n}}{\delta z} + \frac{1}{\delta z}(\rho D)_{\alpha,i+\frac{1}{2}}\frac{Y^*_{ijk,n}-Y^*_{ij,k-1,n}}{\delta z} \end{aligned} \tag{4.13}$$

Source is calcualted using Eqn. 4.7, 4.12 and 4.13 for polystyrene fire at center of RSE geometry. In grid cells where temperatures are below 600°C source term is set to zero. The modified sources are then used with species transport equation as explained in Sec. 4.1. Results of the simulation were not stable. This may occurs because convective and diffusive parts of source term discretization method fails to follow the stiffness of "Lookup" table data. Stable numerical schemes are needed to be searched to solve this problem.

Chapter 5

Fire probability

Appropriate performance based fire protection design can not be well implemented without reasonable fire risk assessment.

5.1 Fire statistics

Fire probability is the assessment of the likelihood that a fire will occur. The probability of a fire can be estimated using fire statistics. World fire statistics [44] contains frequencies of fires and numbers of casualities in different countries of the world for the period 1993-2002. Figure 5.1 presents the average number of fires a year per 1000 inhabitants in different countries. Figure 5.2 shows fire deaths in the countries of the world in 1993-2002.

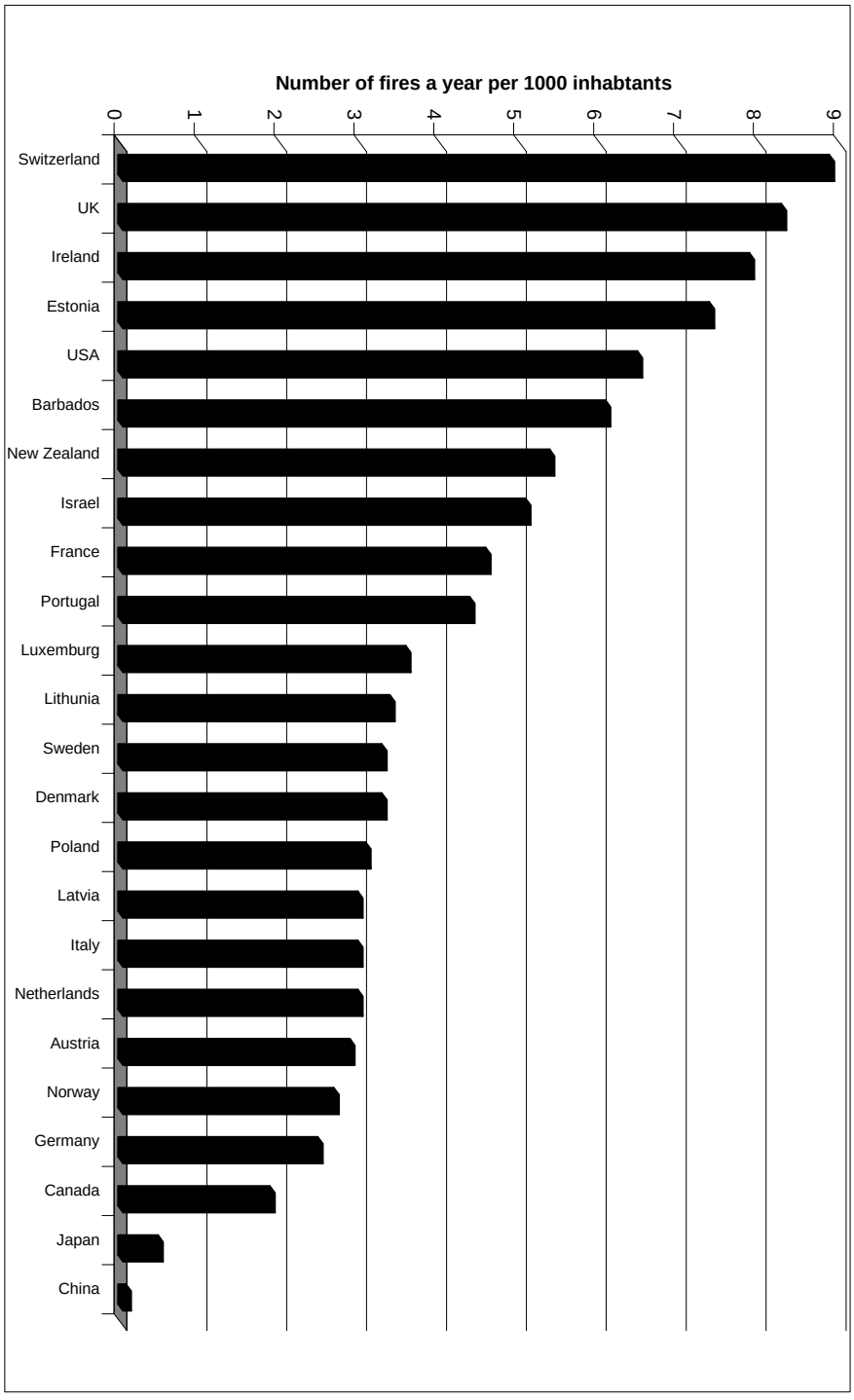

FIGURE 5.1 Fire frequencies in different countries

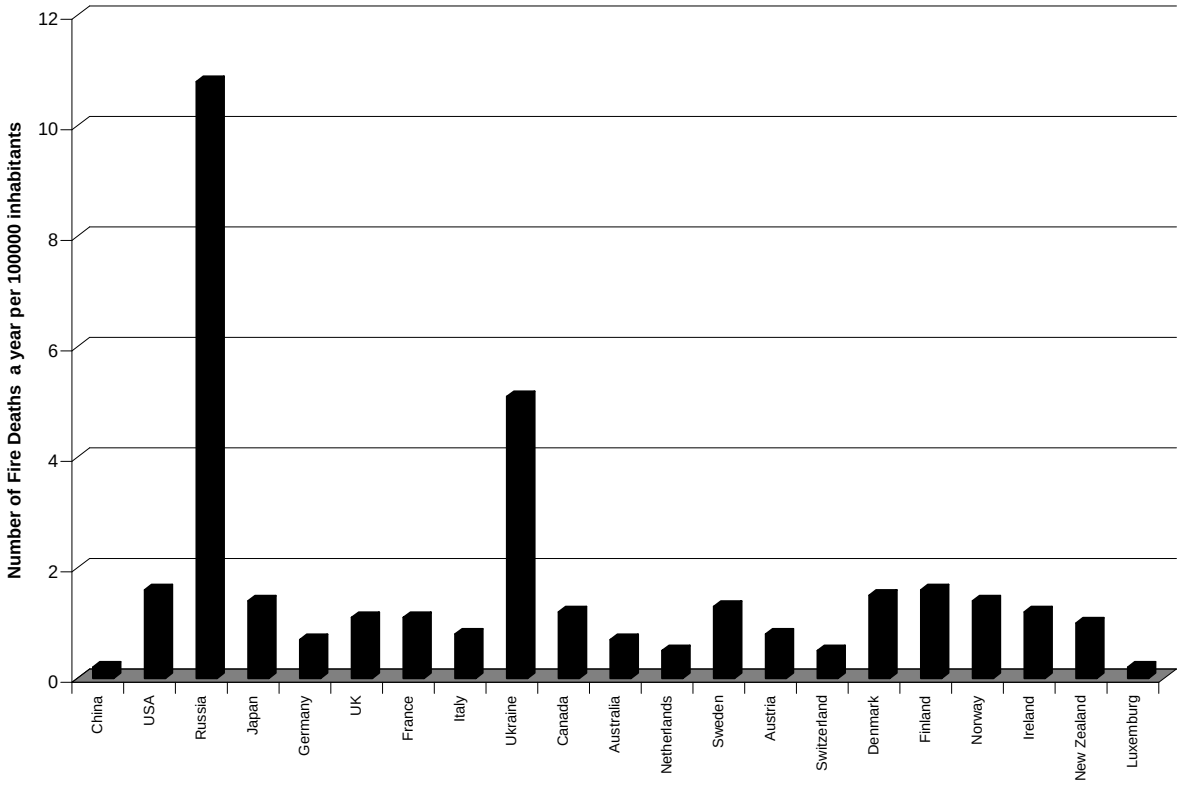

FIGURE 5.2 Fire casualties in different countries

Detailed fire statistics such as source of different types of fires (i.e. house fire, warehouse fire, wildfire), statistics of fire protection device performance in fires etc. are missing and are not available to the public at the national level in Germnay. Therefore,it is difficult to undertake a detailed analysis for the whole country, an improvement of the current system is needed. This could be facilitated by constructing a national data center for fire statistics as part of the "Bundessatistik" [6]. Because of the lack of data availability, US fire statistics are utilized here. There were 1,642,500 fires in 2006 in the United States [7]. Figure 5.3 represent the percentage of different types of fire broken out in 2006 . Residential fires represented 25.1% of all fires and 78.7% of structure fires. 79.5% of all civilian fire fatalities occurred in the home, where home is defined as one- and two-family dwellings and apartments. Of those, approximately 83.5% occurred in single-family homes and duplexes.

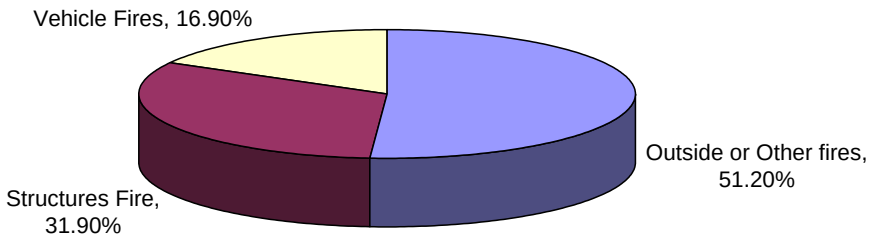

FIGURE 5.3 Fire types in US

Losses from different types of fire in 2006 are shown in Fig. 5.4.

The residential structure fire problem represents approximately 81% of all fire deaths and 79% of the injuries to civilians in 2006. Between 1997 and 2006, an average of 3,090 civilians lost their lives and another 15,340 were injured annually as the result of residential structure fires.

Residential structures include one- and two-family dwellings (including manufactured homes), apartments, hotels, motels, college dormitories, boarding houses etc. Figure 5.5 shows causes of residential structure fires. Cooking is the leading cause of fires and fire injuries in structures. Deaths and property losses due to cooking, however, are among the lowest. The leading type of material ignited in cooking fires is food, especially fats, oils, and grease. Cooking left unattended is the leading factor contributing to cooking fires.

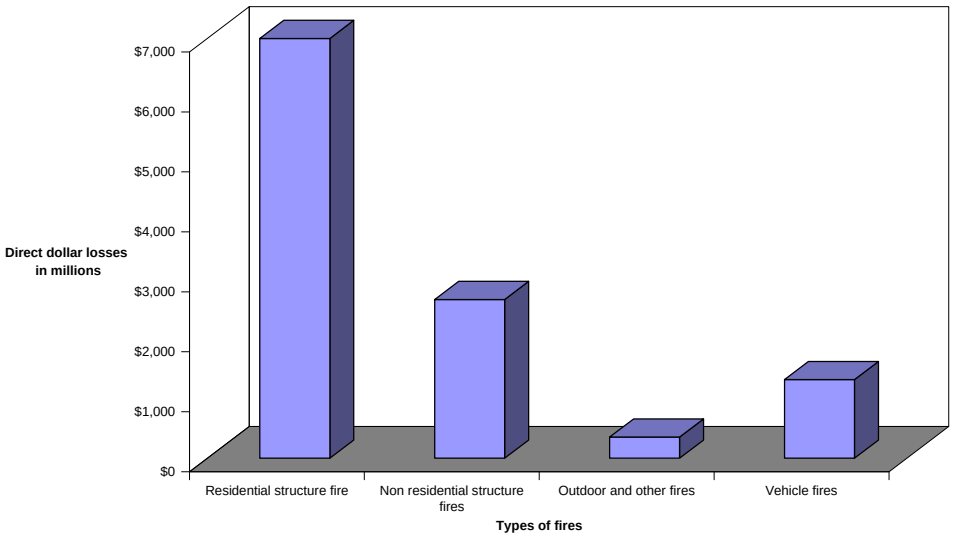

FIGURE 5.4 US fire losses in dollars

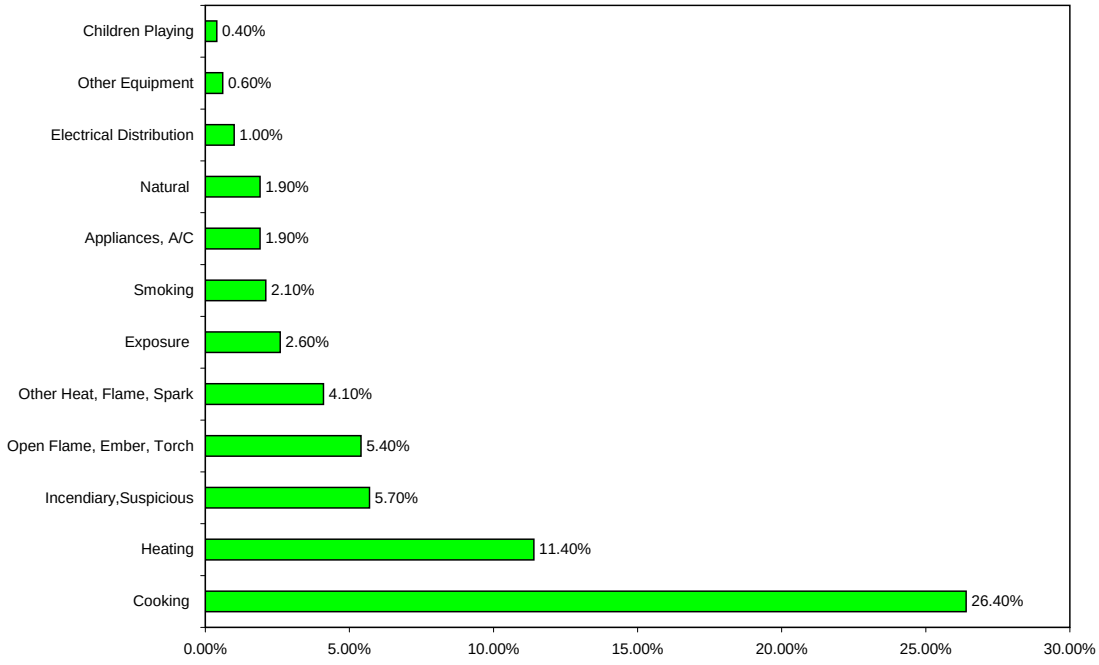

FIGURE 5.5 Causes of residential fires

5.2 Fault tree analysis of initiating event probability of fire

Fault Tree Analyis (FTA) is a most commonly used technique for causal analysis in risk and reliability studies. FTA is a top-down approach to failure analysis, starting with a potential undesirable event (accident) called TOP event, then determining all the ways it can happen. The analysis proceeds by determining how the TOP event can be caused by individual or combined lower level failures or events. FTA is a structured top-down deductive analysis. The causes of the top event are connected through logic gates. References [56, 61, 52] discuss more details about FTA. Figure 5.6 represents a fault tree of initiating event probability that fire will start in enclosures. In Fig. 5.6 combustible materials present and ignition occurs have functional dependency to start fires. Therefore, functional dependency symbol is used.

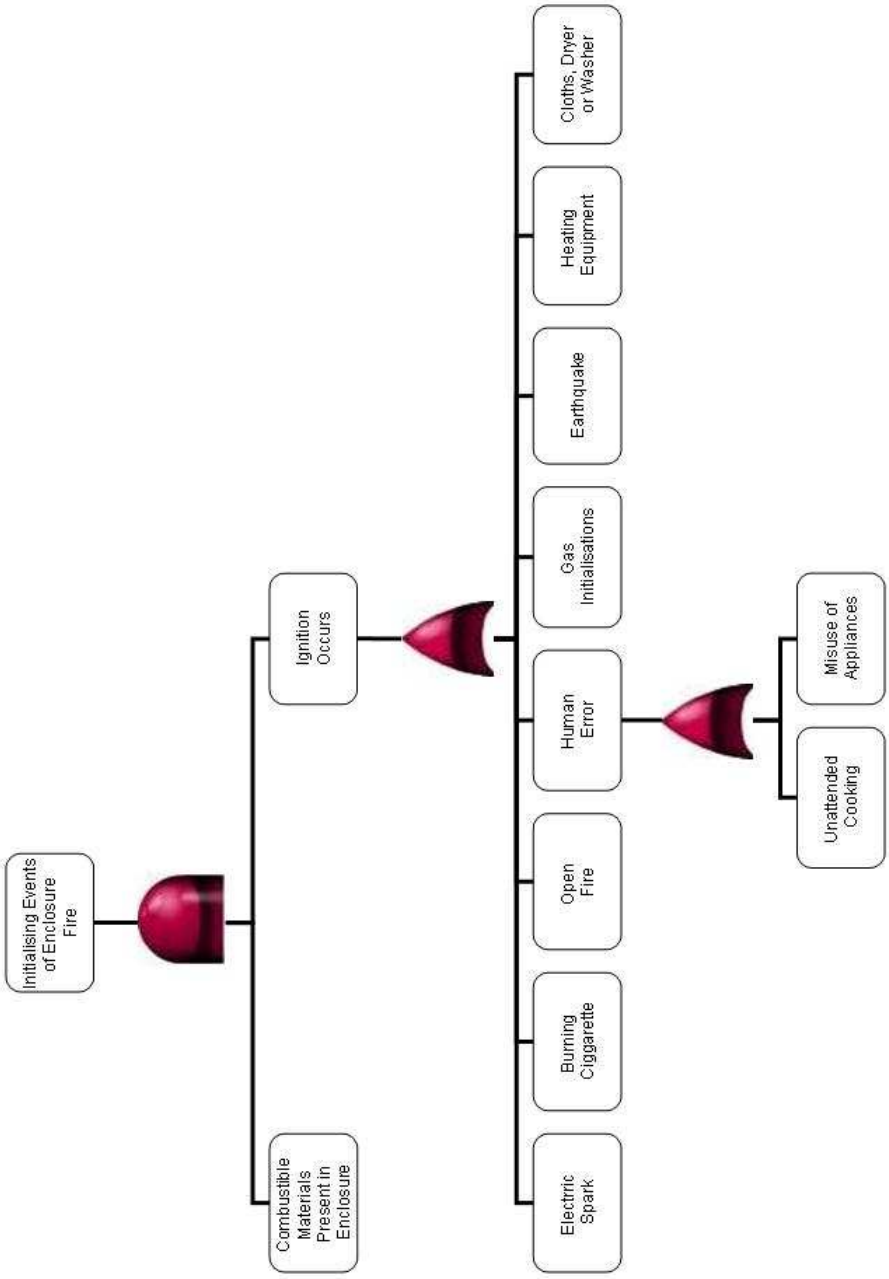

FIGURE 5.6 Fault tree diagram of initiating event probability in enclosure fire

Let assume, probability of top event occuring at time t is $A_0(t)$, probability of basic event i occuring time t is $A_i(t)$, probability of minimum cut set j failing time t $=A_j(t)$. Let $E_i(t)$ denotes the probability that basic event i is in a failed state at time t. For single AND-gate, $A_i(t) = Pr_w(E_i(t))$ for $i = 1, 2$ when basic events are independent, TOP event probability $A_0(t)$ is:

$$A_0(t) = Pr_w((E_1(t) \cap (E_2(t)) = Pr_w(E_1(t)).Pr_w(E_2(t)) = A_1(t).A_2(t) \qquad (5.1)$$

When we have single AND-gate with N basic events. Top event probabiliy $A_0(t)$ is:

$$A_0(t) = \prod_{j=1}^{N} A_j(t) \tag{5.2}$$

For single OR-gate, when basic events are independent, TOP event probability $A_0(t)$ is:

$$\begin{aligned} A_0(t) &= Pr_w((E_1(t) \cup (E_2(t)) \\ &= Pr_w(E_1(t)) + Pr_w(E_2(t)) - Pr_w(E_1(t) \cap E_2(t)) \\ &= A_1(t) + A_2(t) - A_1(t).A_2(t) \end{aligned} \tag{5.3}$$

Using these equations and knowing basic event probabilities from fire statistics, TOP event probability can be estimated. From Fig. 5.1 probability of fire in US is 6.5×10^{-3} where 31.9% of the fires are residential structural fires. 26.4% of residential fires are cooking fires. Hence, probability of cooking fire is $6.5 \times 10^{-3} \times 0.319 \times 0.264 = 5.5 \times 10^{-4}/year$ and *inhabitant*.

5.3 Event tree analysis

This section utilizes the event tree analysis (ETA) for enclosure fire similar to the technique explained for industrial fire risk event tree analysis in [13].
The time dependent event tree technique is used to analyze probable fire scenarios. There are a lot of factors such as fuel characteristics and building environment which dominate fire spread and smoke movement. For a given building, the operational reliability of fire protection system is an important influential factor for probable fire scenarios. Developing credible loss scenarios in fire is an important step in the risk assessment process. A loss scenario represents the sequence of events that can result in undesirable fire incidents. The term "loss scenario development" can be best defined as the reasoning methodology that describes the sequential relationships between time dependent fire loss events. In general, scenario modelling is an abstract representation of a real-world system or subsystem. Time limitations, complexity, and costs generally preclude the development of logic models, which represents every aspect and detail of fire loss exposure potential. Therefore, in most cases fire scenario logic models provide us with a simplified approach that attempts to include the significant aspects of fire events relevant risk-based decisions under evaluation. A comprehensive approach of scenario analysis involves

- Applying a consistent framework and systematic methodology
- Identifying contributing factors associated with fire initiating events
- Evaluating the exposure versus time profile following the initiating event. Exposure elements include fire growth, propagation, incident outcomes, and potential consequence levels

- Assessing the performance of fire protection systems (detection system, passive and active protection systems etc.) in terms of modifying the outcome of the initiating event.

Sequence of events

A scenario represents a set of time related events that can lead to various fire outcomes. One systematic approach towards structuring fire scenarios is the Source, Pathway and Target method:

- Target: The target is the focus of the risk based study and is the first thing to define. To be at risk, the target must be vulnerable to loss from the fire exposure.
- Source: After defining the targets vulnerability and value, the initiating source fire that could expose the target must be identified and screened.
- Pathway: Pathway events include those factors that either propagate or modify the source fire. Pathway propagation factors include fire growth, secondary fuel ignition, uncontrolled flame spread etc. Pathway modification factors, which will reduce the exposure of the target, include fire protection systems such as detection, emergency control systems, suppression systems, manual fire fighting efforts.

An example of scenario development worksheet is presented in a table for an enclosure fire. The table is set up as follows:

1. Evaluation Summary
   - What are the scenario boundaries?
   - What are the specific scenarios under evaluation? What is the risk focus?
2. Target
   - What is the target?
   - What is the fire exposure vulnerability of the target?
     - Temperature effects
     - Radiant heat effects
     - Smoke concentration effects
     - Toxic, corrosive gas effects
   - What is the value of the target?
3. Source
   - What are the potential initiating fire event occurrences?
   - What are the events that should be selected for further evaluation?
4. Pathway
   - What are the pathway propagators? - fire progression potentials - structural failures
   - What are the pathway modifications (i.e. fire protection systems)? - existing - proposed
5. Assumptions/Actions
   - What are the limitations

Event tree structuring

Event Tree Analysis (ETA) conveys the initiating source fire event, fire protection performance, incident outcomes, and consequences. Using ETA provides the major advantage of being able to incorporate time and conditional FPS performance probability into a scenario. ETA is used to analyse both simple and complex processes in which several FPS levels may be in place to respond to specific initiating events. To complete an ETA, a risk analyst must identify initiating source fire events, evaluate the performance of existing or proposed fire protection options, incident outcomes and consequences.

ETA Steps

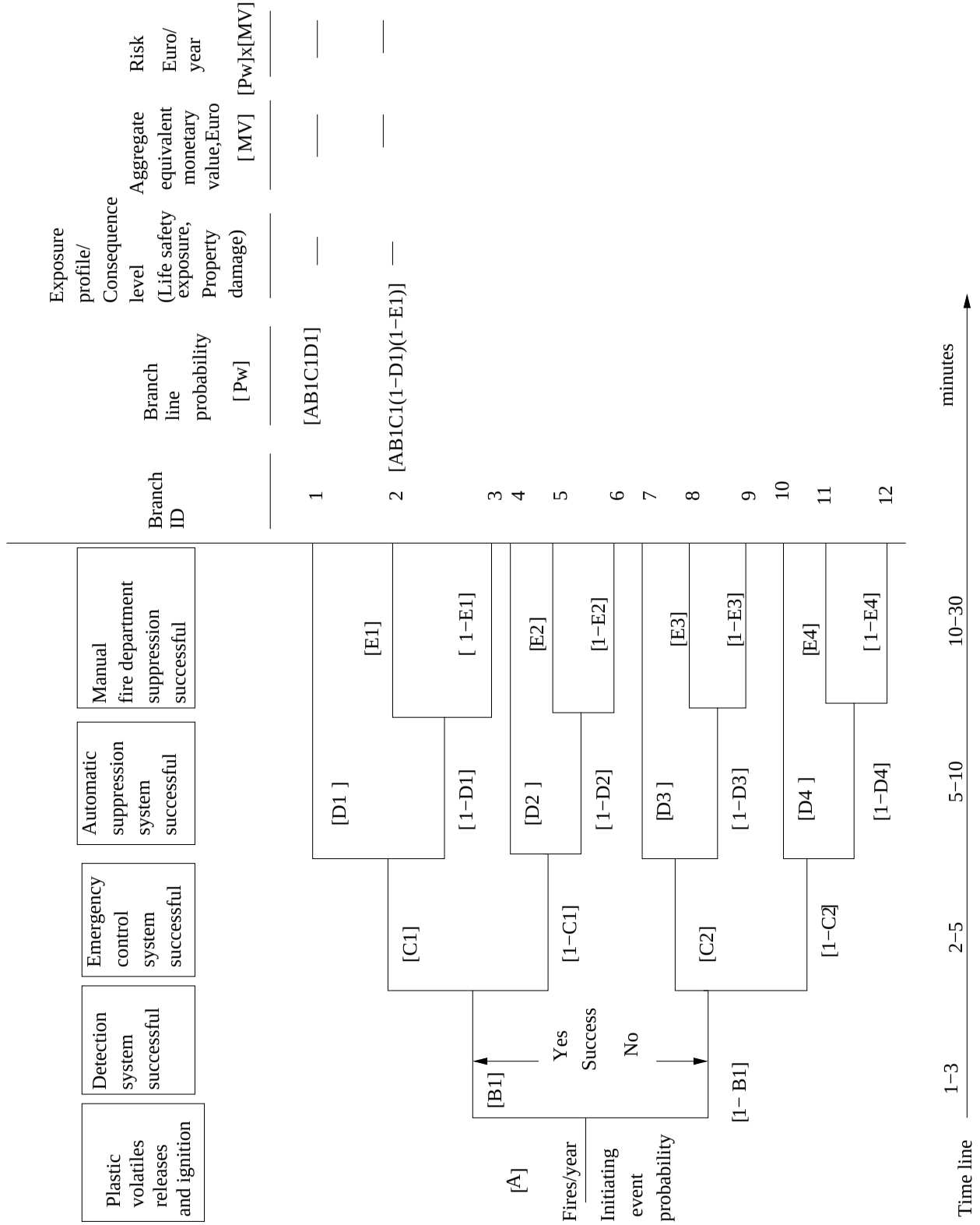

FIGURE 5.7 Fire risk event tree framework

Figure 5.7 presents an example of fire risk event tree framework for cooking fires. Similar approach can be used for other fires mentioned in Fig. 5.6. Event tree development steps include:

- Identifying the initiating fire source event,
- Identifying the pathway factors to be evaluated within the event tree analysis. For example, FPSs, existing or proposed, which will modify the propagation of the initiating fire source event,
- Structuring the event tree branch logic and time line,
- Assessing the incident outcomes,
- Identifying and quantifying exposure and consequences of concern at the target,
- Quantifying branch line probabilities. This involves quantifying the initiating event likelihood and conditional probabilities of pathway factors (i.e. FPS performance success),
- Quantifying the risk.

Identifying pathway factors

Pathway factors are those events that follow the initiating event in sequence. In constructing event tree logic, the analyst must identify significant and relevant pathway factors that will affect fire growth and propagation or mitigation of the initiating event. Intermediate pathway factors represent both a conditional state and a function of time, which is very important to recognize when addressing conditional probabilities. Both propagating and FPS factors need to be identified.

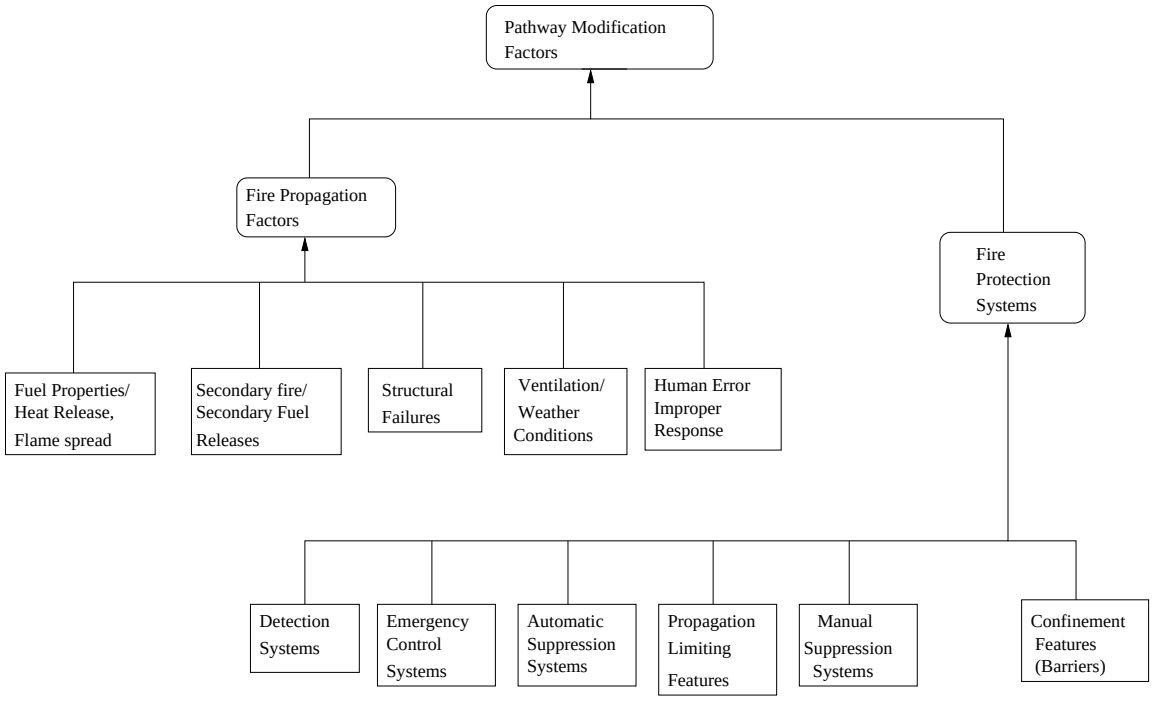

FIGURE 5.8 Pathway factors
[13]

Figure 5.8 provides an example breakdown of intermediate pathway events in terms of:

- Fire propagation factors
- FPSs for protection systems (i.e. fire mitigation)

Some fire growth or propagation factors of interest in scenario development are:

- Fuel properties (heat release rate)
- Flame spread and secondary ignition
- Ventilation effects
- Structural failures
- Operator emergency response

FPS of interest are

- Detection system
- Emergency control system
- Automatic suppression systems
- Propagation limiting features (i.e. fire barriers)
- Manual suppression systems

- Confinement features (construction or separation features that confine a fire to the area of origin)

Structuring the event tree branch logic

The event tree displays the development of accident sequences, beginning with the initiating event and proceeding to the responses of the FPSs. The results are defined fire incident outcomes that can result from initiating event. The FPS function should be depicted chronologically, although many times the events may occur almost simultaneously. Both existing and proposed FPSs can be evaluated. The initiating source event is a frequency or likelihood (i.e. events/year). The pathway factors (FPS performance) are conditional probabilities (i.e. numbers between 0 and 1). The event tree structure concerns:

- Event tree logic from left to right
- This event tree indicates system success in upward (Yes) branch segments. Probability of success = 1 - Probability of failure
- Branch line probabilities are calculated by multiplying the initiating event likelihood and the conditional branch event segment conditional probabilities
- Many fire incident outcomes are possible and are developed through different branches of event tree. The event tree outcomes are then assessed according to potential exposure versus consequence level or category
- The time line establishes a frame of reference for estimating FPS success probabilities and estimating the magnitude of the consequences at the time interval. For example, a 10 min limit could be established as the point where structural steel damage could start to occur from flammable liquid fire exposure. Therefore, to be successful in minimizing damage, we want to detect, shutdown and suppress a fire before 10-min elapsed.

Incident Outcome Assessment

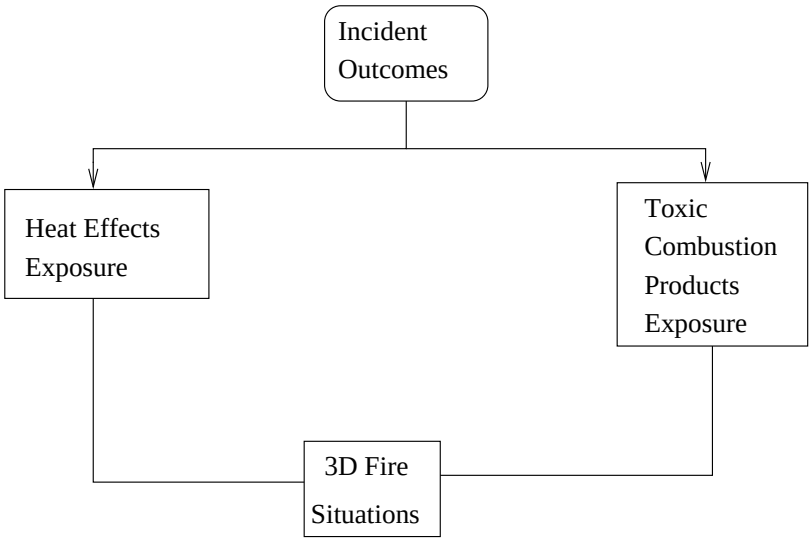

FIGURE 5.9 Fire incident outcome

Figure 5.9 shows potential incidents of primary interest in fire

- Heat from a fire
- Corrosive smoke or combustion product concentration, toxic gas concentrations

Identification and quantification of exposure and consequence levels

Fire incidents represent a multi consequence exposure, including people exposure, property damage, business interruption, environmental impacts, regulatory fines etc. Combined, these consequences can lead to very high monetary loss.

Quantify the risk

The probability of each incident outcome is determined by multiplying the initiating event frequency with conditional probabilities of the FPS performance success along each path leading to that outcome. Risk is the product of multiplying the branch line probability with the consequence value.

In order to quantify risk for cooking fire as shown in Fig. 5.7 as well as other fires, conditional probability of FPS performance success along each path and relevant consequence value are needed. Quantification of risk was not possible since sufficient statistical data do not exist.

Chapter 6

Fire hazard analysis and risk mitigation

The previous chapter describes the importance of identification and quantification of people exposure in fire as a part of risk analysis process. A modelling approach by using the new developed toxic formation model is presented in the following section which can be employed to model toxic exposure in order to mitigate toxic hazard.

6.1 Toxic exposure modelling

Much of the knowledge of materials and products is gained through standard products testing. European fire classification system for construction products does not include any requirement on combustion toxicity. In addition, toxic formation not only depends on material but also burning conditions of enclosure (ventilation, temperature etc.). CO concentrations at different locations of an enclosure can be computed by using the new developed toxic formation model to design e.g. ventilation and safe evacuation.

Smoke property especially CO concentration is estimated and compared with performance criteria based on threshold damage level. CO concentrations of 1000 to 8000 ppm (0.1 -0.8 vol%) may cause human beings to become incapacitated if exposed 1 to 2 minutes. RSE polystyrene fire with different ceiling heights (0.98 m, 1.5 m and 2.5 m) are simulated and CO concentrations are analyzed at door or exit (0.8 m from floor). Results (Fig. 6.1) illustrate that CO concentrations are zero at any time if ceiling height is 2.5 m. Smoke (CO) is transported toward ceiling due to buoyancy and stays above 0.8 m height when 2.5 m ceiling height is used. CO concentration at door increases with decreasing ceiling height.

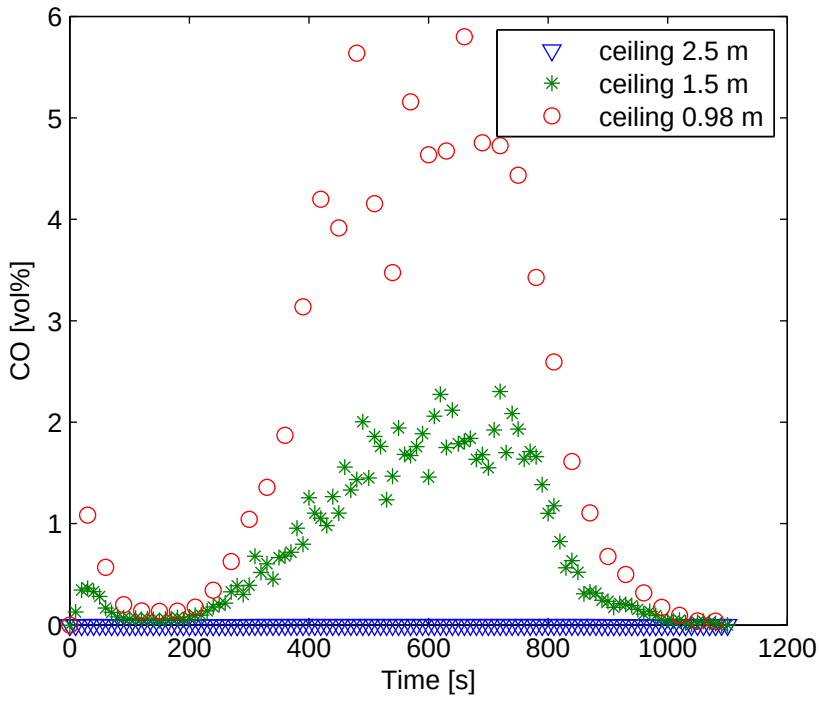

FIGURE 6.1 CO concentrations at exit in an enclosure with varying ceiling height

Influence of ventilation on local CO concentration is analyzed by simulating RSE polystyrene fire (sec. 4.3) with three different door openings: 0.58 m door width, 0.48 m door width and 0.24 m door width. Transient local concentrations decrease with increasing door width which are shown in Fig. 6.2. This occurs because the local equivalence ratios decrease with the bigger opening due to more air-flow through the opening and the volatiles from polystyrene react with more oxygen.

Thus designing appropriate geometry and ventilation conditions can mitigate toxic exposure at a specific area of the enclosure and thereby can lead to a safer evacuation for individuals during enclosure fires. Reduction of toxic exposure results in reduction of fire risk. By providing all the input in ETA (See Fig. 5.7), fire risk and risk mitigation can be estimated for a specific case.

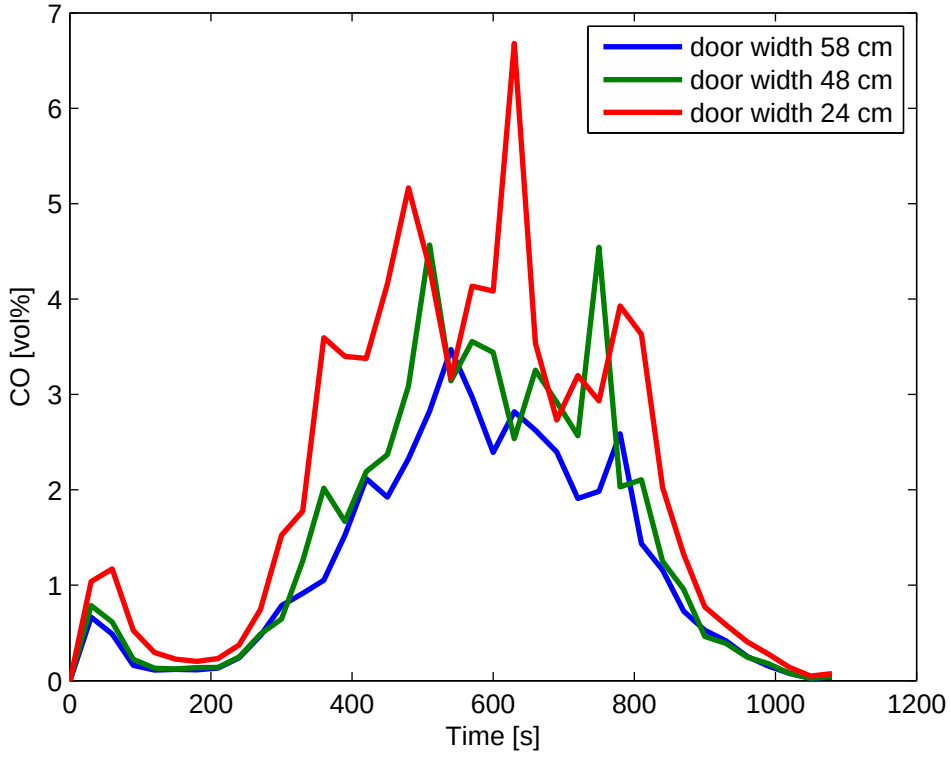

FIGURE 6.2 CO concentrations at exit in an enclosure fire with varying door opening

6.2 Early fire detection

Reliable fire detection is essential to allow for the safe evacuation of occupants. Safe evacuation of the users of the buildings is the primary objective of building regulations. In order to improve safety of the fire fighting efforts as well as to reduce the loss of lives and costs of the public, we need to improve the reliability of detection systems and reduce the time to alarm for real fires. Determination of the response time of the fire detectors at installation location for variables such as smoke (i.e. CO concentration) is conducted.

The current state of the art technology and the European norm EN 45545 contain provisions for installation of fire detection systems. DIN 14676 is adopted in accordance with European norm DIN EN 14604. The regulation for dwellings, regarding the positioning of automatic fire detectors, stipulates one smoke detector must be installed under ceiling center for a room not bigger than 60 m^2. For bigger size room, more detectors should be installed. A number of rules, regulations and recommendations regarding fire detection system are available for public places and industries [2, 8].

In this work, fire detector response time and detector positioning are analyzed based on CO transport in enclosure fire conditions. Fixed temperature and rate of rise detector could also be analyzed. However this is not included here. Smoke detectors are most commonly used detectors in dwellings. Here a smoke detector with capability of CO sensing is analyzed. Fire Dynamics Simulator (FDS) and the new developed toxic (i.e. CO constituent

of smoke) formation model are utilized in order to model transport of CO.

RSE geometry and an enclosure of same floor area with 5 m height have been simulated with polystyrene fires at the center of the both enclosures. According to DIN 14676 one smoke detector is assumed at the center of enclosure just under ceiling. Time required for CO to reach this detector location has been recorded for both cases. Time required for smoke to reach the detector is 5 s for 0.98 m high ceiling whereas 10 s is the estimated time for 5 m ceiling. Detector response time consists of mainly smoke transport time and sensor system response time. Detector response time is higher for higher ceiling. Detector can be set according to optimized response time. This result shows that there is a room for improving early fire warning by designing specific fire conditions at specific enclosures while maintaining codes and standards.

An enclosure, 6 m wide by 5 m tall by 10 m deep with 0.76 m wide by 2.03 m tall door centered at the bottom of the front wall, has been chosen for simulation. Polystyrene fire of 100 kW (set at one of the rear corners) are simulated. According to DIN 14676, one detector must be used for 60 m^2 floor area and location should be set under the ceiling at the center of the enclosure. Two other locations under the ceiling (3 m from a side wall, 1 m from front wall and 1 m from rear wall) have been chosen in order to verify detector response times and select optimized detector positioning and required number of detectors for early warning of occupants to facilitate expeditious evacuation. Time when CO reached 3 detectors is presented in Fig. 6.3. This figure illustrates transient CO concentration at detector locations. Lines parallel to Y-axis indicate the time when CO threshold concentration of 0.003 vol% (30 ppm) is reached to start alarm. This threshold varies depending on the detectors available on the market. The detector at center (D-C in Fig. 6.3) needs 10 s more than the rear detector (D-R in Fig. 6.3). Time needed for CO to reach the detector at front location (D-F in Fig. 6.3) is 35 s more than that of the detector at rear. If there is a fire close to the front wall, the detector at front location will sense earlier than others. Therefore, one detector for 30 m^2 area is capable to detect a fire of any origin inside this area within 10-25 s. Any size of fire can initiate at any location of enclosure. Using two detectors at front and rear location instead of one at center can detect fire from any location while saving detection time. Additionally, US fire statistics show that 22% home fire deaths resulted from homes in which smoke alarm fails to operate [9]. From these statistics, we can assume smoke detectors failure probability is 0.22. One additional smoke detector will reduce this failure probability by 78%. This additional detector costs additional price (30 Euro to 100 Euro). DIN 14676 recommends to use one detector for four years. The cost per year of one detector becomes less than 8.33 Euro. Risk (Euro/year) and estimation of risk mitigation (Euro/year) by additional detector should be quantified for individual cases or in other words, cost-benefit analysis according to targeted safety level should be conducted in risk management decision making process.

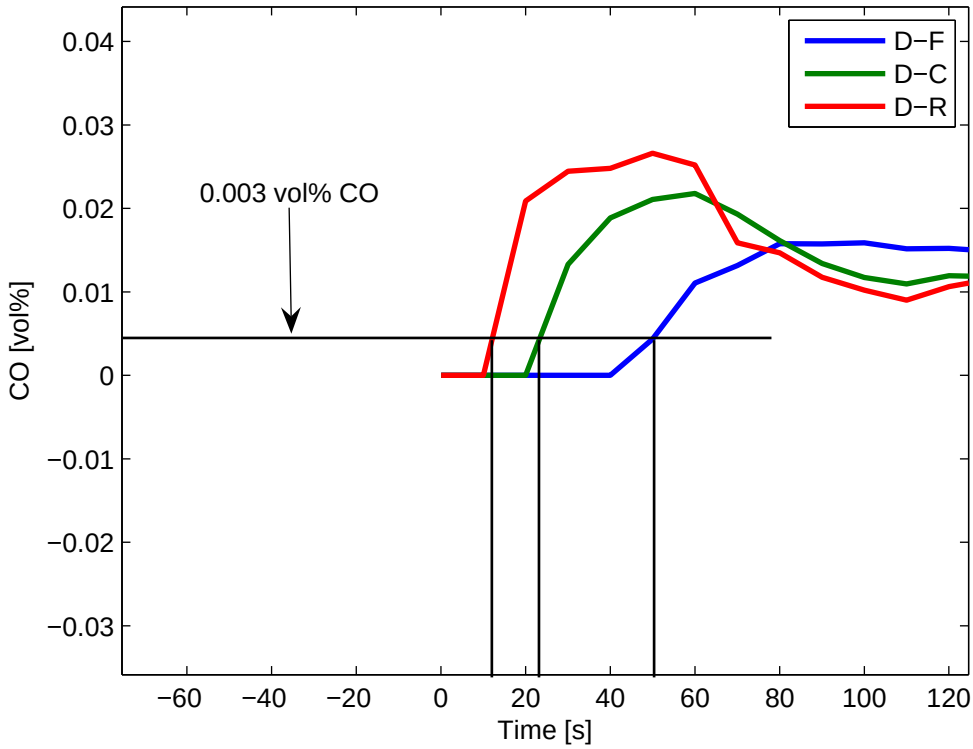

FIGURE 6.3 Detectors response time for 100 kW fire

Chapter 7

Conclusion

The primary aim of this thesis was to develop fire risk mitigation strategies through toxic hazard assessment and fire protection design of enclosure fire. In order to assess toxic hazard with reasonable accuracy, detailed investigation of equivalence ratio and temperature on toxicants formation from different burning substances at enclosure fire conditions is conducted by constrained chemical equilibrium calculations. Because of the multitude of burning materials encountered in fire and the unavailability of chemical kinetics, constrained equilibrium approach is utilized. Currently available CFD codes have either no implemented model or there are toxic models with inaccurate prediction due to the use of empirical data (CO and soot yield). There is no model available for predictions of other toxicants like ($NO_x, SO_x, H_2S, HCN, HCl$ etc.). Three different CFD fire softwares are compared to experimental data and one is chosen based on its ability to predict local transient temperatures while spending same computational time and using same computational resource. A submodel is developed to predict local toxicant concentration by solving species transport equation with artificial source term as postprocessing. Constrained equilibrium concentration are utilized for the calculation of artificial source terms. All spatial derivatives are approximated by second order finite differences and flow variables are updated in time using an explicit second order predictor corrector scheme. Explicit 2nd order Adam-Bashforth scheme is utilized for numerical integration of source term of species balance equation. The developed toxic formation model is coupled with the chosen CFD model FDS 5.

Simulations are performed with the new developed toxic formation model. Modelling results are compared to experimental data of full and reduced scale enclosure natural gas fires as well as reduced scale polystyrene fires. Predictions of CO are in reasonable agreement with experimental data although discrepancies occur also due to errors in temperature and mixture fraction prediction by the chosen CFD model. CO prediction can be improved by better prediction of temperature and mixture fraction at underventilated combustion. The major reason of such discrepancies in temperature prediction is fast chemistry assumption of the combustion model. Due to the lack of detailed chemical kinetics of burning materials, a multi-step reaction mechanism in the form of mixture fraction approach can be used. Additionally, the new developed toxic model ignores heat balance of CO formation during calculation as it is constructed as postprocessing. The use of this model is limited

to unsteady state conditions because source term becomes zero for steady state condition. Despite of these limitations, this simplified model can also be utilized to predict other toxicants (HCN, HCl etc.) in enclosure fire.

The new developed toxic formation model is used to model toxic exposure to occupants in enclosure fires. Results show that the toxic exposure in a specific area can be minimized by choosing appropriate geometry and ventilation. Local toxic concentration in an enclosure fire decreases with increasing ventilation opening. High ceiling height can keep toxicant above occupant head for safer evacuation.

Early fire detection is analyzed by using the CO transport model. The detector response time can be optimized by choosing optimized detector installation location. Using two detectors instead of one as prescribed in DIN norm, can reduce the probability of a dangerous fire and thereby the fire risk by 78%.

Event tree analysis of enclosure fire risk and fault tree analysis of initiating event probability of fires are conducted qualitatively. Quantitative analysis needs event probability data. Event probability can be estimated using fire statistics. Detailed fire statistics (fire protection device performance etc.) are missing and are not available to the public at the national level in Germnay. It is difficult to undertake a detailed analysis for the whole country. Improvement of the current fire statistic system is needed for fire risk analysis and mitigation.

Bibliography

[1] *FDS Technical Reference Guide version 5/2008 , http://www.fire.nist.gov/fds/.*

[2] German norm. Technical report, DIN 5510, Deutsches Institut für Normung e.V.

[3] *International Survey of Computer Models for Fire and Smoke, http://www.firemodelsurvey.com/FieldModels.html.*

[4] *JASMINE Technical Reference Guide , Fire Research Station, BRE,UK.*

[5] *SOFIE Technical Reference guide , http://www.cranfield.ac.uk/sme/sofie.*

[6] *Statistisches Bundesamt Deutschland,http://www.destatis.de/.*

[7] *US Fire Administration,http://www.usfa.dhs.gov/statistics/.*

[8] Tb 04/01 of vfdb- guideline for engineering methods of fire protection. Technical report, vfdb, May 2006.

[9] Marty Ahrens. U.S. experience with smoke alarms and other fire detection/alarm equipment. Technical report, NFPA, Quincy, MA, April 2007.

[10] A.Ostermann and P.Kaps. The solution of a combustion problem with rosenbrock methods. *ACM Transaction on Mathematical Software*, 12(4):354–361, 1986.

[11] A.Tewarson. Generation of heat and chemical compounds in fires. *SFPE Handbook of Fire Protection Engineering, Chapter 3-4*, pages 3.82–3.161, 2002.

[12] C.W Bale, P. Chartrandsfi, S.A. Degterov, R. Ben Mahfoud, J. Melan, A.D. Pelton, G. Eriksson, K. Hack, and S.Petersen. *FactSage Thermochemical Software and Databases , http://www.factsage.com.*

[13] Thomas F. Barry. *Risk-Informed,Performanced-Based Industrial Fire Protection, An Alternative to Prescriptive Codes.*

[14] C.L. Beyler, D.T. Gottuk, and R.J. Roby. The role of temperature on carbon monoxide production in compartment fires. *Fire Safety Journal 24*, pages 315–331, 1995.

[15] Craig Beyler. *Development and Burning of a Layer of Products of Incomplete Combustion Generated by a Buoyant Diffusion Flame.* PhD thesis, Harvard University, 1983.

[16] Kathryn M. Bulter and George W. Mulholland. Generation and transport of smoke components. *Fire Technology.*, 40:149–176, 2004.

[17] M. Bundy, A. Hamins, S. C.Kimm E.L. Johnsson, G.H. Ko, and D.B. Lenhert. Measurements of heat and combustion products in reduced-scale ventilation-limited compartment fires. Technical report, NIST, July 2007.

[18] J.R. Cash. A class of implicit runge-kutta methods for the numerical intregation of stiff ordinary differential equations. *Journal of the Association for Computing Machinery*, 22(4):504–511, October 1975.

[19] C.Beyler. Major species production by diffusion flame in a two-layered compartment fire environment. *Fire Safety Journal*, 10:47–56, 1986.

[20] C.Beyler. Flammabilty Limits of Premixed diffusion Flames. *Handbook of Fire Protection Engineering, NFPA*, 3rd Ed., 2002.

[21] C.L.Beyler and M.M.Hirschler. *Thermal Decomposition of Polymers, section 1 chapter 7,SFPE Handbook of Fire Protection Engineering.* NFPA, 2002.

[22] M.J. Cleary and J.H. Kent. Modelling of species in hood fires by conditional moment closure. *Combustion and Flame*, 143:357–368, 2005.

[23] C.Westbrook and F.Dryer. Simplified Reaction Mechanisms for The Oxidation of Hyrocarbon Fuels in Flames. *Combustion Science and Technology*, 27:31–43, 1981.

[24] F.C.Lockwood and W.M.G. Malalasekera. Fire computation: the flashover phenomenon. In *Twenty-Second Symposium Combustion, Pittsburgh*, pages 1319–1328. Combustion Institute, 1988.

[25] Jason E. Floyd and Kevin B. McGrattan. Multiple parameter mixture fraction with two step combustion chemistry for large eddy simulation. In *Proceedings of the 11th International Interflam Conference*, volume 2, pages 907–918, September 2007.

[26] Burkhard Forell. *A Methodology to assess Species Yields of Compartment Fires by means of an extended Global Equivalence Ratio Concept.* PhD thesis, Faculty of Architecture, Civil Engineering and Environmental Sciences, Technical University of Braunschweig, Germany, Faculty of Engineering, University of Florence, Italy, 2007.

[27] G.Cox. *Combustion Fundamentals of Fire.* Academic Press, 1995.

[28] P. Glarborg, R.J. Kee, and J.A. Miller. PSR: A fortran programm for modeling well-stirred reactors. Sandia National Laboratories. page 27, 1986.

[29] D.T. Gottuk, R.J. Roby, and C.L. Beyler. The role of temperature on carbon monoxide production in compartment fires. *Fire Safety Journal*, 24:315–331, 1995.

[30] James G.Quintiere. Fundamentals of Enclosure Fire Zone Models. *Journal of Fire Protection Engineering*, pages 99–119, 1989.

[31] James G.Quintiere. *Compartment Fire Modeling, section 3 chapter 5, SFPE Handbook of Fire Protection Engineering.* NFPA, 2002.

[32] H.G.Matthies, A. Keese, and J. Steindorf. *Lecture notes Introduction to Scientific Computing.* Institute of Scientific Computing, Technical University of Braunschweig, Germany, 2004.

[33] J.G.Verwer, B.P. Sommeijer, and W. Hundsdorfer. RKC time-stepping for advection-diffusion-reaction problems. *Journal of Computational Physics*, 201:61–79, 2004.

[34] J.H.Morehart. *Species Production in Fires Burning in Two-Layered and Homogeneously Vitiated Environments.* PhD thesis, California Institute of Technology, Pasadena, 1990.

[35] Takashi Kashiwagi. Polymer combustion and flammability-role of the condensed phase. In *Twenty-Fifth Symposium on Combustion*, pages 1423–1437. Combustion Institute, 1994.

[36] S. Kumar and G. Cox. The Application of a Numerical Field Model of Smoke Movement to the Pysical Scaling Compartment Fires. *Numerical Methods in Thermal Problems*, pages 837–848, 1983.

[37] S. Kumar and G. Cox. Mathematical modelling of fire in road tunnels. In *Proceedings of 5th International symposium-on Aerodynamics and Ventilation of Vehicle Tunnels,BHRA, Cranfield, UK*, page 61, 1985.

[38] R. Leithner and H.Müller. CFD studies for boilers. In *Second M.I.T. Conference on Computational Fluid and Solid Mechanics.* M.I.T., June 2003.

[39] M.J. Lewis, J.B.Moss, and P.A.Rubini. CFD modelling of combustion and heat transfer in compartment fires. In *Proceedings of 5th International symposium on Fire Safety Science,Melbourne,Australia*, pages 463–474. International Association of Fire Safety Science, 1997.

[40] A.E. Lutz, R.J. Kee, and J.A. Miller. Senkin: A fortran programm for predicting homogenous gas phase chemical kinetics with sensitivity analysis. sandia national laboratories. page 27, 1988.

[41] F. Markert, B. Andersson, and G. Holmstedt. Scaling experiment to assess chemical warehouse fires. Technical report, Riso National Laboratory, Denmark; Lund university, Sweden, 1996.

[42] I. Nakaya. Prediction model of CO, CO_2, O_2 concentrations in compartment fires using wood fuel. *Fire and Material*, 11:173–178, 1987.

[43] N.L.Crauford, S.K.Cox, and J.B.Moss. Experimental and Numerical Simulation of Buoyant fire. *Combustion and Flame 61*, page 63, 1985.

[44] N.N.Brushlinsky, J.R. Hall, S.V. Sokolov, and P.Wagner. *Center of Fire Statistics.* CTIF, 2005.

[45] V. Novozhilov. Computational fluid dynamics modeling of compartments fires. *Progress in Energy and Combustion Science*, 27:611–666, 2001.

[46] N.P.Bryner, E.L. Johnsson, and W.M. Pitts. Carbon monoxide production in compartment fires-reduced scale enclosure test facility. Technical report, NIST, December 1994.

[47] N.P.Bryner, E.L. Johnsson, and W.M. Pitts. Scaling compartment fires - reduced and full-scale enclosure burns, nist report. Technical report, NIST, Maryland, USA, 1994.

[48] Elaine S. Oran and J.P. Boris. *Numerical Simulation of Reactive Flow.* Cambridge University Press, 2001.

[49] William M. Pitts. Application of thermodynamics and detailed chemical kinetic modeling to understanding combustion product generation in enclosure fires. *Fire Safety Journal.*, 23:271–303, 1994.

[50] William M. Pitts. The global equivalence ratio concept and the formation mechanisms of carbon monoxide in enclosure fires. *Prog. Energy Combust. Sci.21*, pages 197–237, 1995.

[51] W.M. Pitts. An algorithm for estimating carbon monoxide formation in enclosure fires. In *Proceedings of the Fifth International Symposium on Fire Safety Science*, pages 535–546. IAFSS, March 1997.

[52] Marvin Rausand. *System Reliability Theory 2nd edition.* Wiley, 2005.

[53] R.Friedman. An International Survey of Computer Models for Fire and Smoke. *Journal of Fire Protection Engineering*, pages 81–92, 1992.

[54] Hans Richter. *Brandsimulation durch Mikroverbrennung.* PhD thesis, TU Braunschweig, 1999.

[55] Tuomo Rinne, J. Hietaniemi, and S. Hostikka. Experimental validations of the FDS simulations of smoke and toxic gas concentrations. Technical report, VTT working papers 66, ESPOO 2007, VTT Finland, January 2007.

[56] R.Leithner. *Vorlesungskript Risiko und Sicherheit, großtechnischer Anlagen.* IWBT, Technical University of Braunschweig, Germany, 2008.

[57] S.Leonard, G.W.Mulholland, R.Puri, and R.Santoro. Generation of CO and smoke during underventilated combustion. *Combustion and Flame*, 98:20–34, 1994.

[58] S.V.Patankar. *Numerical prediction of three dimensional flows, in Launder,B.E.(ed.) Studies in Convection: Theory, Measurements and Applications,vol.1.* Academic, NewYork, 1978.

[59] T.D.Bui. Some a-stable and l-stable methods for the numerical intregation of stiff ordinary differential equations. *Journal of the Association for Computing Machinery*, 26(3):483–493, 1979.

[60] H. Tuovinen. Validation of Ceiling Jet Flows in a Large Corridor with Vents Using the CFD code Jasmine. *Fire Technology, vol.32 No.1*, pages 25–49, 1996.

[61] W.E. Vesely, F.F.Goldberg, N.H.Roberts, and D.H.Haasl. *Fault Tree Handbook (NUREG-0492)*. U.S. Nuclear Regulatory Commission, 1981.

[62] V.Novozhilov. Computational Fluid Dynamics Modeling of Compartment Fires. *Progress in Energy and Combustion Science 27*, pages 611–666, 2001.

[63] Z. Wang, F. Zia, and E.R. Galea. Predicting toxic gas concentrations resulting from enclosure fires using local equivalence ratio concept linked fire models. *Fire and Materials 31*, pages 27–51, 2007.